الجمهورية الجزائرية الديمقراطية الشعبية
République Algérienne Démocratique et Populaire
وزارة التعليم العالي والبحث العلمي
Ministère de l'enseignement supérieur et de la recherche scientifique

Université Mohamed Khider – Biskra
Faculté des Sciences et de la Technologie
Département : Génie civil et Hydraulique
Réf. :……..

جـامـعـة مـحـمـد خـيـضـر بـسـكـــرة
كـلـيـة الـعـلـــوم والـتـكـنـولـــوجـيـا
قـسـم: الـهـنـدسـة الـمـدنـيـة والـــري
الـمـرجـع:……..

Thèse présentée en vue de l'obtention
Du diplôme de

Doctorat en : Hydraulique

Spécialité (Option) : Hydraulique Urbaine

Préparation et propriétés des adsorbants hybrides à base de charbon : Application dans la dépollution des eaux

Présentée par :

Dhirar BEN SALEM

Soutenue publiquement le : 03/07/2024

Devant le jury composé de :

Youcef Leila	**Professeur**	**Président**	**Université de Biskra**
Ouakouak Abdelkader	**MC-A**	**Encadrant**	**Université d'Eloued**
Nouioua Asma	**MC-A**	**Examinateur**	**Université de Biskra**
Rouahna Noureddine	**MC-A**	**Examinateur**	**Université d'Eloued**
Yahiaoui Khemissi	**MC-A**	**Co-encadrant**	**Université d'Eloued**

الجمهورية الجزائرية الديمقراطية الشعبية
People's Democratic Republic of Algeria
وزارة التعليم العالي والبحث العلمي
Ministry of Higher Education and Scientific Research

Mohamed Khider University of Biskra
Faculty of Science and Technology
Department: Civil Engineering and Hydraulics
Ref: …….

جامعة محمد خيضر بسكرة
كلية العلوم والتكنولوجيا
قسم: الهندسة المدنية والري
المرجع:.....……

Thesis presented with a view to obtaining
the diploma of

Doctorate in: Hydraulics

Specialty (Option): Urban Hydraulics

Preparation and properties of hybrid carbon-based adsorbents: Application in water decontamination

Presented by:

Dhirar BEN SALEM

Publicly defended on: 03/07/2024

In front of a jury composed of:

Youcef Leila	**Professor**	**President**	**University of Biskra**
Ouakouak Abdelkader	**Lecturer-A**	**Supervisor**	**University of El Oued**
Nouioua Asma	**Lecturer-A**	**Examiner**	**University of Biskra**
Rouahna Noureddine	**Lecturer-A**	**Examiner**	**University of El Oued**
Yahiaoui Khemissi	**Lecturer-A**	**Co-supervisor**	**University of El Oued**

Dedications

I dedicate this work

To my dear Mother أمي، أمي، أمي and my dear Father أبي

To my sister Zahra and brothers Saleh, Oussama, and Younes,

To my nephews Bilal and Montasir Bi'Allah.

Dhirar ضِرار

Acknowledgements

First and foremost, I would like to express my gratitude to Allah for the health, patience, courage, and determination. Second, I would like to thank my parents for their encouragement, care, and help. Thank you, *Mom*, thank you, *Dad*. Third, I want to thank me for believing in me and doing all this hard work.

I would like to extend my heartfelt thanks and esteem to my supervisor, Dr Ouakouak Abdelkader, professor at the *University of El Oued*. I thank him for agreeing to guide my research and for his generosity, relevant comments, and constant support throughout my doctoral studies. Also, I would like to thank my co-supervisor Dr Yahiaoui Khemisi (*University of El Oued)* for his support and guidance throughout the process of working on my thesis.

I particularly want to thank Prof. Guergazi Saadia the head of the (*LARHYSS laboratory, University of Biskra*) for providing me with the necessary resources to carry out my thesis work.

I am deeply thankful to Prof. Youcef Leila (*University of Biskra)* for the honour of presiding over my jury. I also want to express my gratitude to those who had the honour of reading and evaluating this thesis and agreeing to be part of the jury: Dr Rouahna Noureddine (*University of El Oued)* and Dr Nouioua Asma (*University of Biskra)*.

I would like to thank all the members of the research laboratory in subterranean and surface hydraulics (*LARHYSS, Biskra, Algeria*) and "*Nanocosas y Catàlisis*" group (*Campus de Puerto Real, Universidad de Cádiz, España*), students, researchers, and professors.

I also want to thank Prof. Maria Bernardo from *NOVA University of Science and Technology* (*Lisbon, Portugal*) for welcoming me to their laboratories during my short internship. I would like to express my gratitude to Profs: Josee Gatica, Hilario Vidal, and Dolores Milla from *Cadiz University* (*Spain*) for allowing me to perform an Erasmus+ internship for four months to complete my thesis research. I am profoundly grateful to Prof. Hai Nguyen Tran (*Duy Tan University, Vietnam*) for his invaluable guidance and support during my doctoral studies.

I thank Prof. Bitam Salim (*Vice Rector, University of Biskra*) for his help and support during my doctoral research.

I greatly thank Dr Bourich Fouzi, Dr Zouai Meftah, Dr Abdeddaim Mehdi from the *University of Biskra*. I also want to thank the PhD student Riah Amel (*Constantine University*) for her help and support.

I'm deeply thankful to Mr Yazid Ayachi and his family, my friends the engineer Mr. Khelifa Amine, Khiouani Tarek, Bendjedidi Abd Nacer, Harrar Mohamed, and Noui Aymen for their support, guidance, and help.

Abstract – Résumé – الملخص

Abstract– This thesis aims to explore, valorise, and develop innovative hybrid adsorbents based on carbon by incorporating the properties of peanut shell biochar or magnetic–biochar with the hydrogel bead of sodium alginate producing biochar/alginate bead (B/A) and magnetic–biochar/alginate (MB/A) beads for adsorbing Cd^{2+} and Cu^{2+} in water, respectively. The two kinds of spherical beads were prepared using the physical cross–linking method. Results exhibited that beads contained between 90% and 93% of water. XRD data proved the successful synthesis of Fe_3O_4 nanoparticles in magnetic–biochar and MB/A samples. The pH, contact times, and isothermal conditions were factors dependent that affected the adsorption efficiency. The maximum capacity of the B/A bead to adsorb Cd^{2+} was 230 mg/g and 234.1 mg/g for the MB/A bead to adsorb Cu^{2+}, calculated from the Langmuir model at 30°C and pH 5.0. The principal metal adsorption mechanisms were described as ion exchange, complexation, and Van der Waals force. Desorption with NaOH or HCl for the laden B/A and MB/A beads exhibited potential reusability. The prices estimated in US$/kg for materials were: initial PS–biochar (0.248), magnetic–biochar (0.38-184.99), B/A bead (1.278-253.62), and MB/A bead (1.348-348.8). The prepared hybrid adsorbents B/A and MB/A can be superior for eliminating cationic heavy metals from aqueous solutions.

Key words: Adsorption; hybrid materials; carbon; biopolymer; pollutants; modelling

Résumé– Cette thèse visait à explorer, valoriser et développer des adsorbants hybrides innovants à base de charbon en incorporant les propriétés du biochar de coques d'arachide ou du biochar–magnétique avec d'hydrogel d'alginate de sodium pour préparer des billes biochar/alginate (B/A) et des billes biochar–magnétique/alginate (MB/A) pour l'adsorption des métaux tels que Cd^{2+} et de Cu^{2+} dans l'eau, respectivement. Les deux types de billes sphériques ont été fabriqués en utilisant la méthode de réticulation physique. Les résultats ont montré que les billes contenaient entre 90% et 93% d'eau. Les données de DRX ont prouvé la réussite de la synthèse des nanoparticules Fe_3O_4 dans le biochar–magnétique et les échantillons MB/A. Le pH, le temps de contact et les conditions d'isotherme étaient des facteurs dépendants qui ont affecté l'efficacité de l'adsorption. La capacité maximale de B/A à adsorber Cd^{2+} était de 230 mg/g et de 234,1 mg/g pour MB/A à adsorber Cu^{2+}, calculée à partir du modèle de Langmuir à 30°C et à un pH de 5,0. Les principaux mécanismes d'adsorption des métaux ont été décrits comme l'échange d'ions, la complexation et les forces de Van der Waals. La désorption avec NaOH ou HCl pour les billes chargées B/A et MB/A a montré un potentiel de réutilisation. Les prix estimés en US$/kg pour les matériaux étaient les suivants : biochar (0.248), biochar–magnétique (0.38–184.99), B/A (1.278–253.62) et MB/A (1.348–348.8). Les adsorbants hybrides préparés B/A et MB/A peuvent être supérieurs pour éliminer les cations métalliques dans des solutions aqueuses.

Mots clés : Adsorption ; matériaux hybride ; charbon ; biopolymère ; polluants ; modélisation.

الملخص– تهدف هذه الأطروحة إلى استكشاف و تقييم وتطوير مواد ممتزة هجينة ومبتكرة تعتمد على الكربون من خلال دمج خصائص الفحم الحيوي لقشور الفول السوداني أو الفحم الحيوي المغناطيسي مع الخرزات المائية لألجينات الصوديوم لإنتاج خرزات الفحم الحيوي/الجينات (B/A) وخرزات الفحم الحيوي المغناطيسي/الجينات (MB/A) من أجل إزالة أيونات الكادميوم والنحاس من الماء. تم تصنيع الخرزات ذات الشكل الكروي باستخدام طريقة التصليب الفيزيائي. أظهرت النتائج أن الخرز تحتوي على ما بين 90% و93% من الماء. أثبتت تحاليل XRD نجاح تصنيع جسيمات Fe_3O_4 في عينات الفحم الحيوي المغناطيسي و MB/A. كانت درجة الحموضة، مدة (فترة) التلامس، وشروط متساوي الحرارة من العوامل التي أثرت على كفاءة الامتزاز. تقدر السعة القصوى لخرزة B/A لامتصاص Cd^{2+} هي 230 ملجم/جم و234.1 ملجم/جرام لخرزة MB/A لامتصاص Cu^{2+}، محسوبة من نموذج Langmuir عند 30 درجة مئوية ودرجة الحموضة 5.0. تم وصف آليات امتزاز المعدن بالتبادل الأيوني، والتعقيد، وقوة فان دير فالس. أظهرت نتائج تجارب تجديد الخرز المحملة B/A و MB/A باستخدام NaOH أو HCl إمكانية إعادة استخدامها في دورات امتزاز جديدة. كانت الأسعار المنخفضة لتكاليف انتاج الممتزات بالدولار الأمريكي للكيلوغرام الواحد هي: الفحم الحيوي الأولي لقشور الفول السوداني (0.248)، والفحم الحيوي المغناطيسي (0.38–184.99)، وخرزات B/A (1.278–253.62)، وخرزات MB/A (1.348–348.8). بشكل واضح، يمكن أن تكون المواد الممتزة الهجينة المحضرة في هذه الدراسة B/A و MB/A متفوقة في إزالة كاتيونات المعادن الثقيلة من المحاليل المائية.

الكلمات المفتاحية: الإمتزاز؛ المواد الهجينة؛ الفحم؛ البوليمر الحيوي؛ الملوثات؛ النمذجة.

Table of contents

Table of contents

Chapter II: Research methodology and procedures

Chapter III: Characterizations and techno–economic feasibility of adsorbents

Chapter IV: Adsorption of cadmium and copper onto the hybrid adsorbents

List of figures

List of figures

Chapter I

Chapter II

Chapter III

Chapter IV

List of tables

List of tables

Chapter I

Chapter III

Chapter IV

Nomenclature

Nomenclature

List of all symbols mentioned in the thesis:

$Ca(OH)_2$	Calcium hydroxide
NaOH	Sodium hydroxide
N_2	Nitrogen
CO_2	Carbon dioxide
S_{BET}	Specific surface area
V_{Total}	Total volume of pores
O_2	Oxygen
HCl	Hydrochloric acid
NaOH	Sodium hydroxide
SA	Sodium Alginate
Fe^{3+}	Iron trivalent cations (ferric ions)
$\alpha–Fe_2O_3$	Hematite
$\gamma–Fe_2O_3$	Maghemite
Fe_3O_4	Magnetite
$FeCl_3$	Iron chloride (III)
$FeCl_2$	Iron chloride (II)
$FeSO_4$	Ferrous sulphate
Ca^{2+}	Calcium divalent cations
$CaCl_2$	Calcium chloride
pH	Potential of hydrogen
pH_{PZC}	The pH of point zero charge
TME	Trace Metal Element
Cd^{2+}	Cadmium ion
CdS	Cadmium sulphide
CdO	Cadmium oxide
$CdCO_3$	Cadmium carbonate

$Cd(NO_3)_2$	Cadmium nitrate
$CdCl_2$	Cadmium chloride
CdSn	Cadmium stannate
Cu^{2+}	Copper ion, also known as Copper (II)
Copper(I), Cu^{+}	Copper iodide
$CuSO_4$	Copper sulphate
PS	Peanut shell
MB	Magnetic biochar
B/A	Biochar/Alginate bead
MB/A	Magnetic–biochar/Alginate bead
KBr	Potassium bromide
C_o	Initial concentration (mg/L)
E	Energy (kJ/mol)
m/V	Mass/Volume ratio (g/L)
DW	Deionized water
q_{exp}	The experimental adsorbed quantity of the adsorbate
q_{cal}	The adsorbed quantity of the adsorbate calculated by the model
$q_{e,\ average}$	The mean of the experimental values (mg/g)
q_{ads}	Adsorbed quantity of the adsorbate
C_e	Concentration at the equilibrium (mg/L)
R%	Adsorption rate (removal efficiency)
T	Temperature (K)
t	Time (min)
q_t	Adsorbed quantity at the time t
q_e	Adsorbed quantity at the equilibrium
k_1	The rate constant of Pseudo–1^{st}–order (PFO)
k_2	The rate constant of Pseudo–2^{nd}–order (PSO)
k_{ipd}	The constant of the Intraparticle diffusion (IPD) model
C_{ipd}	The constant of thickness of the boundary layer of IPD model
m_{PNO}	The exponents of the Pseudo–n^{th}–order (PNO) model
k_{PNO}	The constant rate of the PNO model

k_{Av}	The Avrami kinetic constant (1/min)
n_{Av}	Fractional adsorption order of the Avrami model
α	The initial adsorption rate of the Elovich model [mg/(g×min)]
β	The desorption constant of the Elovich model (g/mg)
K_{Fr}	The constant of the Freundlich model [(mg/g)/(mg/L)$^{n_{Fr}}$]
n_{Fr}	The exponential intensity coefficient of the Freundlich model
Q_{max}	The maximum adsorption capacity (mg/g)
K_L	The energy constant of the Langmuir model (L/mg)
K_{Sips}	The constant of the Sips model (mg/L)$^{-1/n_{Sips}}$
n_{Sips}	The heterogeneity constant of Sips model
$K_{r\text{-}p}$	The constant (L/g) of Redlich–Peterson (R–P)
$a_{r\text{-}p}$	The r–p parameter of the R–P model (mg/L)$^{-g_{r\text{-}p}}$
$g_{r\text{-}p}$	Dimensionless exponential factor of the R–P model (must be ≤1)
$\Delta G°$	Gibbs free energy (kJ/mol)
$\Delta H°$	Change in Enthalpy (kJ/mol)
ΔS°	Change in Entropy (kJ/mol)
R	The molar (ideal) gas constant = 8.31 (J/mol.K)
K_c	Equilibrium constant with non–dimensional
$M_{element}$	Element mass molar (g/mol)
$C°$	The standard reference of solution (1 mol/L)
AI	Artificial intelligence

General Introduction

General introduction

Today's conservation efforts pave the way for a sustainable tomorrow

Water is a vital resource that sustains all life on our earth. Nonetheless, it is also the entire factor for industrial and agricultural development, which can result in air and water pollution, causing severe harm to the environment. Water can purify itself through natural processes, but this operation takes time and is easily overcome by excessive pollution. Undoubtedly, our increasing reliance on some activities, including domestic, urban, industrial, and agricultural, sets drinking water in the grave danger.

Water pollution can be classified as the physical, chemical, or biological alteration of water, making it hazardous to use or disrupting aquatic life (Wasewar et al., 2020). It affects groundwater and surface waters like rivers and the bodies of water. This pollution occurs when substances are discharged into the aqueous solution, degrading its quality, making its use dangerous, and disrupting the aquatic ecosystem. This contamination cannot be naturally treated, and it is improper to introduce any substance into water that exceeds its natural purification capacity. Such a substance is considered a pollutant and must be avoided at all costs.

Nature can sometimes be responsible for pollution, such as when water flows through acidic soils. However, most water pollution is caused by human activities (Ouakouak et al., 2021). There are two main types of water pollution: point and non–point sources. Point sources typically identifiable, such as factories, wastewater treatment plants, septic systems, and other points that directly discharge pollutants into water bodies (Schaffner et al., 2009). Non–point sources are more complex to trace and cannot be linked to specific locations. They represent sediment runoff from farms, construction sites, and mines (Munafò et al., 2005). In prior assessment studies, the elevated levels of cadmium and copper ions in surface and groundwater in certain regions of Algeria represent a pressing public health challenge (Arab et al., 2021; Benhaddya et al., 2020; Khelfaoui et al., 2022). Given the potential for exposure, it is imperative that these hazardous substances are comprehensively addressed and effectively mitigated.

Wastewater discharges from various industrial sectors pose significant health and environmental challenges. Before being released into the environment, these effluents must be treated. Due to their diverse and heterogeneous composition, effluent treatment typically requires

several steps to remove different pollutants. The first usually focuses on removing insoluble contaminants, while subsequent steps often use specific techniques, such as chemical oxidation and biological to decompose pollutants. The choice of the type of treatment depends on the substance targeted, its concentration in water, solubility, and the economic viability of the selected processes (Tran et al., 2016a). Treatment methods include physical–chemical approaches like coagulation–flocculation, chemical methods like chemical oxidation, biological methods involving pollutant decomposition by microorganisms, and adsorption treatment (Nouioua et al., 2023).

Adsorption is a simple and effective operation that has the potential to be cost–efficient if industrial activated carbon, the most commonly used adsorbent, could be replaced by other equally efficient and less expensive alternatives (Rouahna et al., 2023). In recent years, water treatment technologies have significantly advanced with the quality development of new materials, laboratory techniques, and technical processes. Thus, this progress has facilitated the use of agricultural waste (like peanut shells) and the exploration of eco–friendly materials, such as biomass, biochar and biopolymers (i.e., chitosan and alginate) (Heydaripour et al., 2019; Tomul et al., 2020; Wang et al., 2019).

Using agricultural biomass to produce biochar is a trendy way to reduce the consumption of activated carbons. Agri–food activities generate large volumes of waste, and innovative strategies are needed for environmentally sound waste management (Azri et al., 2022; Chahinez et al., 2020). Peanut (PS) production in Algeria has seen a significant increase of 6% from 2018 to 2019, resulting in an estimated production of 126, 022 quintals. El Oued region has emerged as the primary contributor to this increase, accounting for 70% of the total peanut production in the country (*Algerian Ministry of Agriculture*). PS are among the world's most abundant crops, with annual production exceeding 11 million tonnes, where about 200 to 300 grams of waste are yielded per 1 kg of groundnuts. These shells contribute 30% of the entire weight of the legume (Mandala et al., 2023). Therefore, PS wastes can be valorised and used as biochar in many scale applications like water treatment.

Alginates are anionic polysaccharides that are primarily produced from brown algae such as *Laminaria*, *Macrocystis*, and several other species. They are biodegradable and abundant. Alginates have a wide range of applications, including the production of food products,

pharmaceuticals, and water treatment (Ayouch et al., 2020a; Oussalah et al., 2019). By combining or encapsulating materials such as biochar in the alginate matrix, new composite adsorbents can be prepared, which can be used as adsorbents or biopolymers (Aichour et al., 2019; Verduzco-Navarro et al., 2020). These composite adsorbents has the potential to be highly effective in treating heavy metal solutions (Ben Salem et al., 2023; Li et al., 2008; Verduzco-Navarro et al., 2020).

The performance of adsorbent (carbonaceous materials, biopolymers, etc) by its high adsorption capacity toward heavy metals can no longer be considered a sufficient indicator of efficiency. The difficulty of their separation from the solution after the adsorption operation could make them not practical (Ben Salem et al., 2023; Liang et al., 2021). Recent studies have been devoted to finding efficient separation methods for materials after the adsorption process, leading to the adoption of innovative techniques such as flotation and magnetic separation of adsorbent materials (Boukhalfa et al., 2019; Omer et al., 2023; Rocher et al., 2008). In essence, biochar and alginate materials have been modified to be used as magnetic adsorbents in water. Also, the flotation of alginate as hydrogel beads in water was recorded as an advantage for the adsorption operations (Boukhalfa et al., 2019; Hassan et al., 2021; Ben Salem et al., 2023).

This research aims to tackle environmental issues of valorising abundant materials and subjecting them as practical adsorbents for the effective treatment of heavy metals contaminated water while considering the cost of the operation. Therefore, this work seeks to develop low–cost, efficient hybrid adsorbents based on carbon from natural, environmentally friendly materials for the uptake of heavy metal cations (cadmium and copper) in water media. The biomass used to fabricate biochar is peanut shells. The composite material employed to combine with the biochar is a biopolymer: sodium alginate. The two materials were used then to produce non–magnetic and magnetic beads and test their ability to adsorb cadmium and copper cations from water media.

To delve more deeply into each point discussed in this introduction, the thesis was divided into four subsequent chapters with complete consistency. The first chapter was devoted to establishing the problematic matter of this research and proposing the solutions expected to be reached, defining the different absorbent materials, presenting the properties of the element's cadmium and copper, and their presence in nature. Polluted water with cadmium and copper and

methods of treating them, exploring the techniques of separating and reusing absorbent materials after the adsorption process and their importance were discussed.

The second chapter is interested in the materials and methods used in this work. It was shown how to fabricate materials used to prepare the hybrid adsorbents, along with the explanations provided with detailed drawings, followed directly by the advanced technologies used in characterizing samples and determining their physical and chemical properties. Explaining the adsorption theory in detail and accurately had a large share of this section. All the experiments and the conditions controlling them were presented, including thermodynamics and how to analyse the results obtained with various models for modelling the experimental data. The results of the characterization of different samples using the selected techniques were presented and discussed in the third chapter. In addition, the economic feasibility of the prepared materials was discussed, as well as comparing them with materials used in previous studies.

As for the fourth and final chapter, the enormous part of this thesis examined the effectiveness of the hybrid adsorbents fabricated under different experimental conditions, liquefying a lot of ink. The experimental results were presented and modelled to competently understand the behaviour of the adsorption process toward cadmium and copper ions. Adsorption mechanisms were discussed and supported by logical scientific arguments, and previous studies were used to confirm the findings of our research.

Chapter I
Survey of relevant studies

Chapter I: Survey of relevant studies

I.1. Problematic of the research

The industry is one of the main drivers of the global economy, but it is also a primary source of water pollution. Industrial activities generate large amounts of toxic effluents and waste discharged into waterways and oceans. Heavy metals (cationic and anionic elements) can accumulate in aquatic ecosystems and contaminate drinking water sources, causing considerable effects on human health and the environment. In this context, the issue of water depollution by the industry has become a significant priority to overcome this problem for future generations. Therefore, the question is: what can be done to effectively tackle these challenges and guarantee a sustainable source of clean water?

In Algeria (total area of 2,381,741 km^2), groundwater (281,000 wells with capacity of 6.6 billion m^3) and surface water (8.6 billion m^3 were collected by more than 80 dams) present the primary water resources in the country because of their easy extraction and distribution, and this data (studied years: 2020, 2021, and 2022) is available on the Algeria ministry of hydraulic website (https://www.mh.gov.dz). Nevertheless, these necessary resources are threatened by pollution with several contaminants generated by the different industries and other anthropic human activities (i.e., agricultural activities), where the most dangerous are heavy metals solutions such as chromium, lead, cadmium, and copper (Fares et al., 2021) Therefore, many practical and assessment studies have been conducted to track the locations and quantities of these metals and their ability to threaten the water resources of Algeria (Benmostefa et al., 2022; Fares et al., 2021; Khaled-Khodja et al., 2018; Sahli et al., 2011)

Several techniques for treating water containing different kind of pollutants, including precipitation (Harper & Kingham, 1992), coagulation (Kalaitzidou et al., 2020), oxidation/reduction (Marinho, 2019), ion exchange (Maliou et al., 1992), electrolysis (Isarain-Chávez et al., 2014), and adsorption (Dąbrowski, 2001). Among these processes, selective or non–selective adsorption method can be the right choice for treating large volumes of solutions due to its advantages, including efficiency, low cost, and operational simplicity (Dąbrowski, 2001). The method involves selecting adsorbent materials with high adsorption capacity to capture the targeted substances from the solution.

To date, many studies have been performed to apply adsorption technique on a large scale, and thousands of publications are still being published annually in materials engineering to design practical adsorbents with enormous capacities in the treatment of waste liquids.

Commonly used materials for contaminants adsorption are zeolites (Khalid et al., 2004), clays (MARTIN, 1962), biomasses (Kumar & Wyman, 2008), biochar (Chen et al., 2008), and activated carbon (Kadirvelu et al., 2000), etc. In previous studies, iron oxides (magnetite Fe_3O_4 nanoparticles) and polysaccharide materials (i.e., chitosan, alginate, etc.) have effectively eliminated a huge number of harmful metal ions (cationic and anionic metals) in weak or high concentrations of water solutions (Benettayeb et al., 2017; Zare et al., 2016). Combining these materials under specific modifications (chemical or physical) could enhance their quality. The origin and properties of the used materials often control the success of the combination. Meanwhile, recognizing the target element wanted to be removed from the water is also essential to choose the best materials for the operations.

This chapter aims to identify organic and inorganic adsorbent materials for water treatment, exploring biomass and carbonaceous materials (biochar and activated carbon), their preparation methods, and their properties. Iron oxides (Fe_3O_4 materials), alginate, and alginate–based adsorbents (modified) have been defined, explored, and discussed in details. Cadmium and copper metals were introduced and discussed in their: physical and chemical properties, presence, areas of use, maximum concentration allowed in drinking water, and effect on different fields. Different scholar studies in the removing of copper and cadmium from solutions are also cited and examined. Finally, the available methods and the easiest technologies for separating and reusing the different adsorbents in new tests when the adsorption process is completed were also taken as an important part of the current research.

This section allowed us to trace the path of the research problem point by point to achieve the purpose of the study, which is to prepare two different hybrid (composite) carbon–based adsorbents for heavy metals uptake (cadmium and copper): biochar/alginate bead and magnetic–biochar/alginate bead. Peanut shells waste was used to produce the initial biochar and then for the synthesis of magnetic–biochar. Sodium alginate beads were used to fill the biochars in them. The research endeavours to contribute to a cleaner, more sustainable future where industries harmonize with the environment, rather than being at odds with it.

I.2. Adsorbents

I.2.1. General

The term "adsorbent" involves all organic or inorganic materials used for the adsorption of pollutants, while the prefix "bio" in "bioadsorbent" is its extension refers to biological materials capable to do the same operation. Therefore, the term "bioadsorbent" refers to sustainable (green) materials used to remove organic or inorganic pollutants, such as pesticides, organic compounds, heavy metals (also known as trace metal elements TMEs), by binding them to the surface of the adsorbent through their adsorption properties (Bilal et al., 2013; Kyzas & Kostoglou, 2014). These bioadsorbents can be prepared from various sources, including animal–origin waste, plant materials, food waste, organic materials produced by microorganisms (bacteria, fungi, and algae), and synthetic materials of natural origin (Berndes et al., 2003). Consequently, they are sometimes also referred to as biomass (Berndes et al., 2003).

Over the years, biomaterials have undergone continuous improvements and developments to become more efficient and cost–effective. Changes introduced include chemical treatment or carbonization to produce carbonaceous materials such as biochar and activated carbon. Additionally, combining these biomaterials with organic or inorganic materials (i.e., oxide materials) allows the production of effective composite materials (hybrid) for various purposes.

I.2.2. Adsorbent selection criteria

Selecting the adsorbent in wide industrial–scale applications hinge on its quality. The adsorbent subjected to a specific desired component should involve striking a balance between some criteria (Sakhiya et al., 2022; Wang & Wang, 2019b):

- Abundance and preferably biodegradable.
- High adsorption capacity for the target molecule.
- Large surface area with well–defined pores.
- Stability under operational conditions.
- Favourable kinetics, mechanical strength, and ease of handling.
- Selectivity to avoid adsorbing other compounds.
- Efficient regeneration and cost–effectiveness.
- Minimal environmental impact.

I.2.3. Lignocellulosic materials

Lignocellulosic materials are composed of lignin, hemicellulose, and cellulose in varying proportions depending on the properties of the raw material. They are highly present in plants, such as roots, stems, leaves, bark, fruit peels, and shells. Cellulose forms as a crystalline homopolymer of glucose through β–1,4–glycosidic linkages, strengthened by hydrogen bonds. Hemicellulose, on the other hand, is a heteropolymer composed of various sugars like xylose, glucose, and mannose, connected by β–1,4–glycosidic bonds, often featuring acetyl, feruloyl, and glucuronyl groups. Lignin, a three–dimensional polymer of aromatic compounds, is covalently bonded to xylans in hardwoods and galactoglucomannan in softwoods (Sud et al., 2008).

According to Yang et al., (2007), lignocellulosic materials contain different functional groups, such as carboxyl, hydroxyl, methyl, and phenyl groups, which play a crucial role in the physicochemical properties of these materials. These functional groups can influence chemical reactivity, hydrophilicity, and the ability to bond with other materials.

Commonly, evaluation and valorisation of agricultural waste have been studied in many projects for different objectives and the most important one is to discover these materials for effluent treatment. Because of their properties, they are directly used, modified or transformed into carbonaceous materials (i.e., activated carbon, biochar, and hydrochar etc.).

For example, Hameed & Ahmad, (2009) clarified a simple protocol for treating garlic peel (100–300 μm) with distilled water and boiling it (for 30 min) before being used in the dried state for methylene blue adsorption experiments and this method of the biomass preparation obtained from the waste agricultural was also used elsewhere (Garg et al., 2008).

Washing the biomass particles with water (i.e., distilled water, deionized water, pure water etc.) is commonly used to remove any impurity. In essence, biomass could be treated with acidic or basic solutions to ensure the uptake of all undesirable elements from the surface of the subjected materials and also for the activation.

Horsfall & Abia, (2003) published a paper on the activation of biomass for cadmium and zinc removal wherein the first step, they treated biomass derived from cassava waste with thioglycolic acid ($C_2H_4O_2S$) and then used the nitric acid (HNO_3) for the activation step, followed by washing with distilled water.

The chemical polymerization technique of biomass orange peel waste as the based–adsorbent was studied by Feng et al., (2009), where the chemical modification required a specific protocol based on the mixing of the biomass materials with solutions of: saturated calcium hydroxide $Ca(OH)_2$ (1) and sodium hydroxide (NaOH) (2), respecting the mass/volume criteria. The protocol was followed by using HNO_3, ceric ammonium nitrate ($H_8N_8CeO_{18}$), and methyl acrylate ($C_4H_6O_2$) to reach the polymerization state.

On the other hand, the statistical data provided by the (*ASISD*) Agricultural Statistics and Information Systems Directorate (*Ministry of Agriculture in Algeria*) indicates that peanut production at the national level in 2018 was 118,861 quintals over an area of 4,753 hectares. However, a 6% increase in production is estimated at 126,022 quintals by an increase in the cultivated area by only 133 hectares in 2019, with the El Oued region accounting for 70% of the total production (Table I.1).

Table I.1. Summary of areas, productions, yields and growth rates 2019/2018 for peanuts provided by the *Algerian Ministry of Agriculture*.

	Total area (Hectare)	**Total production (Quintals)**	**Yield (Quintals / Hectare)**
Year 2018	4,753	118, 861	25
Year 2019	4,886	126, 022	25.8
Rate of increase (%) (2018/2019)	3	6	3

What is interesting is that most peanut shell residues are still discarded, could pose a pollution to the environment. These residues hold enormous potential for environmental and economic valorisation by avoiding the waste of this resource. Potential applications include the production of construction materials (Ryłko-Polak et al., 2022), organic fertilizers (Hussain et al., 2021), bioenergy (Berndes et al., 2003), and even water purification materials (Bhatnagar et al., 2015). Therefore, it is important to continue exploring the various possible uses of these residues. One significant application of these residues is the adsorption of pollutants in aqueous solutions, where peanut shells can even be transformed into biochar or modified biochar (such as biochar composites) for the same purpose.

I.2.4. Carbon materials

I.2.4.1. General

The use of carbonaceous materials as the main adsorbents in water treatment is due to their effectiveness, low preparation cost, environmental friendliness, and the ability to produce them from abundant and renewable sources. Residues and waste from agricultural activities, resulting from anthropic activity, are rich in carbon and the most commonly used to fabricate carbonaceous materials such as biochar and activated carbon.

Concerning polluted water treatment, activated carbon is regarded to be perhaps more effective than biochar due to its physical or chemical activation. Indeed, the relevance of this comparison also depends on the types of contaminants and precursors present. Discussing cost, activated carbon prices are often higher than those of biochar because of the additional expense of activation required in its production. Moreover, chemical activation can lead to the release of toxic chemicals into the environment after the disposal of activated materials at the end of each water treatment operation. For these reasons, researchers are working to propose new alternative adsorbents like carbon–based adsorbents.

I.2.4.2. Activated carbon

Activated carbon (AC) has a long history in different anthropic activities (i.e., pharmaceutical, environmental, and industrial applications), and its exact origin is unclear (González-García, 2018). Despite this mystery, it remains a valuable resource due to its effectiveness and versatility in modern times. The preparation of activated charcoal from the pyrolysis of biomass that is often derived from agricultural waste as a raw material is followed by a physical (could up to 1100°C) or chemical activation to increase its specific surface area and adsorption capacity, resulting in a final product that is more porous and active (González-García, 2018; Heidarinejad et al., 2020). According to González-García, (2018), physical activation involves exposing the obtained charcoal to a stream of oxidizing gas, such as air (N_2) or CO_2, at high temperatures for 1 to 2 hours. On the other hand, chemical activation involves mixing the charcoal with strong oxidants like $ZnCl_2$, H_3PO_4, KOH and K_2CO_3, and heating it to high temperatures ranging from 400°C to 900°C. However, a hybrid process consisting of physical and chemical methods can be utilized as a two–step process.

AC exists in various forms, with the most common ones being powder (with particle diameters ranging from 1 to 100 µm) and granules (with grain sizes larger than 1 mm). It can also be found in solid blocks or carbon fibre forms. According to a study by Heidarinejad et al., (2020), activated carbon exhibits a porous volume ranging between 0.20 and 0.60 cm^3/g with the potential to reach up to 1 cm^3/g. The specific surface area of AC typically falls within the range of 800 to 1500 m^2/g. However, with specific activation methods, it can exceed an impressive 3400 m^2/g.

Generally, ACs are fabricated from organic compound, such as wood, coconut, coal, and lignin. The percentage of carbon content in these biomass materials is between 40 and 90%, while its density varies from 0.4 to 1.45 g/m^3 (Heidarinejad et al., 2020). Activated carbon is formed of carbon atoms arranged in graphite–like sheets that are then assembled into a granular or monolithic structure. This structure is permeated by pores ranging from a few Angstroms and tens of nanometres in diameter, as illustrated in Fig. I.1a. Its porous structure (micro–, meso–, and macropores) allows for a significant contact surface area with external substances (Fig. I.1b).

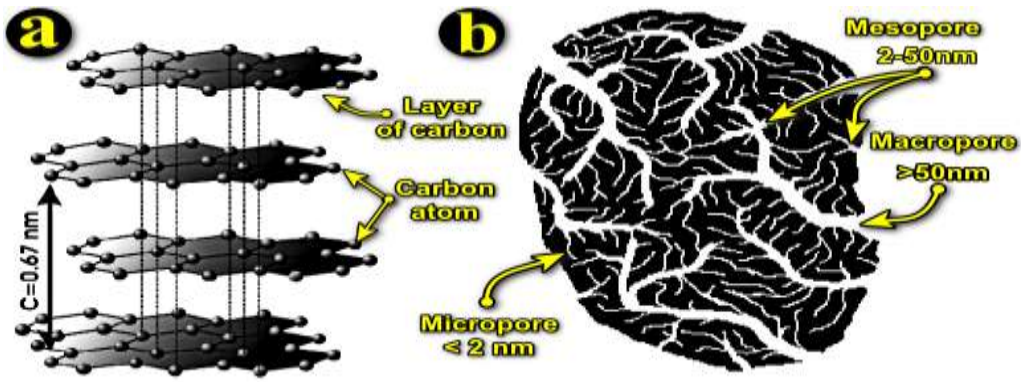

Fig. I.1. Graphitic structure of activated carbon (**a**) and (**b**) schematic presentation of pore size.

Functional groups and atoms like oxygen (O), hydrogen (H), sulphur (S), and nitrogen (N) are typically found in AC in a chemically bonded form to its structure. Among the main functional groups responsible for capturing pollutants in the carbon structure are carboxyl, carbonyl, phenols, lactones, and quinones (Bhatnagar et al., 2013). These groups on the carbon surface come primarily from the activation process, precursor origin, thermal treatment, and post–chemical treatment. To enhance the efficacy of activated carbon for specific contaminant removal purposes, the nature and concentration of surface functional groups can be modified through appropriate thermal or chemical treatments (Bhatnagar et al., 2013; Heidarinejad et al., 2020).

Bouchelta et al., (2008) used nitrogen (N_2) gas with water vapor H_2O (vapor steam) to produce different activated carbons from date stones (at 500, 600, 700, and 800°C). The authors compared between the produced materials in the S_{BET} (surface area; cm^2/g) and V_{Total} (total volume of pores; cm^3/g) obtaining the results: $50 \leq S_{BET} \leq 635$, and $0.20 \leq V_{Total} \leq 0.716$. Furthermore, a previous study performed by Yang & Lua, (2003) employed the physical activation (under N_2 gas) for the production of activated materials at different temperature using pistachio nutshells, and the highest parameters of the surface area reached 1064.2 cm^2/g and total pore volume 0.23 cm^3/g.

Zhao et al., (2017) obtained activated charcoal (S_{BET} and V_{Total} were 1028.88 cm^2/g 0.5378 cm^3/g, respectively) by pre–treating corn straw residues with phosphoric acid (H_3PO_4) before subjecting them to pyrolysis at 300°C. The initial steps of the reaction between H_3PO_4 and lignocellulose primarily involve the acid's reaction with lignin and hemicellulose due to their weaker bonds. Cellulose, being highly resistant, undergoes hydrolysis more slowly as the reaction progresses (Deng et al., 2023). AL-Othman et al., (2012) have also prepared activated charcoal using peanut shells and performed chemical activation with potassium hydroxide (KOH). The material was produced in a nitrogen atmosphere before being heated in the air at a temperature of 450°C to oxidize the charcoal. The S_{BET} was calculated to be 133.31 cm^2/g while the V_{Total} was 0.35 cm^3/g. The formation of cavities within activated carbon occurs due to the evaporation of KOH from sites it previously occupied as an activator (Njoku et al., 2013).

I.2.4.3. Biochar: an alternative material to AC

To promote environmental sustainability and reduce waste, it is crucial to consider the production of biochar from biomass waste. Opting for biochar production using suitable biomass waste materials like crop residues, fields and processing leftovers such as shells can greatly contribute to the conservation of our natural resources.

Till now, researchers have focused on the benefit of biochar in many scale applications, such as fuel, soil improvement, and climate–related subjects. Additionally, biochar has also shown potential in water remediation (Dai et al., 2019). Biochar is typically produced from agricultural biomass which is one of the most abundant sources of renewable resources. Agricultural biomass includes vegetable residues (Pradhan et al., 2020), wood (Shaheen et al., 2019), and animal bones and dung (Chen et al., 2022; Um-e-Laila et al., 2021) (Fig. I.2).

Biochar is carbon–rich material (carbon % ranging from 50 to 93) produced from biomaterial (so–called biomass) that undergoes a high–temperature thermal treatment, typically starting at 200°C and may require temperatures up to 900°C under specific conditions, such as oxygen (O_2) limitation (levels below 0.5%), N_2 atmosphere, or vacuum conditions (Alhashimi & Aktas, 2017; Weber & Quicker, 2018).

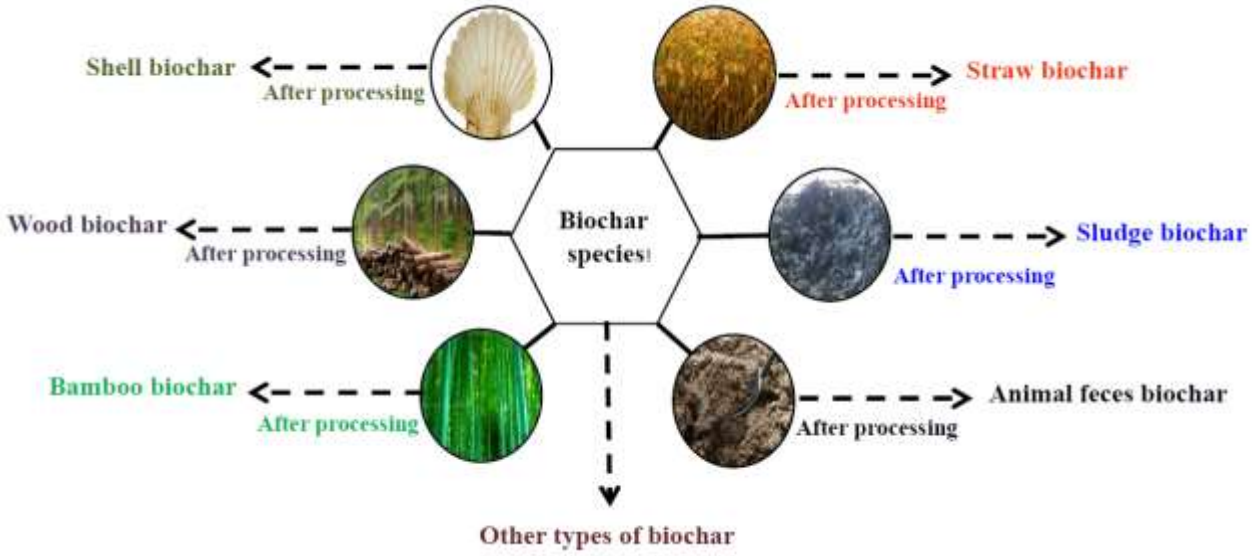

Fig. I.2. The principal origin and classes of biochar (Dai et al., 2019).

Biochar, while porous, does not undergo a physical or chemical activation process like AC, resulting in variations in its properties. However, biochar can be modified (Mahdi et al., 2019), subjected to hydrothermal–treatment (Nouioua et al., 2023) , or used directly to reduce costs resulting from its treatment operations (Chahinez et al., 2020). According to Ambaye et al., (2021), the physicochemical properties of biochar can be affected by various factors, such as the nature of the raw material and the substrate size. Other parameters like the type of pyrolysis (slow, fast, or flash), temperature, heating rate, and pyrolysis duration can also play a vital role in the final quality and the elemental composition (i.e., C, N, K, and Ca) of the produced biochar (Dai et al., 2019).

In essence, biochar contains several functional groups on the surface, including hydroxyl, methylate, carbonyl, and carboxyl. Its structure is influenced by various factors, including high carbon content, aromatic functional groups containing oxygen, and high porosity. Biochar has a stable molecular structure and a large surface area that facilitates the adsorption of pollutants present in the environment (Ahmad et al., 2014).

In many studies, non–modified biochars have been prepared from plant residue sources at different specific temperature of heating, such as palm petiole pyrolyzed at 700°C of 640 m^2/g from BET method calculations S_{BET} and V_t of 0.403 cm^3/g (Chahinez et al., 2020), peanut shells at 300, 500, and 700°C with S_{BET} = 0.890, 58, and 376 m^2/g, and V_{Total} = 0.0058, 0.053, and 0.23 cm^3/g, respectively (Wang et al., 2019).

As known, the temperature of pyrolysis is affected the textural properties and the feedstock of the produced biochar. For example, Gai et al., (2014) have fabricated many biochars from waste: wheat straw (1), corn straw (2), and peanut shells (3), at different temperature of heating: 400, 500, 600, and 700°C, where their textural characteristics changed (S_{BET} = 3 to 185 to m^2/g; V_{Total} = 0.006 to 0.110 cm^3/g). A similar study performed by Hadj-Otmane et al., (2022), where the surface area of the waste petiole obtained from date palm and heated at different temperature (500, 600, and 800°C) was varied from 200.27 to 767.44 m^2/g. The same observation was recorded for the total pore volume parameter, where was affected and changed (0.15 to 0.53 cm^3/g). It can conclude from the past studies that the choice of the pyrolysis temperature is an important key factor in the production of biochars, and it affects the textural parameters and also the morphology of the feedstock transformed to carbon materials, and this factor play a vital role for the choice of the best biomass precursor for the carbonization.

On the other hand, many researchers have used water (i.e., distilled water) and chemical solutions of different reagent materials to wash and activate the resulting biochar product. The chemical treatment allows for the avoidance of the presence of impurities from the material surface. The most common reagents utilized for this operation are hydrochloric acid (HCl), sodium hydroxide (NaOH), sulfuric acid (H_2SO_4) and phosphoric acid (H_3PO_4) solutions. Often, the final step of this chemical treatment ends with washing the adsorbent with water.

In support of this, Vo et al., (2019) used HCl to wash the final biochar produced from tectona grandis tree sawdust in their study. Li et al., (2017), in their experiments used NaOH to treat rape straw biochar, H_3PO_4 for treatment corchorus capsularis L derived biochar (Chen et al., 2020), and rice straw biochar treated with H_2SO_4 (Yakout et al., 2015). However, treating the initial biochar with different chemicals or by physical activation can be a valuable strategy to activate its sites, change its surface properties, and improve its suitability for diverse contaminant adsorption.

Like AC, the properties of biochar can be modified using various methods: acid (Rajapaksha et al., 2016) or alkalinity (1) (Wang et al., 2015), oxidizing agents (2) (Huff & Lee, 2016), metal– salt and oxide (3) (Wang & Wang, 2019a) and steam and gas purging (4) (Wang & Wang, 2019a). In general, the selection of the activation method of biochar depends on its environmental application. When it comes to the water treatment field, this also will depend on the target contaminant. Organic and inorganic compounds are different to be effectively removed from water. Hence, choosing the activation method is required to ensure the efficiency of the process. The possible methods of biochar activation are depicted in Fig. I.3.

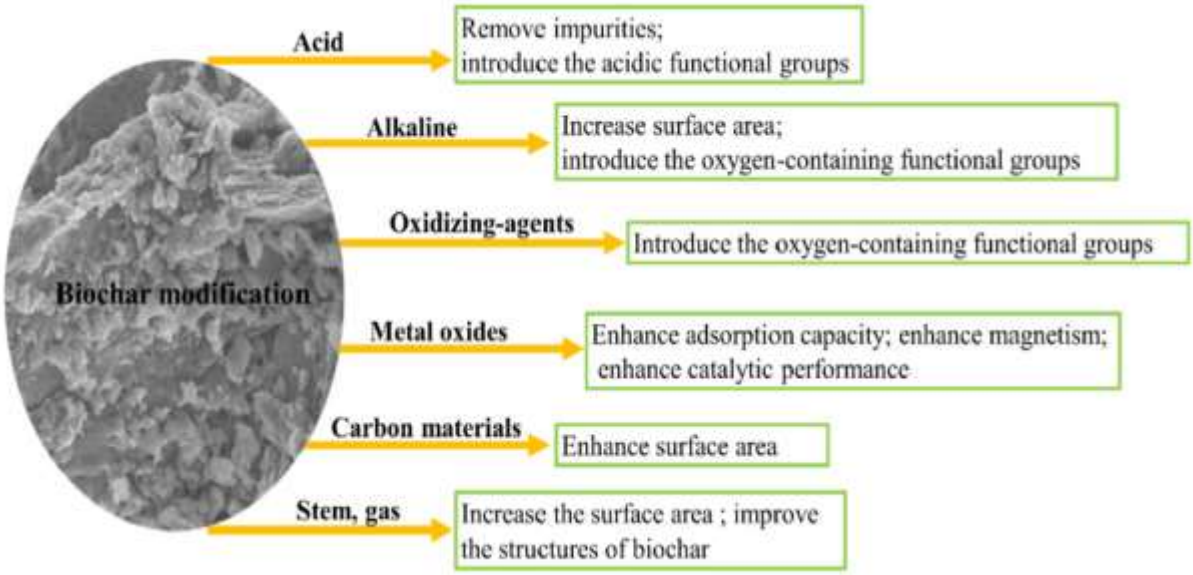

Fig. I.3. The possible methods for the modification of biochar (Wang & Wang, 2019a).

I.2.4.4. Comparison between non–modified biochar and activated carbon

In general, the comparison between materials is usually based on certain aspects, but when it comes to comparing AC and biochar this is sometimes difficult. Although biochar is frequently mentioned in literature as the supposed alternative to several adsorbents, AC is prevalent for its effectiveness. Unlike physical activation, the chemical differences between biochar and activated carbon influence their adsorption capacities, making activated carbon more effective at removing specific contaminants due to its altered chemical structure. However, this activation makes AC very expensive, and its residual concentration of chemicals could not be eco–friendly. Table I.2 briefly shows a comparison between initial biochar and activated carbon from different aspects.

Table I.2. Comparison between non–modified biochar and activated carbon (González-García, 2018).

Aspect	Biochar (based)	Activated carbon
Origin (source)	Organic materials	Organic materials
Production	-Thermal decomposition -No activation	-Thermal decomposition -Chemical or physical activation -Modification
Porosity and surface area	-Lower specific surface area -Varied porous structure and depends on feedstock and pyrolysis conditions	-High surface area and a well-developed pore structure
Adsorption capacity	Acceptable adsorption capabilities	Renowned by its high adsorption capacity
Environmental impact	-Low energy for production -Safe and potential for capable for environmental issues	-Energy-intensive in the production processes -Chemical activation could be not safe
Cost of production	Low cost (not expensive)	Expensive, especially for chemical activation
Regeneration	Capable	Capable

I.2.5. Magnetite nano–sized materials (Fe_3O_4)

Iron oxides were widely recognized and vastly studied magnetic materials, where the knowledgeable forms include zero–valent iron (nanoscale ZVI), hematite materials (α–Fe_2O_3), magnetite particles of Fe_3O_4, and another form derived from magnetite: maghemite (γ–Fe_2O_3).

This thesis is focused on the characteristic of magnetite (Fe_3O_4 nanoparticles) and its application as a part of the research. Magnetite has a deep black colour and a polymorph compound with an inverse spinel structure, wherein the crystalline lattice carries Fe^{2+} ions. Its chemical formula is represented as $[Fe^{3+}]_A[Fe^{2+}Fe^{3+}]_BO_4$. Ferrous ions (Fe^{2+}) inhabit octahedral sites, while ferric ions (Fe^{3+}) manifest in octahedral and tetrahedral sites (Fig. I.4). This remarkable mineral adopts an Fd3m crystalline structure of the cubic system, with its lattice parameter established as a = 8.396 Å. Each fundamental unit cell assembles 8 Fe^{2+} atoms, 16 Fe^{3+} atoms, and 32 O_2 atoms.

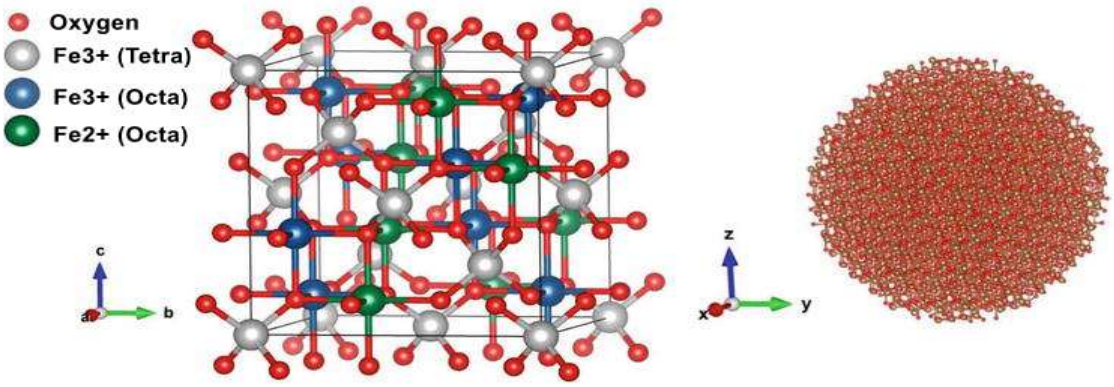

Fig. I.4. The crystal structure of magnetite (Fe_3O_4) (Fouad et al., 2020)

Magnetite, Fe_3O_4, is a mineral with unique properties. It has a cubic crystal structure, a density of 5.18 g/cm^3 and a hardness level of 5.5. Its melting point falls between 1583 and 1597°C, while its boiling point is 2623°C. Magnetite is characterized by its deep black colour and displays ferrimagnetic behaviour. It has a Curie temperature of 580 K and a magnetic susceptibility (Ms) ranging from 92 to 100 A·m^2/kg at 300 K. In nanoparticle form, it exhibits superparamagnetic properties. It appears opaque with a metallic lustre and has an isometric crystal system with no birefringence. It has a refractive index value of n = 2.42, which contributes to its optical characteristics (Dudchenko et al., 2022).

According to Wei et al., (2012), nanoparticles have excellent physical and chemical properties compared to atomic or bulky counterparts because of different decisive factors, such as the related surface, mesoscopic physic, small entity, and quantum size. In fact, Fe_3O_4 nanoparticles can be easily synthesized due to its abundance and low operational costs. Therefore, scientists use different physical and chemical methods to fabricate magnetic nanoparticles (MNPs) for diverse scale applications. To ensure that MNPs are in the right size and shape and safe for use, researchers utilise techniques such as thermal decomposition (1), ball milling (2), hydrothermal (3), co–precipitation (4), sol–gel (5), microemulsion (6) and biological (7) (Fig. I.5). Among the mentioned techniques, the co–precipitation of Fe^{2+} and Fe^{3+} ions in a basic solution remains one of the most commonly used methods for synthesis (particle size < 20 nm with a super–magnetic). Intermediate states can arise through the partial oxidation of Fe^{2+} ions into Fe^{3+} ions (temporary stages in the overall transformation) (Boukhalfa, 2019).

Furthermore, Wei et al., (2012) in their work utilized the co–precipitation method and selected analytical reagents ($FeCl_3$, $FeCl_2$, NaOH and C_2H_6O) to synthesize Fe_3O_4 nanoparticles

at different temperatures (40 and 80). They went through the investigation of their magnetic properties, crystal structure, and morphology. In brief, they conclude that the modification in the proportion of the material used for the preparation affected a little on the crystalline structure of the magnetite particles. The superparamagnetic of the prepared sample were varied from 50.6 to 55.4 emμ/g while the bulk of Fe_3O_4 was very high (90 emμ/g).

In another study, Hariani et al., (2013) mentioned in their study that the chemical co–precipitation technique is easy and has a successful rate of 96 and 99.9% for Fe_3O_4 synthesis. The researchers applied N_2 gas, $FeCl_3$ and $FeCl_2$ in the co–precipitation process (at 70°C) of Fe_3O_4 particles with diameter ranging between 5 and 20 nm and superparamagnetic (89.46 emμ/g). In another study, Wu et al., (2011) fabricated superparamagnetic Fe_3O_4 particles (74.86 emu/g) with a 15 nm diameter using $FeSO_4$, $FeCl_3$ and d $C_{12}H_{25}OSO_3Na$, based on ultrasonic–assisted co–precipitation techniques (at 65°C). In general, magnetite nanoparticles (Fe_3O_4) have versatile applications in biomedicine, environmental remediation, electronics, energy storage, construction materials, agriculture, and smart textiles (Ali et al., 2021; Dudchenko et al., 2022; Petrov & Chubarov, 2022).

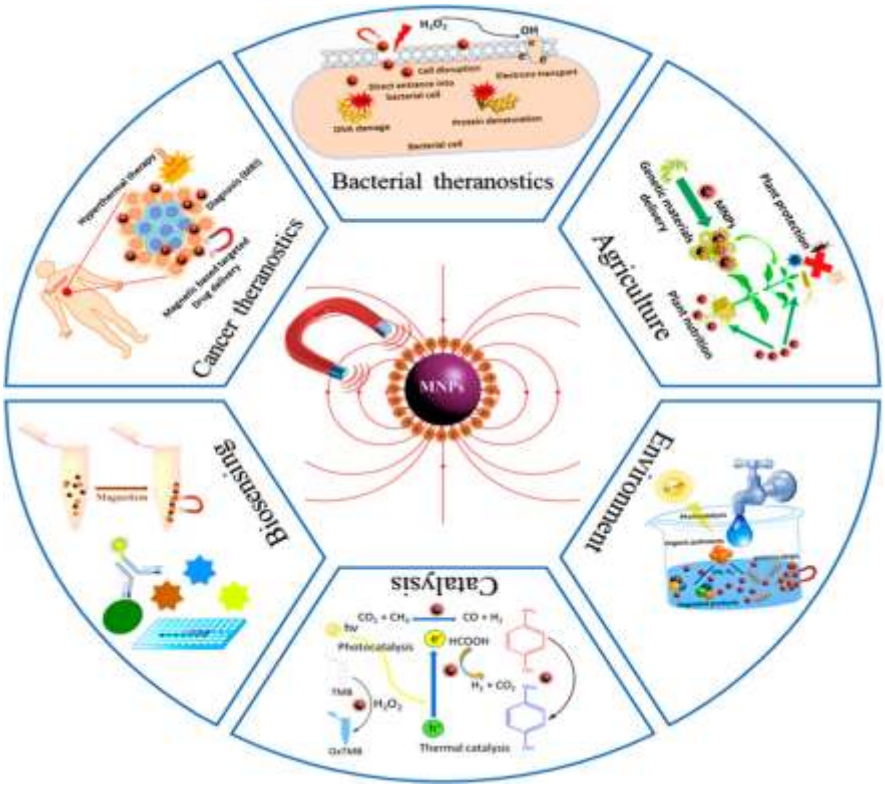

Fig. I.5. Different applications of the magnetic nanoparticles (Fe_3O_4) (Ali et al., 2021).

By delving into the field of water treatment, magnetic Fe_3O_4 nanoparticles have a high adsorption capacity and were used to capture anionic metals: chromium (VI) (Zhao et al., 2010) and phosphate (Wang et al., 2015), and cationic metals: copper (Yang et al., 2018) and cadmium (Kataria & Garg, 2018) due to their large specific surface area and surface polarity, making them potentially useful for water treatment applications aimed at decontaminating water.

I.2.6. Sodium alginate

I.2.6.1. General

One of the materials whose name is associated with bioadsorbents in the field of water purification is among the most versatile biopolymers, alginates. These are biodegradable anionic polysaccharides primarily produced from brown algae such as *Laminaria*, *Macrocystis*, and several other species.

Historically, the English researcher Edward Charles Cortis Stanford was the first chemist to conduct initial experiments on extracting alginic acid from brown algae, and his discovery was patented on January 12, 1881. Subsequently, most commercial alginates were developed in the United States in the 1920s and 1930s. Today, there are several salts of alginic acid, but the most well–known are calcium alginate (CA) and sodium alginate (SA).

Alginates are also used in a variety of applications, such as the production of food products, pharmaceuticals, cosmetics, industrial products, and also in water treatment applications. SA is abundant, biodegradable, and highly versatile due to its ability to associate with other components and retain them. It has a significant capacity to bind inorganic pollutants, mainly heavy metal cations, because of its numerous free hydroxyl and carboxyl groups. However, while sodium alginate serves its purpose effectively in various applications, it does exhibit certain limitations in terms of mechanical properties, stability, and heat tolerance (Wang, et al., 2020).

According to Fig. I.6, the polysaccharide is a linear binary copolymer composed of two types: acid residues linked together by glycosidic bonds of the β–(1–4) and α–(1–4) types. These residues, namely β–D–mannuronic acid (M) and α–L–guluronic acid (G), are spontaneously distributed in blocks of repetitive M residues (MM blocks), blocks of repetitive G residues (GG blocks), and blocks of mixed M and G residues (MG blocks) (Wang et al., 2019).

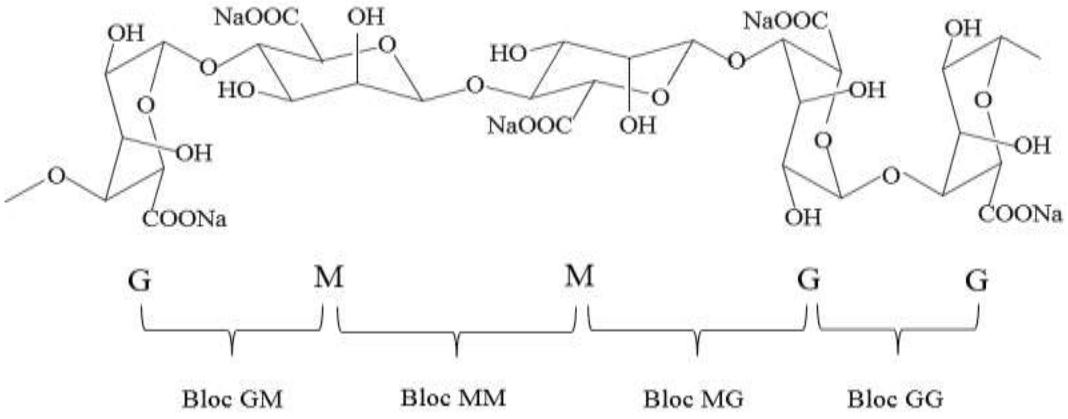

Fig. I.6. Molecular structure of Na–alginate (SA).

I.2.6.2. Solubility and gelling

Sodium alginate is a soft and water–soluble substance. Its solubility is influenced by several factors, such as the pH of solvent, the ionic strength of the medium, and the presence of ions (Pawar & Edgar, 2012). To dissolve alginate, the pH of the solvent must be higher than a critical value, and the carboxylic acid groups must be deprotonated. The ionic strength of the medium significantly influences the solubility of a solution, along with several other critical properties, including viscosity, chain extension, and polymer conformation. It is essential to use a solvent free of cross–linking ions to ensure proper dissolution (Aichour, 2019). A gelation method proposed for this study is called the ionotropic method, where the gelation of sodium alginate is easily formed in the presence of multivalent cations such as Ba^{2+}, Sr^{2+}, Fe^{2+}, Ca^{2+} (divalent cations), or Al^{3+} and Fe^{3+} (trivalent cations). In the case of the most commonly used divalent cation, Ca^{2+}, gel formation is induced by interactions between the G blocks, which associate to form closely held junctions until saturation of available sites (Boukhalfa, 2019).

Additionally, the MG blocks also participate, forming weaker junctions. Thus, high G content alginates form regions of rigid junctions, resulting in more resistant gels. The ionotropic gelation mechanism can be schematically presented as an "egg–box" model of an alginate hydrogel in the presence of calcium ions as described in Fig. I.7 (Aichour, 2019; Boukhalfa et al., 2019).

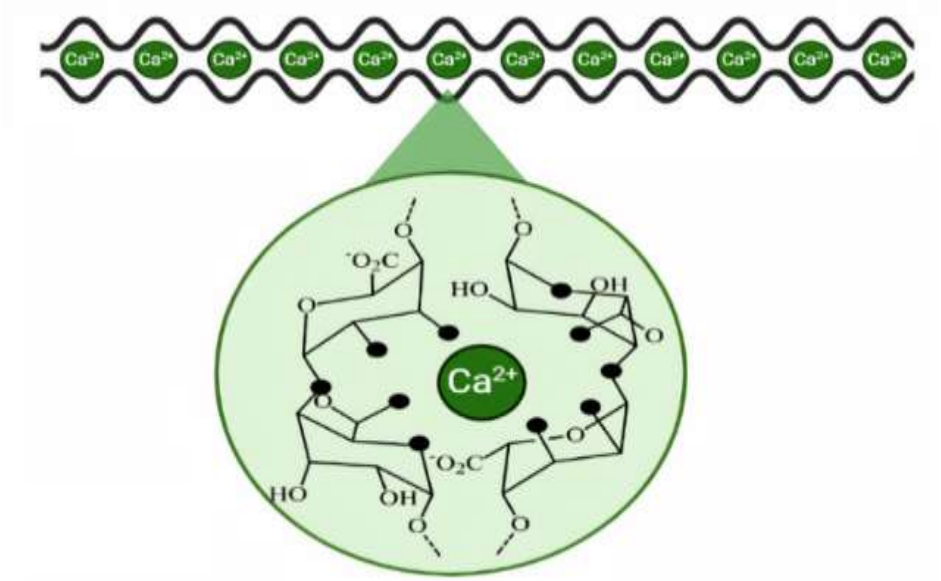

Fig. I.7. Formation of alginate hydrogel matrix egg–box–like (Aichour, 2019).

I.2.6.3. Encapsulation: principal and techniques

Based on the properties of sodium alginate mentioned before, commixing or encapsulating adsorbents in a polymer matrix allows the combination of adsorbents to prepare a new composite material, adsorbent/biopolymer. The encapsulation in water treatment aims to offer significant adsorption sites and a high affinity for the target molecules in the solution. The effectiveness of the composite material comes not only from the encapsulated adsorbent but also from the active sites of the alginate polymer matrix.

The development, structuring control, and shape of the alginate capsules or beads depend on the properties of the alginate used in the preparation, the nature and origin of the combined adsorbent, the cross–linking agent, and the encapsulation and gelation method. These beads are easy to separate and regenerate, reducing the cost of the process. Different encapsulation techniques have been developed for the preparation of alginate beads. The most common ones are synthesis by extrusion, gelation by aerosol, and synthesis by emulsion, and these methods are mechanical processes (Aichour, 2019; Boukhalfa, 2019).

Extrusion is a method based on introducing a solution of alginate salt or alginate combined with an adsorbent drop by drop into the cross–linking bath using a syringe (Rocher et al., 2008).

The rapid reaction between alginate and the cross–linking agent on the surface solidifies the spherical shape of the drops within the solution. Subsequently, the internal volume of these drops gelifies when the cross–linking agent diffuses through the surface of the forming beads.

The aerosol gelation technique relies on the micrometric spraying of an alginate salt solution using an electro–spray towards a cross–linking solution to solidify the shape and size of the formed droplets (Serp et al., 2000).

According to Zhao et al., (2007), the emulsion method involves introducing a calcium–bound alginate solution, which is then emulsified in oil. The release of Ca^{2+} ions by lowering the pH allows the gelation of the alginate droplets. Although this method allows for large–scale production, it has the disadvantage of less homogeneous droplet size distribution.

I.2.5.4. Encapsulation in previous studies

Numerous studies focused on the preparation of composites or the fabrication of beads, having different types, natures and origins. They were based on diverse methods and protocols of manufacturing, which eventually resulted in the successful design and excellent efficacy of the resulting materials.

For example, Andreas et al., (2021) published an interesting scientific paper for those interested in the development of new composite materials, such as hydrogel beads and their applications. The researchers used 3% of $CaCl_2$ bath (gelation solution) and 3% of alginate powder in 100 mL of several solutions containing different compounds to produce different types of beads, including a solution containing extracted fresh red cabbage. In their laboratory experiments, the researchers relied on the help of a micropipette of a specific diameter. The results showed that the diameter of the obtained spherical beads in wet form (4.7 – 6.11 mm contained 98% of water) extended when the pH of the used solution (3 – 11) increased. The prepared materials were used to remove methylene blue.

Other studies concerned with methylene blue removal were performed by Aichour et al., (2019), Boukhalfa et al., (2019), Oussalah et al., (2019) in the same laboratory at Setif university, using the same protocol (2% (w/v) of alginate solution dropped to 4% $CaCl_2$ bath) to prepare effective composite beads from biomaterials citrus peel, bentonite, and carbon nanotubes,

respectively. They successfully controlled the preparation of hard beads containing different proportions (ratios) of the materials involved in their protocol.

On the other hand, alginate–based modified or non–biochar beads have gained attention in the water remediation field and have been reported in many studies: using alginate/water hyacinth biochar beads to treat cadmium solutions (Liu et al., 2020), subjecting alginate/ modified biochar for copper recovery from water (Xiao et al., 2019), and effective adsorption of copper ions by alginate/biochar derived from pitch pine (Park et al., 2022). Their unique combination of alginate and biochar (carbon–rich material) properties holds the potential to address challenges in pollutant removal from solutions (i.e., heavy metals).

There is no doubt that the use of composite beads is very typical in the field of contaminated water treatment. Although it is very applicable in several respects, the most essential is their ease of separation from liquids. Nevertheless, magnetic beads cannot be overlooked as they are essentially a development of simple beads. They have taken an enormous part of the existing literature and confirmed their efficacy and superiority in many studies.

For example, Metin et al., (2020) and Boukhalfa et al., (2019) published excellent papers on the fabrication of magnetic beads. They operated a similar experiment to prepare magnetic materials using iron (III) ($FeCl_3$) solution at 90°C. A previous study was achieved by (Yu et al., 2017a), where the authors used $FeCl_3$ and $FeSO_4$ to synthesize Fe_3O_4 particles in modified biochar by co–precipitation method. The resulting materials were dropped then in alginate beads and used to treat copper solutions.

A composite of organic and inorganic materials combination: magnetic bentonite (1) and carboxymethyl chitosan (2), have been used to produce beads based on alginate hydrogel in a study (for copper adsorption) conducted by Zhang et al., (2019). By focusing on the magnetic nanoparticles, their experiments involved using $FeCl_3$ and $FeCl_2$ chemicals to synthesize Fe_3O_4 in bentonite materials. The authors optimize a vital study on the formulation of the magnetic beads by varying the mass ratio (%) of the combined materials six (6) times which enhanced the removal rate (%) from 74 to 94.

I.3. Adsorbates: Cadmium and copper

I.3.1. General

The term "adsorbate" refers to the substance that is retained on the surface of an adsorbent through the process of adsorption. In other words, it is the molecule, particle, or ion that is captured by the adsorbent during this reaction.

Heavy metals can be considered adsorbates due to their properties of being adsorbed by various surfaces such as soils, biomasses, and carbonaceous materials. Heavy metals like lead, zinc, copper, and cadmium, when present in high concentrations, can be dangerous to the environment and human health, causing irreversible damage.

Cadmium and copper are two trace metal elements (TME) naturally present in the crust of the ground. They are formed through complex geological processes such as rock metamorphism, volcanic eruptions, sedimentary deposits, and hydrothermal processes.

Although the presence of cadmium and copper is relatively low in the natural environment, their levels can increase due to anthropogenic activities such as mining, fuel industry, and agricultural applications, as well as air pollution caused by industrial activities and motor vehicle emissions. However, copper is an abundant metal widely used, whereas cadmium is rarer and often associated with zinc deposits.

I.3.2. Cadmium

I.3.2.1. Physico–chemical characterization of cadmium

Cadmium (Cd) is a silvery–white metal belonging to the zinc family with atomic number 48. It is characterized chemically by an electron configuration of [Kr] 4d10 5s2 and an atomic mass of 112.411 g/mol. Its density is 8.65 g/cm^3, with a melting point of 321 °C, and a boiling point of 765 °C. It is also a suitable electrical and thermal conductor but relatively weaker when compared to other metals. Cadmium has several stable isotopes, with the most common ones being ^{112}Cd (0.89%), ^{113}Cd (11.14%), ^{114}Cd (22.96%), and ^{116}Cd (24.13%).

According to (Ford et al., 2007), cadmium can exist in various crystalline forms, including cadmium sulphide (CdS), cadmium oxide (CdO), cadmium carbonate ($CdCO_3$), cadmium nitrate

($Cd(NO_3)_2$), cadmium chloride ($CdCl_2$), and cadmium stannate (CdSn). The pH can influence the chemical form of cadmium present in a medium.

Depending on its value, cadmium can be found in different forms. When the pH is below 5.0, cadmium is present as Cd^{2+} ions. If the pH is between 5.0 and 7.0, it exists as cadmium hydroxide complexes. Finally, if the pH is above 7.0, cadmium may be found as cadmium carbonate complexes (Fig. I.8).

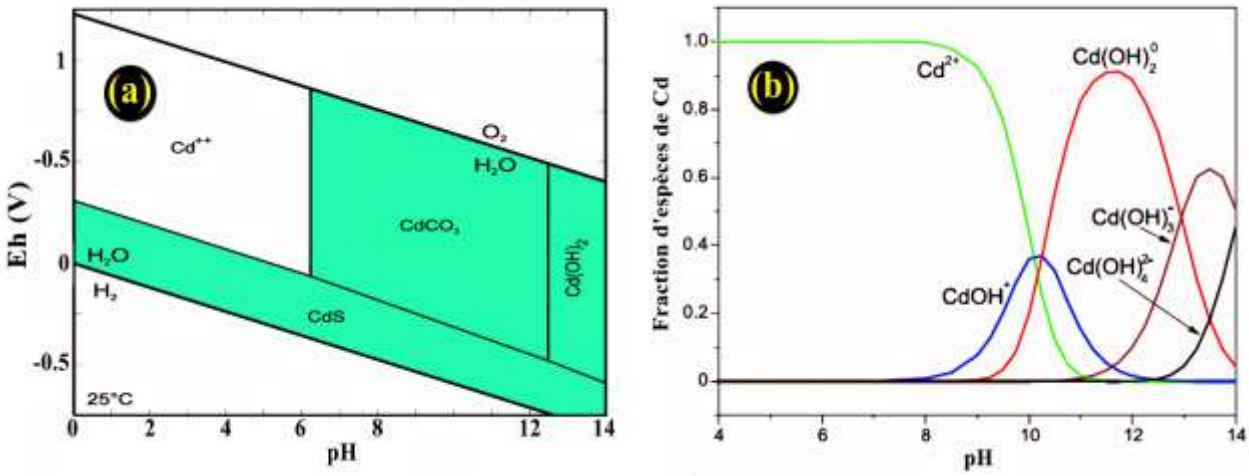

Fig. I.8. (**a**) Pourbaix diagram for the Cd/Water system and (**b**) Distribution of cadmium species as a function of pH (Ford et al., 2007).

I.3.2.2. Applications of cadmium

Indeed, cadmium is not directly used in the food industry due to its potential contamination of the environment and human health. However, it has an essential position in numerous industries and commercial activities thanks to its durability, reliability, corrosion resistance, and mechanical properties. One notable application is in the production of rechargeable batteries, such as Nickel–Cadmium batteries, which are highly popular in electronic devices and industrial equipment. It is utilized to improve the corrosion resistance and mechanical properties of certain metals like steel and iron by alloying them with other elements. Also, it is employed to manufacture pigments for paints, ceramics, and rubber products. This use benefits from the resistance of the metal to light and fading, and its ability to produce bright and long–lasting colours.

I.3.3. Copper

I.3.3.1. Physico–chemical characterizations

Copper (Cu) is a chemical element with an atomic number of 29. It has an electron configuration of [Ar] 3d10 4s1 and an atomic mass of 63.55 g/mol. Its melting point is 1083 °C, its boiling point is 2567 °C, and its relative density is 8.96 g/cm^3. Copper is also known for its high electrical conductivity, which depends on various factors such as temperature, purity, and impurities (Ouakouak, 2017). Generally, the electrical conductivity of copper at a standard temperature is approximately 59.6 x 106 S/m and 57 under a specific condition with a normalization factor of Hg = 1. Copper isotopes are distinct atomic forms that vary in the number of neutrons. In nature, copper is composed of two stable isotopes: ^{63}Cu and ^{65}Cu. The most abundant of these is ^{63}Cu, representing 69.17% of all–natural copper, while ^{65}Cu accounts for only 30.83%. Additionally, other unstable isotopes of copper can be produced through nuclear reactions, either natural or artificial. Copper exists in various forms, including pure Cu, Cu(I) (Cu^+), Cu(II) (Cu^{2+}), and Cu(IV) (Cu^{4+}), with the most common ones being Cu(I) and Cu(II). A Pourbaix diagram establishes the potential–pH equilibrium of the Cu–H_2O system, with another graph represented in Fig. I.9, both of which illustrate the distribution of different copper species depending on the pH of the environment. This helps to understand how pH influences the balance between different copper forms (Cu^+, Cu^{2+}, Cu^{3+}, and Cu^{4+}) and how these different forms react with other ions in the environment to form stable complexes (Meshram et al., 2020).

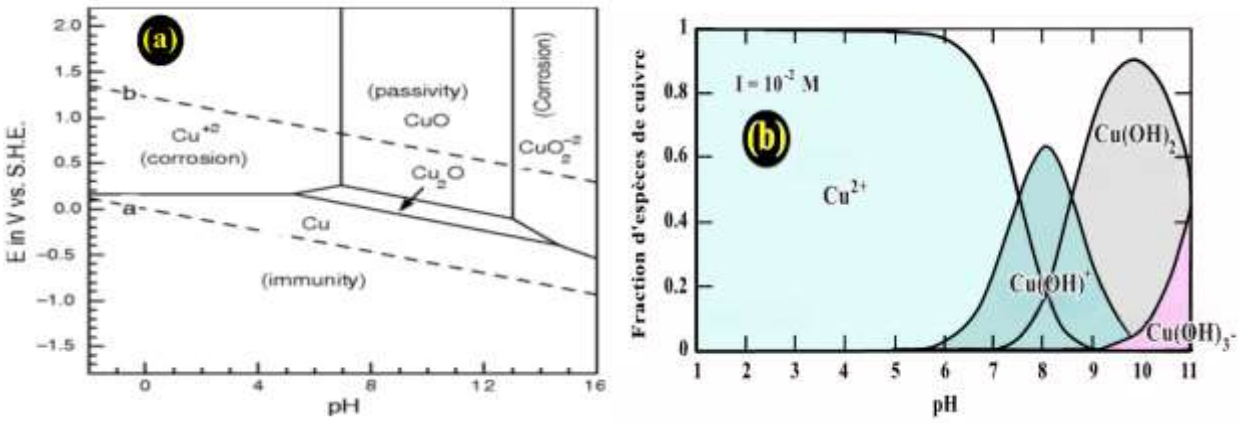

Fig. I.9. (**a**) Pourbaix diagram for the Cu/Water system and (**b**) Distribution of copper species as a function of pH (Meshram et al., 2020).

Graphs are based on the equilibrium reaction of each copper species with hydrogen ions (H^+) and hydroxide ions (OH–) present in the medium. At a pH lower than 5.5, there is a high concentration of hydrogen ions, leading to the formation of poorly soluble Cu(I) H^+ complexes. As the pH increases, the concentration of hydrogen ions decreases, and the concentration of hydroxide ions increases, which can lead to the formation of Cu (II) OH– complexes. The pH can affect the solubility of different copper compounds. At a pH lower than 7.5, copper (II) salts are generally poorly soluble, resulting in their accumulation in the medium. At a pH higher than 7.5, copper (II) salts can become more soluble and precipitate in the medium as $Cu(OH)_2$.

I.3.3.2. Copper in daily activities

Copper is a versatile metal widely used due to its unique properties. It is known for being an excellent conductor of electricity and heat, making it an ideal material for producing electrical wires, electronic components, engine parts, radiators, and heating appliances. Its resistance to corrosion makes copper a durable choice for products exposed to humid environments, such as water and gas pipes. Copper is relatively hard and strong, and its applications include the production of jewellery, currency, kitchen utensils, and sporting goods. In agriculture, copper is used as a fungicide, growth stimulator, pest control agent, and soil quality enhancer (Ouakouak, 2017; Verduzco-Navarro et al., 2020).

In the food industry, copper is used to manufacture food containers such as pots and pans. Additionally, it can be added to foods as a food additive to provide an essential source of trace elements for supporting regular growth and development. Furthermore, copper can stabilize colours and flavours in food products by preventing their decomposition and alteration. The daily source of copper for an average person may include foods from various sources such as fruits and vegetables, seafood, whole grains, red meat products, and nuts, contributing to a total intake of about 2 mg of copper per day. In medicine, copper possesses antimicrobial properties, making it a practical component to fabricate catheters, stents, and medications such as sulphonamides.

I.3.3.3. The importance of copper for human health

In the human body, copper plays a vital role in numerous biological functions and is involved in several essential metabolic processes. It is necessary to form many proteins and enzymes, including haemoglobin, which carries oxygen and iron in the blood, and collagen, a vital

structural protein for the skin, bones, and tendons. Copper is also involved in carbohydrates, lipid metabolism, and producing energy within cells.

Copper absorption takes place in the small intestine, where it binds to proteins such as ceruloplasmin before being transported into the bloodstream. Once in the blood, it is carried to tissues where it is utilized for necessary enzymatic reactions. It can also be stored in the liver, kidneys, brain, and muscles. Copper metabolism is regulated by feedback mechanisms to maintain stable levels in the body. For instance, when copper levels are high, the production of ceruloplasmin is reduced, limiting the amount of copper available for absorption into the blood, and the excess is eliminated through the kidneys and faeces.

Adequate levels of copper are necessary for overall good health, and its absence can lead to severe health problems. Conversely, high levels can result in unfavourable effects such as liver disorders, nerve degeneration, and developmental issues.

According to the *World Health Organization* (WHO, 2011), a recommended minimum daily intake of copper is 30 mgCu/kg of body weight for adults and 40 mgCu/kg for infants. However, these requirements may vary due to many factors, such as pregnancy, breastfeeding, ageing, and certain health conditions. Therefore, it is crucial to go through the assessment of the copper needs of each individual.

I.3.4. Cadmium and copper contamination in Algerian water sources

The WHO has recommended the maximum permissible levels in drinking water for Cd^{2+} to be 0.003 mg/L and for Cu^{2+} to be 2 mg/L (WHO, 2011). At the national level, the Algerian standard has recommended the limit values in surface waters to be and 0.005 mg/L for Cd^{2+} and 2 mg/L for Cu^{2+}, and in groundwater to be 0.005 mg/L for both metals (JORA, 2011). This means that prolonged exposure to excessive amounts of these metals can hurt human health (Ouakouak, 2017). Cadmium is considered a potential carcinogen and may cause cancers such as prostate and lung cancer. It can cause kidney damage, interfere with bone formation, and cause osteoporosis. Moreover, copper overload can lead to liver disorders like cirrhosis and reproductive problems (i.e., infertility) (Feng et al., 2009). Some investigations in previous studies conducted in different locations in Algeria have revealed the presence of cadmium and copper levels in surface and groundwater that exceed the recommended limits. Arab et al., (2021) indicated extreme pollution

in the Kaf Om Taboul area in El Kala. This contamination is caused by the presence of high concentrations of cadmium (1.435 mg/L) and copper (28.67 mg/L) in water samples (named W3) collected from the mining waste site in the same area. These fluids flow directly into Lake Tonga and the Mediterranean Sea through Wadi El Barita. Studies by Djorfi et al., (2010) reveal a risk of groundwater pollution by copper in the Berka Zerga area in Annaba, with a minimum concentration of 4.05 mg/L at the source and a maximum of 26.74 mg/L at point "P5". It has been reported that hazardous pollution results from the indiscriminate discharge of vast quantities of solid and liquid waste. Furthermore, numerous studies indicate the presence of toxic cadmium in water due to anthropogenic activities. A minimum concentration of 0.26 mg/L and a maximum of 2.67 mg/L were observed in the El Souk River in Skikda (Khelfaoui et al., 2022). At Chott Marouane in El M'Ghaier, the content ranged from 0.05 to 0.9 mg/L (Benhaddya et al., 2019). In the surface waters of Oued Righ, concentrations ranging from 0.025 to 0.065 mg/L were noted in Touggourt, and from 0.024 to 0.082 mg/L in the Djamaa and M'Ghaier regions (Benhaddya et al., 2020). Based on these previous assessment studies, the elevated concentration levels of cadmium and copper ions in surface and groundwater in some areas in Algeria have become a critical public health issue. This situation is alarming because the recommended limits have been exceeded, posing a significant threat to human health. For these reasons, cadmium and copper metals were selected as candidates to prepare hybrid adsorbents for treating them.

I.3.5. Cadmium and copper removal by adsorption

Ensuring the safety of drinking water by monitoring heavy metal levels is of utmost importance, as it not only safeguards water quality but also plays a vital role in protecting human health. Various methods for controlling these metals were used, such as chemical precipitation, membrane filtration, ion exchange, reverse osmosis, electrochemical treatment, and adsorption. Some of these methods are more effective in removing certain pollutants than others, so it is crucial to choose the most appropriate method based on the types of pollutants and adsorbents. One of the most common methods is the adsorption technique due to its simplicity of design, reasonable cost, and effectiveness.

Several studies have examined the adsorption potential of biomasses for retaining organic and inorganic pollutants, showing remarkable efficiency, especially for heavy metals. A study by Liu et al., (2019) focused on the adsorption of cadmium and copper ions by camellia oil tea

biomass revealed adsorption capacities of 14.2 mg/g and 12.1 mg/g for Cd^{2+} and Cu^{2+}, respectively. By studying copper removal in a study performed by (Feng et al., 2009), a modified orange peel biomass (polymerization product) by three chemical reagents showed high adsorption capacity of 289 mg/g, while the initial orange peel waste provided a capacity of 44.28 mg/g. In their notable study, Yang et al., (2019) employed unmodified Ca–alginate beads as green biomass to remove Cd^{2+} and Cu^{2+}. It was reported that their adsorption data are well–fitted by the Langmuir isotherm. The maximum adsorption capacities were measured at 216.82 mg/g for Cd^{2+} and 140.55 mg/g for Cu^{2+}. These studies also indicated the role of solution pH and temperature in the efficiency of pollutant adsorption. Wang et al., (2020) presented a study examining biochar produced from willow wood to adsorb cadmium and copper metals. Factors such as the initial pollutant concentration, temperature, and agitation time have a meaningful role during the adsorption study. The results showed that the biochar had a maximum adsorption capacity of 35.2 mg/g for cadmium and 12.2 mg/g for copper. The authors also noted that the Langmuir model fitted the obtained results better than the Freundlich model.

Zhou et al., (2018) published a study on subjecting a composite material composed of ferromanganese binary oxide and biochar to treat cadmium and copper solutions. They demonstrated the material's adsorption efficiency, with a maximum adsorption capacity of 101 mg/g for cadmium and 64.9 mg/g for copper, as measured by the Langmuir isotherm model. They found that pH is a crucial factor in heavy metals removal. Activated carbon prepared from Tunisian date pits showed a maximum copper removal value of 31.25 mg/g (Bouhamed et al., 2012). On the other hand, the adsorption of cadmium on activated carbon from olive pits showed 11.72 mg/g (Alslaibi et al., 2013).

Composite materials of alginate/carbonaceous materials have also garnered attention in several studies. A study performed by Li et al., (2010) focused on copper removal using a compound of Carbon nanotubes/Alginate, which showed an effective copper removal rate of 69.9%. The authors also indicated that the adsorption process is pH–dependent, and the maximum capacity was 84.88 mg/g. Other work has been carried out by Park et al., (2022) on the adsorption of copper ions using alginate beads alone and combined with biochar produced from rigid pine at different rates (1% and 4%) of biochar. The results showed high copper removal rates, reaching 122 mg/g at 0% biochar, 93.5 mg/g (1%), and 62.5 mg/g (4%). They also observed that the adsorption process for all adsorbents required 8 hours to reach equilibrium, indicating the role of

stirring time, and the kinetic data followed the pseudo 2nd order of model. Similar outcomes in suitable kinetic model were also published elsewhere (Feng et al., 2009). In another study, the removal of cadmium using modified carbon–based alginate beads derived from water hyacinth (700°C) exhibited a high adsorption capacity for cadmium, reaching 45.8 mg/g, and the rapid adsorption process occurred in just 9 to 15 hours (Liu et al., 2020). Competitive adsorption condition for copper and cadmium ions using different materials was studied in many papers.

Bakhtiari et al., (2022) investigated the uptake of Cu^{2+} and Cd^{2+} in two adsorption systems using Fe_3O_4 particles. The Single–metal adsorption is performed for only one metal in solution, while the binary mode uses more than one metal. The author found competition between the Cu and Cd ions explained by the decrease in the adsorption capacity and confirmed by a comparison study between the two metal systems. However, they observed that the removal efficiency for Cu and Cd ions in the solution of competition was higher at low initial concentrations and lower at elevated initial concentrations.

Overall, the adsorption technique shows promising applications for removing heavy metals from water. Although some adsorbents provided excellent removal for cadmium and copper removal in the adsorption capacity, it is necessary to continue studying and improving adsorbents to ensure maximum efficiency and minimize negative environmental impacts. Based on this, our research is a step to explore and develop new adsorbents.

I.4. Technologies of separation and reuse of adsorbents

I.4.1. General

While different types of adsorbents are widely used for practical applications, there are difficulties in separating them and the problem of mass loss after each adsorption process, especially for powdery materials such as clays, biomasses, and carbonaceous substances. This problem can also affect negatively the reuse of the absorbent materials in further adsorption operations. However, the adsorption capacity alone can no longer be considered a sufficient indicator of efficiency, and it is imperative to develop innovative methods for the effective separation of materials without facing issues with filtration or decantation. As of writing these lines now, recent studies have been devoted to finding efficient separation methods for materials

after the adsorption process, leading to the adoption of innovative techniques such as flotation and magnetic separation of adsorbents.

I.4.2. Techniques of separation

The flotation separation technique is based on the use of polymeric materials such as chitosan and alginate to create floating spheres on water (Fig. I.10a). This technique has been the subject of numerous previous studies and has been considered an effective means of separating different materials (Abd El-Monaem et al., 2022; Qiao, Tian, Bai, Zhao, et al., 2020). On the other hand, magnetic separation has proven to be the most effective and typical method (Fig. I.10b). It relies on modifying the properties of target materials by incorporating magnetic components. This technique has been applied to different types of adsorbents, such as biochar (Oladipo et al., 2019), chitosan (Fan et al., 2018), and alginate (Hong et al., 2016).

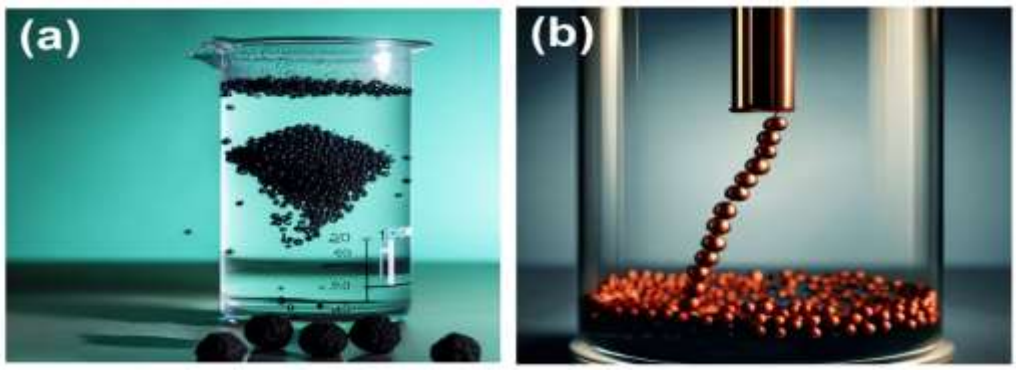

Fig. I.10. Separation techniques of beads: (**a**) floatation and (**b**) magnetically (AI; bing.com)

I.4.3. Reuse possibility of adsorbent materials

Frequent replacement of adsorbents can be costly, while reusing them can reduce the expenses of the adsorption process and even improve environmental efficiency by reducing the amount of waste produced. However, the reuse of the adsorbent can affect its ability to adsorb pollutants, making it necessary to regenerate the material to restore its adsorption capacity.

Various techniques can be used to regenerate materials and separate pollutants from the adsorbent. These techniques include thermal separation by using heat to dissociate adsorbates from the adsorbent; the electrolysis method uses electric currents to perform separation; chemical desorption uses reagents or solvents, and the simple water washing technique (Kulkarni & Kaware,

2014). However, these techniques may not be suitable for all types of adsorbents due to their different physical and chemical properties. For example, alginate cannot be regenerated using the thermal method if its structure needs to be preserved based in its weak properties toward elevated temperature (Zhang et al., 2019).

According to Lata et al., (2015), the chemical desorption method is the most common, as it involves the use of chemical additives as mentioned in many previous studies, such as hydrochloric acid (HCl) (Aichour et al., 2018; Park et al., 2022) and sodium hydroxide (NaOH) (Zhang et al., 2021). Batch desorption of Cd^{2+} and Zn^{2+} solutions from cassava biomass was studied by (Horsfall & Abia, 2003). The experiment of their study was performed under 0.1 M of HCl to desorb the metal ions for 30 min. They obtained excellent results for the desorption of selected metal ions. In support of this, the regeneration of sunflower carbon filled in Ca–alginate beads was successfully examined in the column system (Jain et al., 2013). The authors used an HCl (0.5 M) flow of 0.2 mL per minute to desorb cadmium ions, followed by a washing step using distilled water (pH between 5 and 6) to remove the excess H^+. The regenerated beads were used again in new adsorption tests.

Azri et al., (2022) subjected their biochar fabricated from pepper stem waste to 0.1 M NaOH for the desorption process of ibuprofen molecules after 04 cycles of continuous adsorption operation. This reagent was effective, and the adsorbent was used subsequently in other cycles. HCl and NaOH reagents approved their positive impact in the desorption of the loaded molecule onto adsorbent materials from the Contaminant/H_2O system. For these reasons, our research will test these chemicals as candidates to desorb cadmium and copper ions and reuse the prepared hybrid adsorbent.

Chapter II
Research Methodology and Procedures

Chapter II: Research methodology and procedures

II.1. Introduction

The chapter of this thesis serves as the linchpin for understanding the intricate details of the research. It explains the tools, methods, materials, simplifies the concepts and details the protocols utilized to achieve the purposes of the thesis: the preparation of hybrid adsorbents based on carbon for water treatment.

Herein, in this chapter, a great effort has been made to understand the study in terms of applied work related to the different experiments in the laboratory and the other side related to the techniques of analysing and interpreting the obtained results.

Over the years, many different research plans have been pursued by researchers to accomplish their work. Therefore, a research plan was followed that integrates in a very thoughtful manner each research element that has been explained and employed. Previous studies were employed to clarify all points related to the methodology of this research and the reasons for choosing the protocols or techniques used in the experiments and their purpose.

To express all of that, essential points related to this study were presented carefully:

- The precursor materials and chemical reagents used for the study.
- Preparation of adsorbents: protocols and methods conducted.
- Analytical techniques employed to identify the samples: SEM, FTIR, XRD, TGA-DTG, Ash content, Physical N_2 adsorption/desorption, and pH_{PZC}.
- Preparation of the used metals solutions (cadmium and copper): dosage and measurement of concentrations methods.
- Adsorption technique: theory (definition), principle, hypotheses, physical and chemical adsorption, and its steps.
- Presentation of the tests in the batch system: design of experiments (adsorption and desorption) and the performed tests.
- The used software along with the models (kinetics and isotherm) employed for the simulation of the equilibrium data.
- Thermodynamics study: the importance of the study and presentation of the method and their equations used for the parameters of the thermodynamic calculation.

II.2. Precursor material and chemical reagents

The precursor materials used in this study come from a natural source: peanut shells waste. The waste materials were collected from agricultural fields located in El Oued, Algeria. Sodium alginate was acquired from Aldrich (United States of America). Calcium chloride ($CaCl_2$•$5H_2O$), cadmium chloride ($CdCl_2$), 99% copper sulphate ($CuSO_4$•$5H_2O$), anhydrous iron (III) chloride ($FeCl_3$), and 99.5% ferrous sulphate ($FeSO_4$•$7H_2O$) were purchased from Riedel de Haën (Germany), Sigma–Aldrich (Germany), BIOCHEM Chemopharma (Quebec, Canada), and Arcos Organics (Spain) respectively. Distilled water with low conductivity (around 10 µS/cm) was used, and chemical additives such as HCl (≥ 38%) and NaOH (≥ 98.8%) were added to adjust the pH of the medium.

II.3. Preparation of the hybrid adsorbents

The term "hybrid adsorbent" refers to a material or substance that combines two or more different components or structures. Hybrid adsorbents are designed to take advantage of the unique properties of their constituent components to enhance their adsorption capabilities. Therefore, two hybrid adsorbents with spherical bead design biochar/alginate (1) and magnetic–biochar/alginate (2) were prepared based on the initial peanut shell biochar. The fabrication of the adsorbent materials was performed at the *LARHYSS laboratory* and some services were provided by the *pedagogical–Lab, Department of Civil Engineering and Hydraulics, University of Biskra, Algeria*.

II.3.1 Preparation of initial biochar

The steps for the fabrication of peanut shell biochar are illustrated in Fig. II.1. After collecting peanut shell biomass, the first step is to wash them with tap water several times to remove any presence of impurities, and then with distilled water. Subsequently, they are dried at room temperature for 24 hours. After that, the collected materials were meticulously cut into pieces with diameters ranging from 0.5 to 1 mm using a state–of–the–art laboratory grinder and washed with distilled water. The materials are then dried using the same method as before. Finally, in the last step, the product undergoes direct pyrolysis at 700°C for 3 hours (with a heating increase–rate of 10°C/min) using a muffle furnace (*DAIHAN Scientific*, Model *FHX–05, Korea*) under limited oxygen conditions to obtain the labelled PS–biochar.

After the fabrication of biochar, each sample weighing between 11 and 15 g is immersed in 400 mL of HCl (0.1 M) solution and vigorously agitated at a speed of 600 rpm. It is then rinsed multiple times with distilled water until the average pH reaches a value between 6.5 and 7.5, ensuring the absence of excess chlorine in the solution, and subsequently dried at 60°C for 24 hours. After the drying phase, the samples are stored in a clean container until their use in the adsorption experiments.

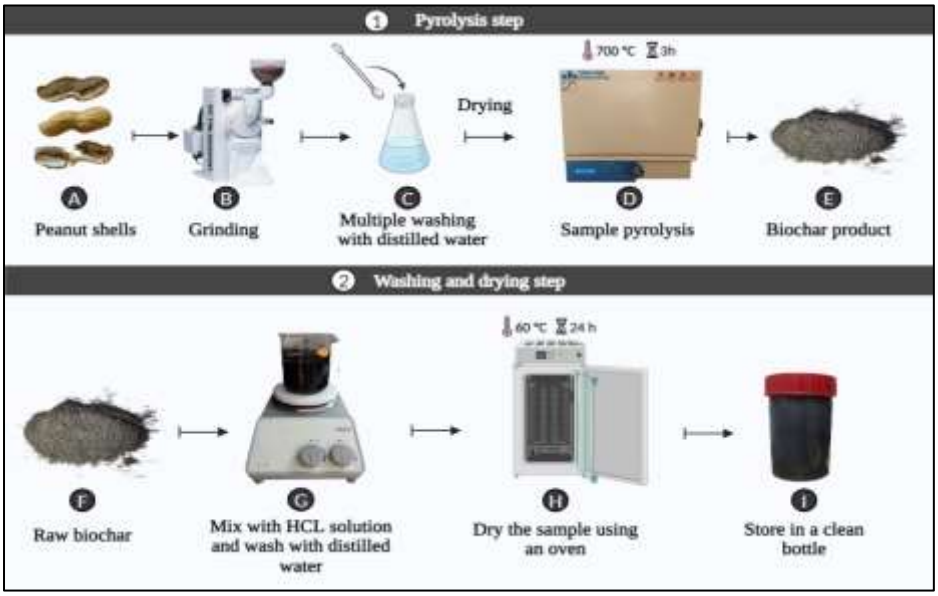

Fig. II.1. The used equipment for biochar preparation.

II.3.2. Magnetic–biochar (MB) preparation

Fig. II.2 illustrates the protocol for the preparation of magnetic–biochar. The synthesis operation of MB by co–precipitation was conducted following a method previously described by (Thines et al., 2017). For this purpose, a solution containing 2.98 g of $FeCl_3$ and 1.52 g of $FeSO_4 \cdot 7H_2O$ in 200 mL of distilled water was mixed with 4.6 g of the initial PS–biochar under an inert atmosphere for 20 minutes. To ensure the complete precipitation of Fe_3O_4, a NaOH solution (4.5 M) was added to reach a pH of 11 ± 0.1 at 80°C, and then the mixture was stirred for 3 hours. In the final step, the produced magnetic biochar powder was immersed in a 0.1 mol/L HCl solution and agitated for 240 minutes to remove impurities. It was then rinsed several times with distilled water before being dried at 60°C for 24 hours to eliminate any remaining moisture.

The chemical reaction achieves the following equation:

$$Fe^{2+} + 2Fe^{3+} + 8OH^- + PSB \rightarrow Fe_3O_4 - PSB + 4H_2O \quad \text{(II.1)}$$

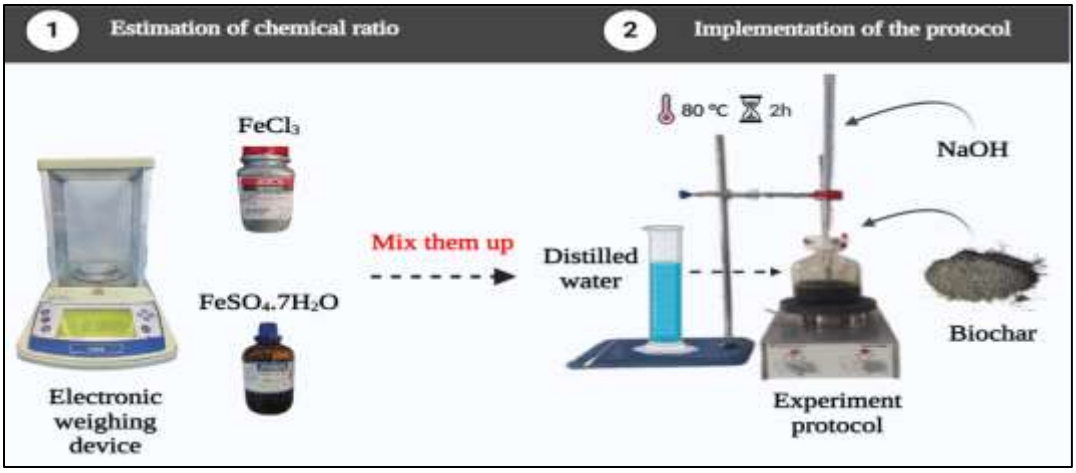

Fig. II.2. Protocol of magnetic–biochar synthesis.

II.3.3. Preparation of B/A and magnetic MB/A beads

The synthesis of composite alginate beads based on biochar or magnetic biochar was carried out by cross–linking method (Fig. II.3). To do this, 2 g of acid salt powder (SA) was dissolved in 100 mL of distilled water, and the mixture was stirred for 4 hours, intermittently adding 2 g of PS–biochar or magnetic–biochar during the first hour of stirring. After ensuring optimal homogeneity by continuously stirring the mixture, it was poured into a 10 mL syringe and immersed in a 4% (w/v) calcium chloride solution under gentle agitation to form hydrogel beads.

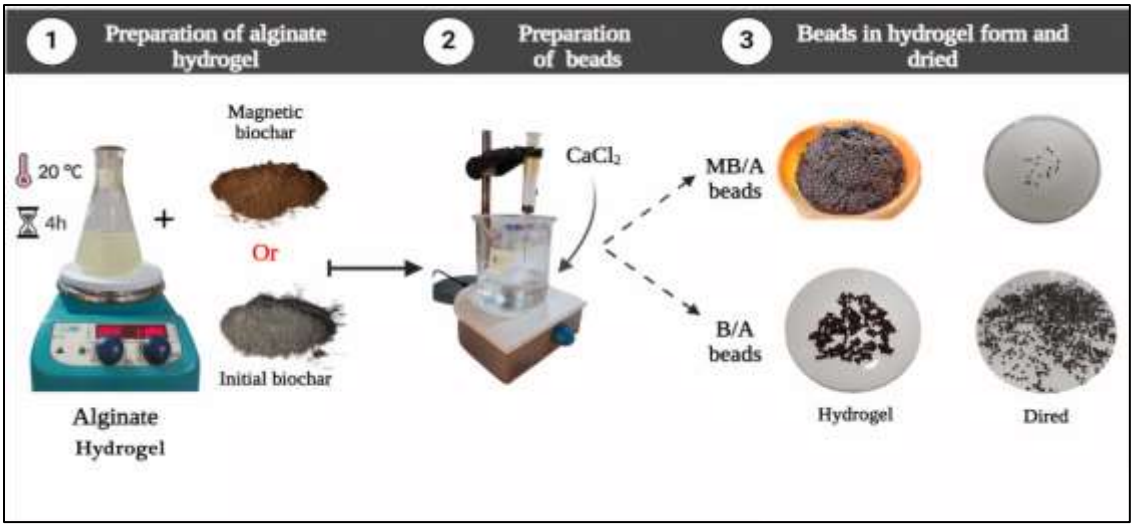

Fig. II.3. Protocol of samples preparation.

The spherical beads were left in the $CaCl_2$ bath overnight to complete the gelation and improve the hardness of the beads. Subsequently, the obtained beads were separated from the

solution using a magnet or flotation method and then washed four times to remove excess calcium ions and chloride from their surface. The beads were left to dry for 48 hours at room temperature and were eventually stored in a clean bottle until their use. SA bead was also synthesized for further experiments using the same protocol.

II.4. Materials characterization

II.4.1. SEM graphs

SEM "Scanning Electron Microscopy" is a highly versatile material characterization technique that allows visualizing the surface of a sample with high resolution and detecting elements present in the sample (HAMIMED, 2016). SEM uses the principle of electron–matter interactions to produce high–resolution images of the surface sample by sending an electron beam onto it. This technique also enables the measurement of the chemical composition of samples through various spectroscopy techniques such as Auger electron spectroscopy and X–ray spectroscopy. Furthermore, SEM offers other applications, including morphology, chemical element mapping, particle size measurement, and material texture characterization. This study used the high–resolution SEM *ZEISS–EVO 15* (Fig. II.4). SEM analysis of the prepared materials (the samples are in the form of powder: PS–biochar, MB powder, B/A bead, and MB/A bead) was performed at *CRAPC, Ouargla, Algeria*.

Fig. II.4. SEM equipment (*CRAPC, Ouargla, Algeria*).

II.4.2. Fourier Transform Infrared Spectroscopy (FTIR)

Fourier Transform Infrared Spectroscopy (FTIR) analysis is a widely used method in materials characterization (Derafa, 2021). It is practical for studying adsorbents as it allows the determination of functional groups present on the surface of the adsorbent and their reactivity with other elements like heavy metals. The infrared spectra obtained through this technique are powerful tools for identifying chemical components. The characteristic bands observed in the spectrum enable the identification of different functional groups present in the sample, such as C–H bonds, carbonyl groups, hydroxyl groups, amine groups, etc. This information is invaluable to characterize samples as it helps predict their adsorption capacity based on their functional surface groups. Sample preparation is a necessary step in Fourier Transform Infrared Spectroscopy analysis. In this study, a ground sample (1 mg) was mixed with KBr (300 mg) to produce a transparent pellet that can be used for transmission analysis (Fig. II.5). This technique is common in solid materials analysis and provides high–quality infrared spectra.

The infrared spectra were obtained in this study using a spectrophotometer (*SHIMADZU–IR Affinity^{-1}, Japan*) controlled by a computer, over a wavelength range of 4000 to 400 cm^{-1}. This infrared spectral analysis consists of two main parts: the first, ranging from 4000 to 1500 cm^{-1}, highlights functional groups common to all materials. The second part, between 1500 and 400 cm^{-1}, reveals groups specific to each material, thus creating a unique fingerprint for each analyte. This characterization technique was performed at the *Department of Chemistry, University of Biskra, Algeria*.

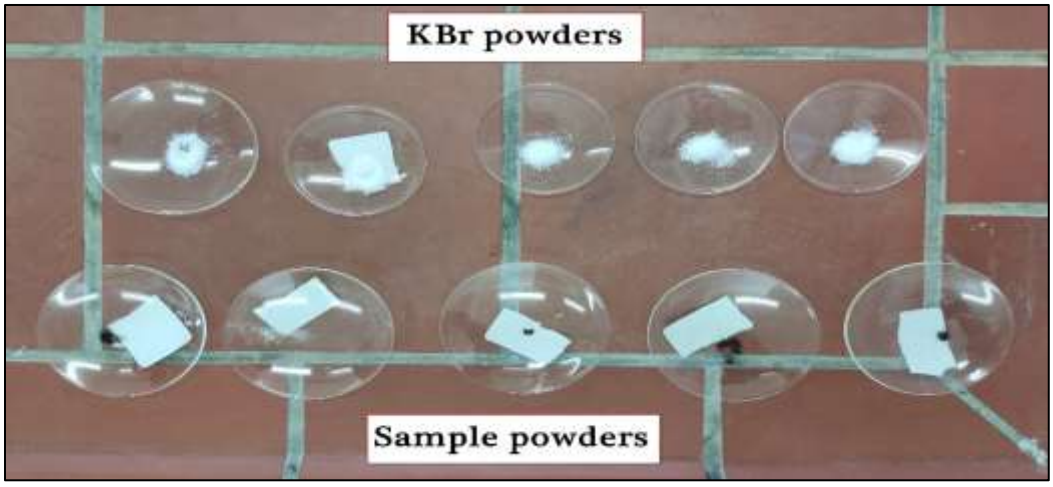

Fig. II.5. KBr powder used for the different samples for the FTIR analysis.

II.4.3. X–ray Diffraction Analysis (XRD)

X–ray Diffraction (XRD) is a technique used to identify and study the crystalline or amorphous structure of materials (i.e., biochar, biopolymer, oxides) (Aichour, 2019). In our study, we employed this analysis to examine the structural properties of adsorbents before and after the adsorption of molecules on the sample surface to investigate the structural changes that occur in the adsorbent when it interacts with the adsorbed molecules. These analyses include measuring changes in interatomic distance and deformation of the crystalline lattice resulting from adsorption. XRD is utilized to characterize the adsorbent materials by determining their crystalline structure and discovering their purity and homogeneity. The results of these analyses can be used to ensure the quality and performance of the adsorbent materials. The expression of Bragg is employed to measure the diffraction angles within the crystalline plane, according to the following equation:

$$\lambda_w = 2 \times d \times \sin\theta \qquad \text{(II.2)}$$

Where:

λ_w: is the wavelength of the X–ray beam.

d: is the spacing between two successive parallel planes of the crystal lattice.

θ: is the angle between the incident beam and the plane lattice.

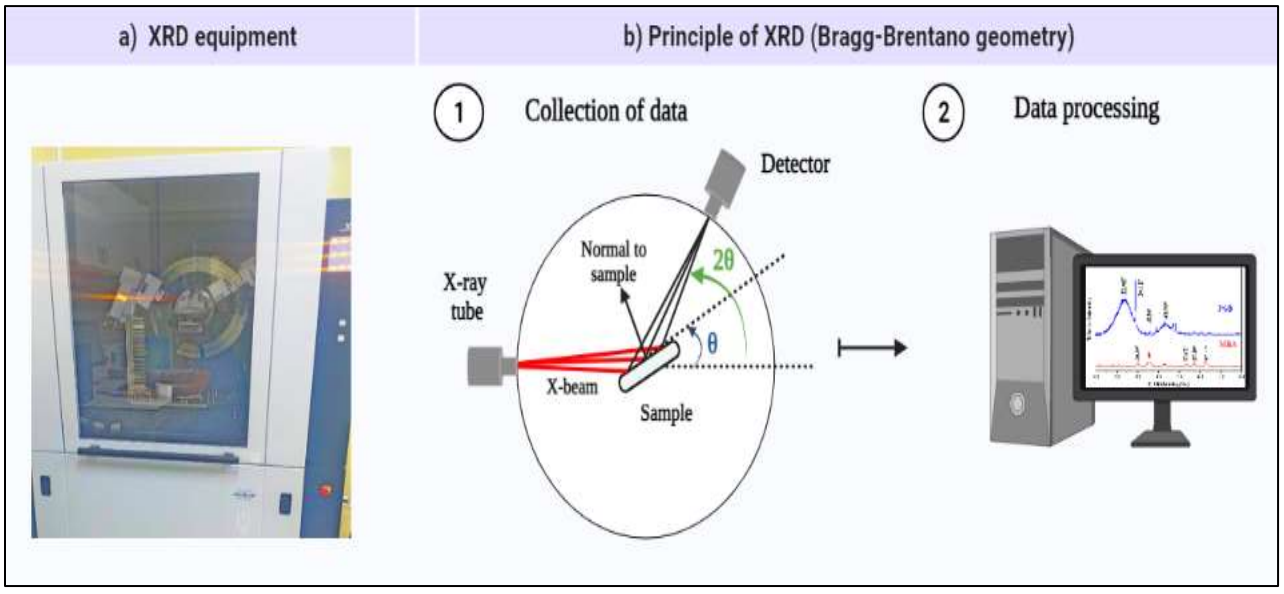

Fig. II.6. (**a**) XRD device (*CRAPC, Biskra, Algeria*) and (**b**) Principal of XRD technique.

In this study, the samples were analysed using X–ray diffraction with a *Bruker Model D8* Advance instrument (Fig. II.6.a), from Germany, operating with CuKα1 radiation (λ = 1.5406 Å) at a voltage of 40 kV and a current of 30 mA. The range of 2θ was from 5° to 80° (with a step size of 0.02°). This characterization technique was performed at the physical and chemical analysis platform *CRAPC, Biskra, Algeria*.

II.4.4. Thermal degradation TGA and DTG analyses

The determination of beads' thermal behaviour designed to encapsulate materials (i.e., PS–biochar and magnetic–biochar) utilizing alginate biopolymer is critical from the viewpoint of the temperature effect (Lussac & Ely, 2010). Therefore, the temperature behaviour of naturally dried beads (B/A and MB/A) at room temperature of 20°C, PS–biochar and magnetic biochar (70°C of drying temperature in the oven) was performed by studying the thermogravimetric analysis TGA and DTG using *TA* equipment model *Q50* (Fig. II.7).

Fig. II.7. The used device for the thermal degradation analysis (*University of Cadix, Spain*).

The temperature ramp rate was set at 10°C/min, ranging from 30°C to 900°C. This technique involves determining the quantities of volatile constituents released (or sometimes re–adsorbed) by the analysed sample as a function of temperature. This analysis technique was performed at the *Department of Chemistry, University of Cadix, Spain*.

II.4.5. Proximate analysis of ash content

The Ashe content protocol *(ASTM D1762*) combines two integral steps for accurate ash content determination. Firstly, the sample is ground, and its moisture content is determined through weight loss at 105°C in a drying oven. Secondly, the residual material from the moisture determination is heated to 750°C in a muffle furnace, burning off organic components to leave inorganic ash. Once a constant weight is achieved, the difference from the initial residue weight indicates the ash content. This test was performed at the *Department of Chemistry, Nova University (FCT), Lisbon, Portugal* (Fig. II.8). Ash content was also calculated using the TGA data.

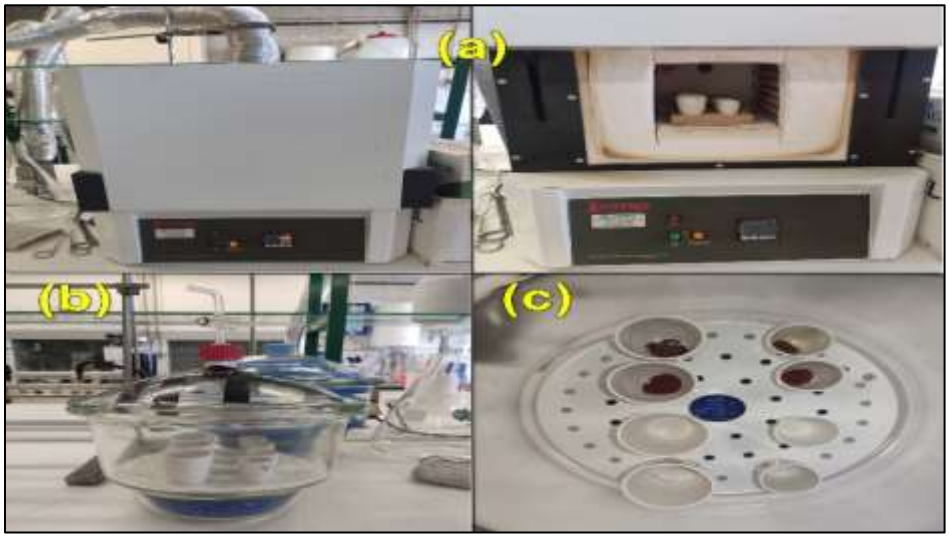

Fig. II.8. The used devices for ash content analysis: (**a**) muffle furnace, (**b**) dryer, and (**c**) crucible contain samples after the tests.

II.4.6. Textural property of adsorbents

Discovering the porous texture of samples is an essential step in material preparation, and determining their specific surface area is a crucial technique to achieve this. The most common methods for calculating the specific surface area and pore size distribution involve the adsorption–desorption of gases such as nitrogen, argon, krypton, or carbon dioxide. The nitrogen adsorption–desorption method at 77 K is necessary for determining the specific surface area, volume and diameter of pores, and evaluating the adsorption potential of materials. In this context, the nitrogen adsorption–desorption isotherms at 77 K of the prepared materials were obtained using the *ASAP2020* instrument at the *platform of CRAPC* for *physical and chemical analysis* in *Algeria* and at the *Department of Chemistry, University of Cadix, Spain*.

II.4.6.1. BET Specific Surface Area

The abbreviation "BET" defined to Brunauer, Emmett and Teller, and this method is used to determine the specific surface area of adsorbents by measuring the adsorption of gas in multiple layers on the material, represented by the Eq. II.3. This method is based on Langmuir's theory of adsorption in a monomolecular layer, which states that the adsorbed molecules do not distribute uniformly on the surface of material but rather form concentrated adsorption sites at specific locations (Rocher, 2008). Moreover, the BET method uniquely considers the interactions among the adsorbed molecules, enabling a remarkably accurate measurement of the material's specific surface area.

$$v = \frac{v_m c P}{(P_O - P)[1 + (c-1)(P_O / P)]} \tag{II.3}$$

Where: v is the volume of gas adsorbed per unit mass, v_m is the volume of gas adsorbed on a monolayer (L/g), P is the gas pressure, P_o is the saturation pressure, and c_{BET} is the BET constant for interaction between the adsorbed molecules. Using an Arrhenius−type exponential relationship, this constant can be related to the enthalpy of adsorption of molecules on the solid surface. This relationship is characteristic of the adsorbate/adsorbent pair. When the gas pressure is well below the saturation vapor pressure ($P << P_o$), the expression can be simplified, and the Langmuir equation (Eq. II.4) can be retrieved. In other words, when the pressure is low, there is insufficient gas to form more than one layer on the surface, which corresponds to the Langmuir assumption.

$$v = \frac{v_m c (P_O - P)}{1 + (c-1)(P_O / P)} \tag{II.4}$$

The BET equation can also be rewritten in a linear form (called the BET plot) to calculate the quantity V_m using the following transformation:

$$\frac{v_m c (P_O - P)}{v[(P_O / P) - 1]} = \frac{1}{v_m c} + \frac{(c-1)P}{v_m c P_O} \tag{II.5}$$

By plotting the quantity $\frac{v_m c (P_O - P)}{v[(P_O / P) - 1]}$ as a function of P/P_o in the linear domain ($0.05 < P/P_o < 0.35$), a straight line with a slope $\frac{c-1}{v_m c}$ and intercept at the origin $\frac{1}{v_m c}$ is obtained.

By using nitrogen (N_2) with an adsorption section s = 0.1620 nm^2, a molar volume V = 13.540 L/mol, and N_a (number of Avogadro; L/g) the specific surface area (S_{BET}) in m^2/g is calculated by applying Eq. II.6.

$$S_{BET} = \frac{v_m.N_a.s}{V} = 7205.v_m \quad \text{(II.6)}$$

II.4.6.2. Distribution of pore volume and diameter

This research employed the BET and BJH methods to assess the textural attributes concerning pore volume and size in porous materials. These methodologies rely on the analysis of N_2 physical adsorption isotherms conducted at a temperature of 77 K, facilitating the elucidation of pore dimensions and their distribution within our adsorbents.

II.4.7. The pH_{PZC} (drift method)

The pH_{PZC} is an abbreviation of "Point of Zero Charge". It is a critical factor in understanding the interactions between the adsorbent and the ions or molecules present in water. It is often determined using an acid–base titration method to measure the surface potential of the adsorbent at different pH levels.

The drift method allows us to determine the pH at which the net surface charge is zero. The pH_{PZC} is essential for optimizing the undertaking of the adsorbent under specific environmental conditions (Azri et al., 2022).

In this study, the pH_{PZC} was calculated following the previously reported works (Ouakouak et al., 2021) using the following method: 30 mg of dried adsorbent was added to each 30 mL of 0.01 M NaCl solution with an initial pH (pH_o) ranging from 2 to 9. After 4 hours of agitation, the final pH (pH_f) was recorded. Finally, the pH_{PZC} value was graphically defined by plotting the intersection point of the ΔpH curve ($pH_f - pH_o$) as a function of pH_o. In this study, a *Hanna pH 210 instrument* (*LARHYSS laboratory, University of Biskra, Algeria*) was used to measure the pH of all experimental solutions (Fig. II.9).

Fig. II.9. (**a**) pH meter device and (**b**) pH_{PZC} experiment.

II.5. Dosage of cadmium and copper

II.5.1. Atomic absorption spectrometry method (AAS)

AAS is a technique first described by the Australian chemical engineer Alan Walsh in 1955 (Walsh, 1955). It provides a decisive quantitative analytical instrument. This analytical method is used to determine the concentration of an unknown element in a sample by measuring the ability of atoms of that element to absorb light at specific wavelengths (λ) that depend on the energy levels unique to that element. The principle of AAS involves directing light emitted from a source into a flame containing the element to be assayed in ionized form. The atoms of the element absorb a portion of the light at a specific wavelength characteristic of the element. To measure the amount of absorption, a radiation detector calculates the difference in light intensity before and after passing through the flame (see Fig. II.10). From the measured absorbance, the concentration of the element present in the sample can be determined by applying the Beer–Lambert equation:

$$A = \varepsilon.l.C \qquad \text{(II.7)}$$

With: In absorbance (A), ε is the molar absorption coefficient (L/mol/cm), l is the length of the optical path traversed by light in the sample (cm), and C is the concentration of the element in the sample.

According to the Beer–Lambert law, the absorbance of a sample is proportional to the concentration of the absorbing species and the length of the optical path traversed by light in the

sample. Absorbance is defined as the negative logarithm of the ratio between the intensity of light incident on the sample and the intensity of light transmitted through the sample (Eq. II.8).

$$A = -log\left(\frac{I_t}{I_o}\right) \quad \text{(II.8)}$$

With: I_t is the intensity of the light transmitted through the sample, and I_o is the intensity of the light incident on the sample.

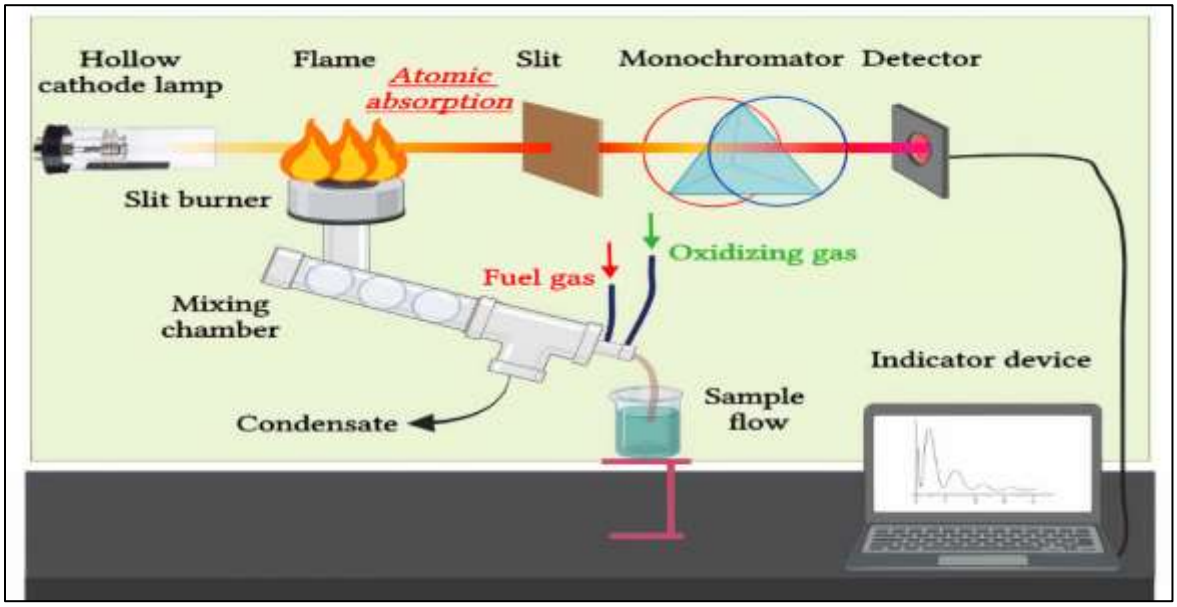

Fig. II.10. Principal of AAS method in details.

II.5.2. Dosage method

To plot the calibration curve of each metal cadmium and copper, a stock solution with a concentration of 100 mg/L was prepared. From this stock solution, a series of solutions with known concentrations ranging from 10 to 50 mg/L was obtained through successive dilution, while maintaining a constant pH. These solutions were analysed using flame atomic absorption spectrometry with the *240FS–AA* spectrometer (*CRAPC, Bousmail, Tipaza, Algeria*) and *Thermo–Scientific iCE–3000* spectrometer (*Department of Analytical Chemistry, Cadiz, Spain*) to determine the variation of absorbance measured as a function of the initial concentrations C_o (mg/L) of the aqueous solutions of Cd^{2+} and Cu^{2+} (Fig. II.11). The calibration curves for cadmium and copper were represented in Fig. II.12.

Fig. II.11. AAS instrument (**a**) *CRAPC, Bousmail, Algeria* and (**b**) *Cadix, Spain.*

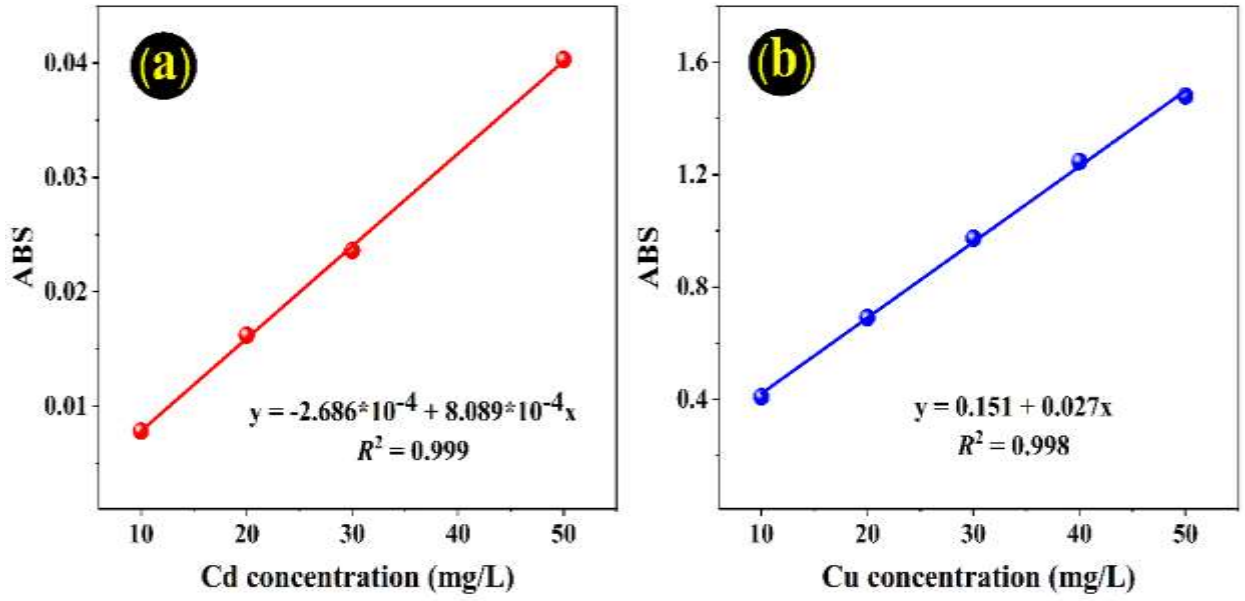

Fig. II.12. Calibration curves and detail for: (**a**) cadmium ions and (**b**) copper ions.

The variations of absorbance as a function of concentration were plotted on the calibration curve, which showed a straight line with a correlation coefficient greater than 0.99. This line was used to determine the concentrations of the unknown solutions after adsorption. All the measurements were performed at *CRAPC, Bousmail, Tipaza, Algeria* and *Department of Analytical Chemistry, Cadiz, Spain.*

II.6. Adsorption technique

II.6.1. Principle

Adsorption is the process by which molecules of a substance, whether it is a gas, liquid, or solid, adhere or bind to the surface of a solid or liquid material. Adsorption is a versatile and essential physicochemical technique used in various fields, including catalysis, separation, and water purification, among others (Ali & Gupta, 2007). The adsorption theory postulates that the process typically occurs in a porous solid medium, which acts as an adsorbent. The molecules of the adsorbate are attracted to the surface of the adsorbent, leading to a simultaneous variation in the concentration of the adsorbate in the solution and on the solid surface. Commonly used terms in this theory include the adsorbent (the solid material providing the adsorption surface) and the adsorbate (the species that will be adsorbed) and this is illustrated in Fig. II.13.

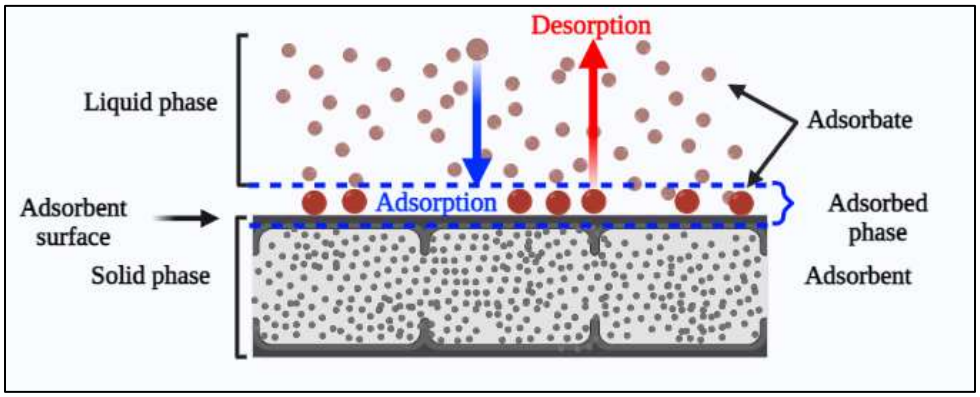

Fig. II.13. Principal of adsorption and desorption phenomenon (Gherbi, 2008).

Desorption is the reverse process of adsorption, during which the adsorbed species are released and transferred from the surface of the adsorbent to the liquid phase. The properties of the liquid phase, such as concentration, temperature, and pH, can be modified to facilitate desorption. According to (Gherbi, 2008), adsorption studies are generally based on three types of experiments:

- Kinetics: these experiments measure the rates of adsorption in kinetic studies.
- Isotherms: involve studying the quantities adsorbed at equilibrium, obtained through isotherm adsorption studies.
- Desorption: involves studying the properties of the adsorbed molecules concerning their chemical structure and ability to desorb.

II.6.2. Adsorption theories

According to the literature (Ouakouak, 2017), there are three main hypotheses to describe adsorption on solids:

- Monomolecular layer theory suggests that molecules form layers on a solid surface due to attractive forces between them. Langmuir and Brunauer developed this theory.
- Adsorption occurs when vapours of the substance condense inside tiny pores due to a decrease in saturation pressure. Capillary condensation can occur in materials with very small pores.

II.6.3. Adsorption steps

The adsorption process of solute molecules initially present in the solution onto porous solid adsorbents can be described as a four–step progression:

- First, solute molecules are transported from the solution to the boundary layer or the superficial film that surrounds the particles of the adsorbent.
- Next, these solute molecules move through the boundary layer and reach the external surface of the adsorbent particles.
- Subsequently, the solute molecules diffuse into the pores of the adsorbent material.
- Finally, the solute molecules undergo a reaction, either physical or chemical, at the internal surface of the adsorbent.

The four steps represent a series of successive phenomena that control the mass transfer of the adsorbate from the solution medium to the adsorption sites on the adsorbent (Reffas A, 2010).

II.6.4. Physical and chemical adsorption

The process of physical adsorption involves the fixation of adsorbate molecules to the surface of the adsorbent primarily through Van der Waals forces and electrostatic interactions like polarization, dipole, and quadrupole effects, especially for adsorbents with an ionic structure (Karge & Weitkamp, 2008). This type of adsorption, known as physisorption, does not cause any changes to the molecular structure and can be reversed, allowing the adsorbed molecules to be released under specific conditions (Claude Cardot, 2010). This phenomenon occurs as a result of

weak energy forces being exchanged between the solid surface and the nearby molecules (Raymond Desjardins, 1997).

According to Krou (2010) and Salah (2012), physisorption is a type of physical adsorption resulting from relatively weak intermolecular forces, which are less than 24 kcal/mole in strength (Fig. II.14a). It involves three types of interactions between: permanent dipoles (Keesom forces), permanent dipoles and induced dipoles (Debye forces), and induced dipoles (Van der Waals forces). These forces decrease in energy (*E*) in the following "*E*" order: Keesom > Debye > Van der Waals. Among them, Van der Waals forces arise due to the movement of electrons within molecules, leading to the creation of momentary dipole moments. These local dipole moments can induce similar temporary dipoles in neighbouring molecules, resulting in attractive interactions between them. Additionally, electrostatic interactions can combine with Van der Waals forces, playing a significant role in the interactions between polar or ionic molecules (Slasli, 2002).

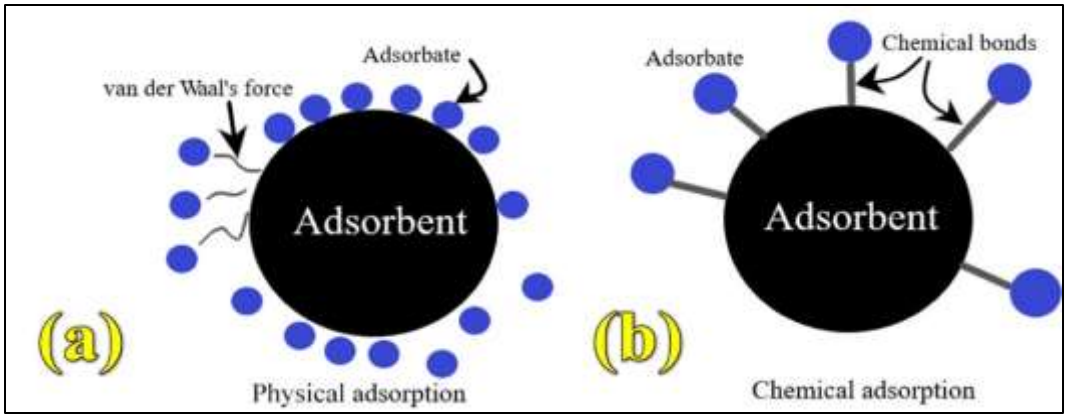

Fig. II.14. (**a**) physical adsorption and (**b**) chemical adsorption (Moosavi et al., 2020).

Chemical adsorption (Fig. 14b) is a process where adsorbate molecules react with the surface of the adsorbent, forming chemical bonds (Sun & Meunier, 2003). It involves high–energy chemical bonding forces (ranging from 25 to 400 kcal/mole), which develop between ionizable compounds and functional groups located on the edges of graphite microcrystals (Claude Cardot, 2010).

Chemisorption is a crucial element in the mechanisms of heterogeneous catalytic reactions and is considered irreversible. When all active centres on the surface have established bonds with adsorbate molecules, chemisorption is complete. Two distinct behaviours are distinguished in

chemical adsorption: heteropolar when electrons exchange exists between a donor and acceptor, forming a layer of ions on the adsorbent surface, and homopolar occurs when a covalent bond is formed, involving the sharing of electrons. In chemical bonding, only the first layer attaches to the adsorbent surface and undergoes strong adsorption, while additional layers are held by weaker adsorption (physisorption) (Bouziane & Zertal, 2007).

II.6.5. Types of bonds involved in adsorption

Adsorption depends on different types of interactions between the molecules of the adsorbent and the adsorbed molecules:

- Ionic bonds: formed from the electrostatic attraction between oppositely charged ions in a chemical compound. The energy of bonding can exceed 200 kJ/mol.
- Hydrogen bonds: Electrostatic bonds between atoms with free electron pairs, like oxygen, nitrogen, or sulphur, and hydrogen atoms linked to electronegative atoms (N or O). Energies of bonding range from 2 to 63 kJ/mol.
- Hydrophobic interactions: Result from the hydrophobic nature of certain organic pollutants. These non–ionizable, weakly polar, and poorly water–soluble pollutants partition between the aqueous and solid phases.
- Covalent bonds: Specific chemical bonds between certain sites of the organic pollutant and specific sites of the adsorbent (high bonding energies).
- Van Der Waals interaction: Weak electrostatic interactions, with bonding energies below 100 kJ/mol.

II.7. Batch adsorption study

II.7.1. General

Batch adsorption studies find extensive application in environmental engineering, wastewater treatment, purification processes, and the development of adsorbent materials for diverse industrial uses (Ali & Gupta, 2007). The procedure entails combining a known amount of the adsorbent material with a solution containing the adsorbate, permitting them to interact under controlled conditions. These studies are carried out in small–batch reactors or containers, wherein the adsorbent is introduced to a fixed volume of the solution containing the adsorbate.

Subsequently, the mixture undergoes stirring or shaking to facilitate optimal contact between the adsorbent and the adsorbate.

Data analysis, interpretation, and modelling are essential elements that should rely on to extract meaningful insights from experimental data of adsorption, understand underlying mechanisms, and predict system behaviour. Therefore, in chemistry, material science, and environment, two critical data analyses are kinetic and isotherm models. These models are invaluable tools in comprehending complex systems, and their applications are of utmost importance in our research endeavours. This thesis used *Origin pro (2021) software* to modulate the different equations of models. The different adsorption batch experiment performed in this thesis were done in research *laboratory in subterranean and surface hydraulics (University of Biskra, Algeria*. Additional studies and experiments were done at *NOVA University (FCT), Lisbon and Cadix University, Spain.*

II.7.2. Design of experiments

In this study, the first aspect of the experiment involved preparing cadmium and copper solutions from a mother solution of 500 mg/L for adsorption tests. A mass ratio of 1 g/L between the adsorbent and the volume of the metal solution was used for all adsorption experiments (Fig. II.15). The solid–liquid mixture was consistently stirred at a speed of 200 rpm (within the duration specified by the kinetics equilibrium time), leading to their uniformity, and enabling the disregard of species diffusion within the solution volume, while varying different parameters: the pH of solutions (from 2 to 9), the stirring time (from 5 to 360 min), the initial concentration (from 5 to 200 mg/L), and the temperature (from 15 to 45°C). After complete adsorption, the solid–liquid mixture was separated and filtered using a magnet (for the magnetic beads) and a 0.45 µm membrane filter before measuring the residual metal ions.

The second aspect of the experiment is dedicated to the reusability of the adsorbent (Fig. II.15). Scholars explored different ways to regenerate laden adsorbents and reduce the cost of the overall process. The reuse of adsorbent materials supports environmental matters by lowering the waste resulting from the adsorption operation.

In our case, a portion of 1 g/L of adsorbent/solution (200 mg/200 mL) was performed for the first adsorption experiment, and the ratio was maintained for the subsequent tests. After stirring

the mixture for 4 hours, the laden beads were collected (magnetically or by flotation technique) and dried for the new test (cycle). At 50% or less of the adsorption process efficiency, the operation stopped to start the desorption test.

In the desorption step (regeneration of materials), the beads were subjected to a 0.1 M solution of NaOH or HCl vigorously agitated at a speed of 600 rpm for 4h. Thus, this method allows the liberation of the adsorbed metal cation. Washing the materials by DW is the final operation for the reuse test.

The adsorbed quantities (Eq. II.9) and the adsorption rate R% (Eq. II.10) of cadmium and copper ions are calculated as follows:

$$q_{ads} = \frac{(C_o - C_e) \times V}{m} \tag{II.9}$$

$$\mathrm{R\,\%} = \frac{C_o - C_e}{C_o} \times 100 \tag{II.10}$$

Where: q_{ads} is the adsorbed quantity of the adsorbate; C_o and C_e denote the metal concentrations (mg/L) at baseline and at equilibrium, respectively.

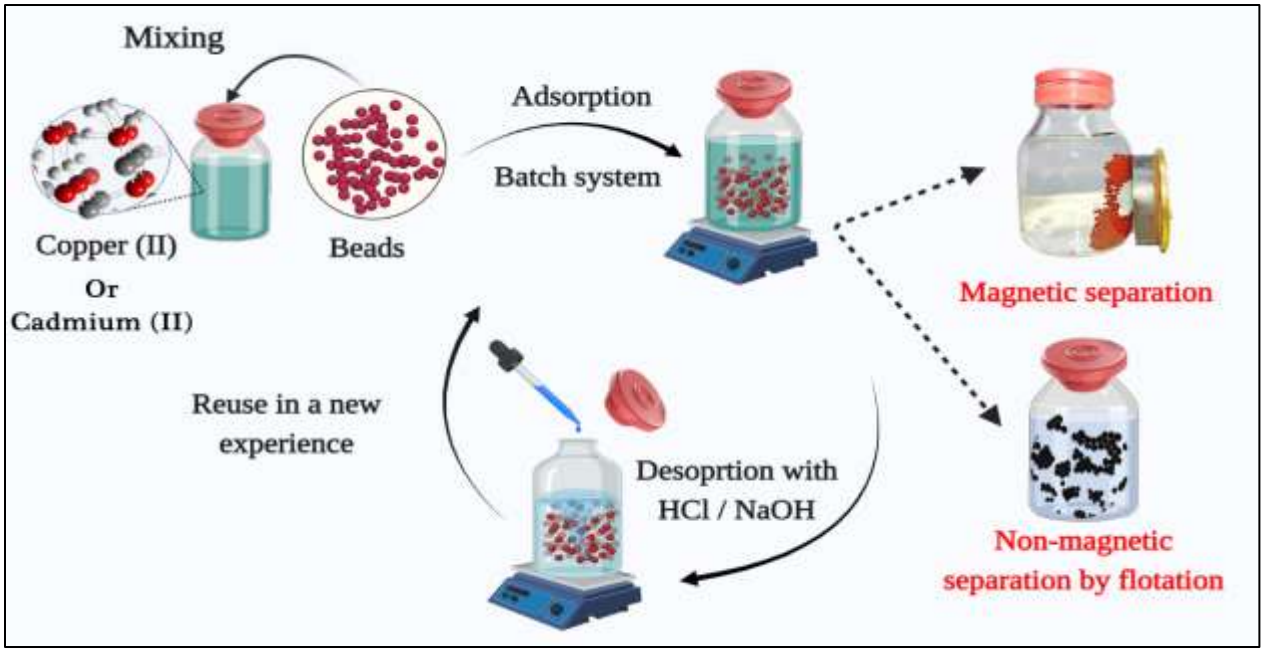

Fig. II.15. Simple explanation of the batch adsorption and desorption experiments.

II.7.3. Adsorption kinetic

II.7.3.1. General

The kinetics of adsorption involves studying how the concentration of the adsorbate in the solution changes over time when it comes into contact with the adsorbent. The data obtained from this study are then represented graphically as a curve, denoted as $q_t = f(t)$. This study delves into the exploration of chemical reaction rates and the many factors that influence their speed. It involves utilizing different mathematical models to describe the changes in concentration or quantity of reactants and products as time progresses. By delving deeply into kinetic data, the adsorption study gains valuable insights into the underlying reaction mechanisms, reaction rates, and how different variables impact the overall reaction kinetics.

This thesis used different kinetic models based on literature to approach the experimental data and understand the adsorption mechanism.

II.7.3.2. Pseudo–1st–order (PFO) model

In reality, the reaction may have a more complex mechanism, but the PFO model simplifies it by assuming that the activated complex formation is fast and in a steady state. This oldest model was proposed by (Lagergren, 1898). It provides the adsorption rate of the adsorbate by the equations Eq. II.11 and Eq. II.12.

❖ Linear form:

$$\ln(q_e - q_t) = \ln q_e - k_1 t \quad \text{(II.11)}$$

❖ Non–linear form:

$$q_t = q_e(1 - e^{-k_1 t}) \quad \text{(II.12)}$$

Where q_t and q_e (mg/g) are the adsorbed at contact time t and at the equilibrium, respectively; while k_1 (1/min) is the rate constant of PFO.

II.7.3.3. Pseudo–2nd–order (PSO) model

This model was studied by (Blanchard et al., 1984) regarding aspects related to adsorption and this model is commonly used to describe the kinetics of chemical reactions or processes. In 1998, Ho and McKay (1998) proposed a ground–breaking model (represented by Eq. II.13 and Eq.

II.14) that elegantly captures the concept of equilibrium between species present in solution and those adsorbed onto surfaces.

❖ Linear form:

$$\frac{t}{q_t} = \frac{1}{k_2 \times q_e^2} + \frac{1}{q_e} t \qquad \text{(II.13)}$$

❖ Non–linear form:

$$q_t = \frac{q_e^2 . k_2 . t}{1 + q_e . k_2 . t} \qquad \text{(II.14)}$$

Where k_2 (g/min.mg) is the rate constant of PSO equation.

II.7.3.4. Intraparticle diffusion (IPD) model

The model proposed by Weber Jr, Morris, and Stumm (1962) and was later studied by Allen, Mckay, and Khader (1989). Their subsequent research demonstrated that the quantity of adsorbed solute is intricately linked to the square root of time (t) (Eq. II.15).

$$q_t = k_{ip} t^{(1/2)} + C_{ip} \qquad \text{(II.15)}$$

Where: k_{ipd} is the IPD constant, and C_{ipd} represents the constant associated with the thickness of the boundary layer.

II.7.3.5. Pseudo–nth–order (PNO) model

Except for the first (1st) and second (2st) order models, and as reported by their equations, there is an additional order of fitting named The Pseudo–nth–order (PNO) that might be better suited for explaining the experimental data concerning adsorption kinetics (Tseng et al., 2014).

PNO equation (Eq. II.16 and Eq. II.17) is a development originating from the kinetics of first–order reactions. Including "pseudo" in its name signifies that the reaction is not strictly first–order (PFO) but exhibits analogous behaviour under specific conditions (Leyva-Ramos et al., 2010; Marczewski, 2010). The actual mechanism contains multiple sequential stages and interplays among diverse reactants.

❖ Linear form:

$$(q_{e,PNO} - q_t)^{1-m} = (m-1)k_{PNO}t + q_{e,PNO}{}^{1-m} \quad \text{(II.16)}$$

❖ Non–linear form:

$$q_t = q_{e,PNO} \times \left[1 - \left[\frac{1}{(1+(m-1)\times(q_{e,PNO}{}^{(m-1)})\times k_{pno}\times t)}\right]^{\frac{1}{m-1}}\right] \quad \text{(II.17)}$$

Where: $q_{e,PNO}$ (mg/g) referred to the quantity adsorbed calculated by PNO model; m_{PNO} and k_{PNO} are their exponents and the constant rate, respectively.

II.7.3.6. Avrami model

The Avrami kinetic model finds application in understanding and predicting the adsorption behaviour of substances in various systems, such as gas or liquid adsorption. The mathematical equation of this model elucidates the kinetics of adsorption processes (Eq. II.18 and Eq. II.19). Also, the Avrami equation helps to predict the rate at which a solute (molecule or particle) is adsorbed onto the surface of a solid adsorbent.

❖ Linear form:

$$ln\left[ln\left(\frac{q_e}{q_e - q_t}\right)\right] = n_{Av}lnK_{Av} + n_{Av}lnt \quad \text{(II.18)}$$

❖ Non–linear form:

$$q_t = q_e(1 - e^{-(K_{Av}t)^{n_{Av}}}) \quad \text{(II.19)}$$

Where: K_{Av} (1/min) represents the Avrami kinetic constant, and n_{Av} is its fractional adsorption order.

II.7.3.7. Elovich model

In 1962, Elovich and Larionov (1962) developed this model. Also, there was a previous study on the kinetics process by (Elovich & Zhabrova, 1939). The Elovich equation (Eq. II.20 and Eq. II.21) proposes a two–step adsorption process: fast initial adsorption due to the availability of

the active sites on the adsorbent surface, followed by slower adsorption as these sites become saturated.

❖ Linear form:

$$q_t = \frac{1}{\alpha}\ln(\alpha.\beta) + \frac{1}{\alpha}\ln t \quad \text{(II.20)}$$

❖ Non–linear form:

$$q_t = \frac{1}{\beta}\ln(\alpha.\beta.t + 1) \quad \text{(II.21)}$$

Where: α [mg/(g×min)] represents the initial adsorption rate, while β (g/mg) characterizes the Elovich desorption constant.

II.7.4. Adsorption isotherm

II.7.4.1. General

Studying the adsorption of a selected element by varying its initial concentration (C_o) with specified adsorbent mass (m) and at a fixed temperature (T) allows us to describe the adsorption process. This study is the key to understanding adsorption behaviour and mechanism.

II.7.4.2. Classification of isotherms

The relationship between the amount of adsorbate on an adsorbent surface and the equilibrium concentration of the adsorbate in the surrounding liquid at a constant temperature is known as isotherms (Rouquerol et al., 2013). Ouakouak, (2017) provided a comprehensive synthesis of the classification of isotherms, identifying cases now widely recognized as the primary forms of isotherms commonly observed.

a) Classification of Brunauer

Brunauer, (1943) classification of sorption isotherms groups into five primary types based on their shape and the underlying physical processes (Fig. II.16):

❖ Type I is characterized by Langmuir-like isotherms, which display a typical increase in water content with increasing water activity. The first derivative of the isotherm increases with

moisture content, making it typical of filling a monomolecular layer on the internal surface of a material.

- ❖ Type II is characterized by Sigmoidal or S-shaped isotherms, which account for the existence of multilayers on the internal surface of a material.
- ❖ Type III, known as the Flory-Huggins isotherm, takes into account the existence of a solvent or plasticizer, such as glycerol, above the glass transition temperature.
- ❖ Type IV describes the adsorption of a swellable hydrophilic solid until a maximum site hydration is reached.
- ❖ Type V observed for the adsorption of water vapor on charcoal, is the Brunauer-Emmett-Teller (BET) multilayer adsorption isotherm.

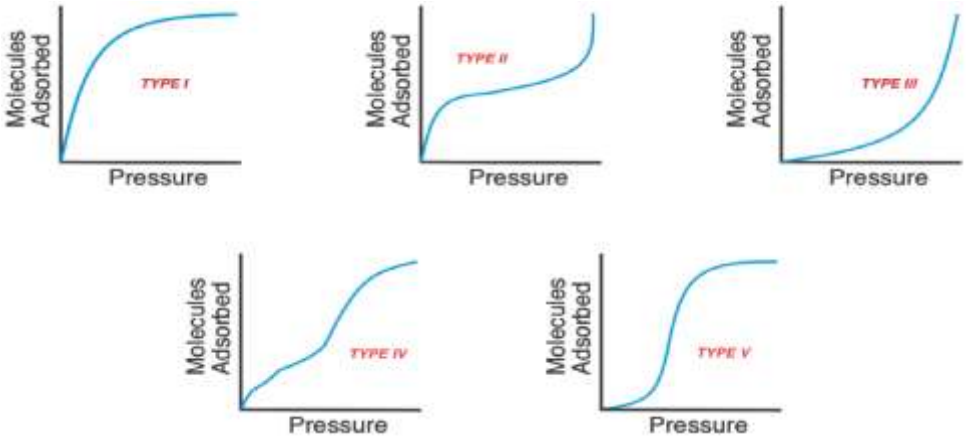

Fig. II.16. Classification of Brunauer (San-Pedro et al., 2020)

b) Classification of Giles

Giles et al., (1974) distinguished different shapes of adsorption isotherm curve based on its shape and initial slope. According to Fig. II.17, the different types of curves that represent various molecular adsorption behaviors on a surface are as follows:

- ❖ "L Curves" (Langmuir isotherms): typically indicating molecules adsorbed flat on the surface or vertically oriented adsorbed ions with strong intermolecular attraction.
- ❖ "S Curves": indicative of a vertical orientation of adsorbed molecules at the surface.
- ❖ "H Curves": represent high-affinity solutes, often ionic micelles or high-affinity ions exchanging with low-affinity ions.
- ❖ "C Curves": linear curves indicating solutes that penetrate the solid more easily than the solvent.

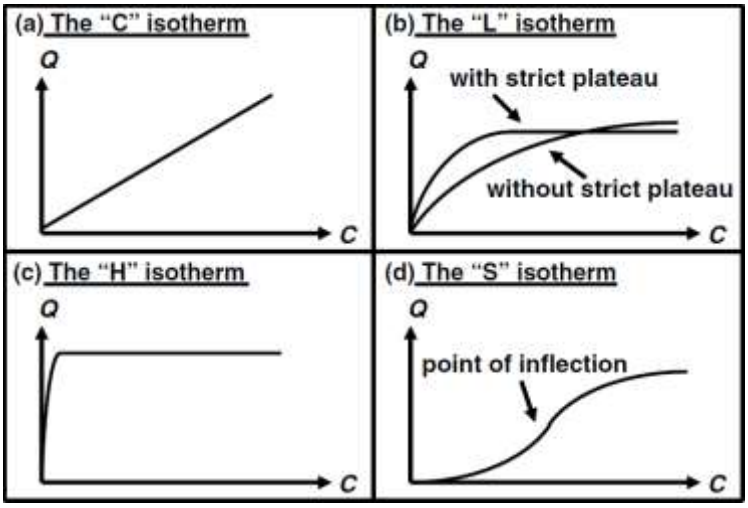

Fig. II.17. The main types of isotherms of Giles et al., (1974).

II.7.4.3. Freundlich model

The model of Herbert Freundlich introduced in 1909 (Eq. II.22 and Eq. II.23), delves into the intricate nature of surface interactions (Freundlich, 1909). This empirical approach sheds light on the relationship between solute and equilibrium concentration. This model mainly finds relevance in physical scenarios, assumes the formation of multiple layers of adsorbed molecules on the solid surface, and accounts for adsorption on heterogeneous surfaces.

❖ Linear form:

$$\log q_e = \log K_{Fr} + n_{Fr} \log C_e \tag{II.22}$$

❖ Non–linear form:

$$q_e = K_{Fr}.C_e^{(1/n_{Fr})} \tag{II.23}$$

Where K_{Fr}[(mg/g)/(mg/L)$^{n_{Fr}}$] and n_{Fr} represent the constant and the exponential intensity coefficient of the Freundlich model, respectively.

II.7.4.4. Langmuir model

This model was proposed by Irving Langmuir in 1918. It describes a reversible process of adsorption and desorption occurring on specific, energetically identical sites. In this model, the adsorbed molecule is located at a well–defined adsorption site on the adsorbent material, and each site can bind only one molecule. The Langmuir isotherm assumes monolayer adsorption on a

homogeneous adsorbent surface, implying that multiple layers of molecules are not considered (Langmuir, 1918). The mathematical equations of this model are presented in Eq. II.24 and Eq. II.25.

❖ Linear form:

$$\frac{C_e}{q_e} = \frac{1}{Q_{\max}.K_L} + \frac{C_e}{Q_{\max}} \quad \text{(II.24)}$$

❖ Non–linear form:

$$q_e = \frac{Q_{max}.K_L.C_e}{1 + K_L.C_e} \quad \text{(II.25)}$$

$Q_{\max}$ (mg/g) is the maximum adsorption capacity; and K_L (L/mg) represent its energy constant.

II.7.4.5. Sips (Langmuir–Freundlich) model

The Sips isotherm is a hybrid model that extends from the Langmuir and Freundlich isotherm models to better describe the adsorption behaviour. The model described by Eq. II.26 and Eq. II.27 assumes that the adsorption exists at multiple sites on the adsorbent surface and incorporates monolayer and multilayer adsorption (Ahmed & Dhedan, 2012).

❖ Linear form:

$$\ln\left(\frac{q_e}{Q_{\max} - q_e}\right) = \frac{1}{n}\ln C_e + \ln(k)^{1/n} \quad \text{(II.26)}$$

❖ Non–linear form:

$$qe = \frac{Q_{max}.K_{Sips}.C_e^{n_{Sips}}}{1 + K_{Sips}.C_e^{n_{Sips}}} \quad \text{(II.27)}$$

Where K_{Sips} $(\text{mg/L})^{-1/n_{\text{Sips}}}$ and n_{Sips} are the constant and heterogeneity constant of Langmuir–Freundlich, respectively.

II.7.4.6. Redlich–Peterson (R–P) model

The Redlich–Peterson model is a mathematical equation (Eq. II.28 and Eq. II.29) employed to elucidate the adherence of liquids to solid surfaces (Redlich & Peterson, 1959). It serves as an

expanded version of the Langmuir isotherm model, offering enhanced adaptability for systems that deviate from its assumptions.

❖ Linear form:

$$\ln\left(\frac{C_e}{q_e}\right) = a_{r-p}\ln C_e - \ln K_{r-p} \tag{II.28}$$

❖ Non–linear form:

$$q_e = \frac{K_{r-p}.C_e}{1 + a_{r-p}.C_e^{\,g_{r-p}}} \tag{II.29}$$

Where: $K_{r\text{-}p}$ (L/g) and $a_{r\text{-}p}$ (mg/L)$^{-g_{r\text{-}p}}$ represent are the constant and the R–P model parameter and $g_{r\text{-}p}$ (must be ≤1) is its dimensionless exponential factor.

II.7.5. Thermodynamic study

Increasing the temperature of the solution is well known to accelerate the diffusion of adsorbate molecules through the external boundary layer, and inside the pores of the adsorbent particles, due to the decrease in solution viscosity (Doğan et al., 2006). Scholars reported that adsorption operation is affected by change in temperature, resulting in the change of the adsorbent adsorption capacity (Liu & Liu, 2008). The standard parameters of thermodynamics (given in kJ/mol) concerning the Gibbs free energy (also known as available energy) ($\Delta G°$) associated in terms of both enthalpy ($\Delta H°$) and entropy ($\Delta S°$) can be used to recognize the temperature change impact on the adsorption operation. To investigate this purpose, some computations were applied using the Gibbs and Van't Hoff equations in the order as follows:

$$\Delta G° = \Delta H° - T\Delta S° \tag{II.30}$$

$$\Delta G° = -RT\ ln\ K_L \tag{II.31}$$

$$Ln\ \mathrm{K}_c = -\frac{\Delta H^{\circ}}{R} \times \frac{1}{T} + \frac{\Delta S}{R} \tag{II.32}$$

Where: R = 8.31 (J/mol.K) relate to the molar (ideal) gas constant, the temperature T is measured in kelvin (K), and K_c is an equilibrium constant with non–dimensional.

The constant K_C (Eq. II.33) was calculated based on the K_L energy constant of Langmuir, "$M_{element}$" element mass molar and "$C°$" standard reference solution (1 mol/L) to solve the unit problem, as mentioned in the literature (Tran, 2022). The following equation can simplify the change in units:

$$K_C \approx K_L\left(L/mg\right) \times M_{element}\left(mg/mol\right) \times C°\ \left(mol/L\right) \tag{II.33}$$

II.7.6. Determine the appropriate model

The applicability of different models is determined by tracing the suitability of their parameters using the correlation coefficient (R^2) (Eq. II.34), adj–R^2 (Eq. II.35), standard deviation (SD) (Eq. II.36), and Chi–square (χ^2) (Eq. II.37). Their equations are in the order as follows:

$$R^2 = \frac{\sum(q_{e,\exp} - q_{e,cal})^2}{\sum(q_{e,\exp} - q_{e,average})^2} \tag{II.34}$$

$$R^2_{adj} = [1-(1-R^2)\times(\frac{n-1}{n-p-1})] \tag{II.35}$$

$$SD = \sqrt{(\frac{1}{n-p})\times\left[\sum_{i=1}^{n}(q_{e,\exp} - q_{e,\mathrm{cal}})^2\right]} \tag{II.36}$$

$$\chi^2 = \sum\frac{(q_{e,\exp} - q_{e,cal})^2}{q_{e,cal}} \tag{II.37}$$

Where: "$q_{e,exp}$" and "$q_{e,cal}$" (measured in mg/g) denote the different adsorption capacities at the equilibrium obtained from the experimental results and model simulation data, respectively. "$q_{e,\ average}$" (measured in mg/g) signifies the mean of the experimental values, while "n" exhibits the entire number of experiments accomplished.

These parameters are integrated initially into *Origin software* (Version 2021). After the modelling operation of the adsorption data, the values of the mentioned parameters were automatically calculated, checked, and outlined in the different tables.

II.8. Conclusion

In conclusion, the materials and methods chapter lay a strong foundation for understanding the intricacies of your research. It not only outlines the tools, methodologies, and materials but also simplifies complex concepts and details the protocols used in the fabrication of hybrid adsorbents B/A and MB/A based on carbon for water treatment.

Key points covered in this chapter include the precursor materials and chemical reagents, protocols for material preparation, analytical techniques, preparation of metal solutions (cadmium and copper), the theory and principles of adsorption, design of experiments, and models for data simulation. A well–thought–out research plan integrates previous studies to elucidate the methodology's rationale and the selection of protocols and techniques.

Chapter III

Characterizations and techno-economic feasibility of adsorbents

Chapter III: Characterizations and techno–economic feasibility of adsorbents

III.1. Introduction

This chapter delves into the critical aspect of adsorbent design, encompassing shape and properties and the nuanced interpretation of characterization results obtained from the materials meticulously prepared during this study. The objective is to discern and comprehend their intricate textural, morphological, and physicochemical attributes. Utilizing the techniques introduced in *Chapter II* (SEM–EDS, FTIR, XRD, TGA–DTG, Ash content, Physical N_2 adsorption/desorption, and pH_{PZC}), embarking on a comprehensive journey to extract invaluable insights from these analytical tools. By doing so, they unlock a deeper understanding of how the materials interact with contaminants and their suitability for specific applications.

Furthermore, this chapter delves into the techno–economic feasibility of the prepared materials, namely PS–biochar, magnetic–biochar (MB), biochar/alginate (B/A) bead, and magnetic–biochar/alginate (MB/A) bead. Through a thorough examination, we assess the economic viability of these innovative adsorbents and discuss their potential practical implications. This evaluation is reinforced by drawing upon insights from prior studies that have explored similar materials and their applications.

III.2. Digital images and deep study in adsorbent design

The meticulous design of adsorbents is a multifaceted process that considers crucial aspects like shape, mass requirements for manufacturing, and particle size. This attention to detail is pivotal as it underpins the smooth and efficient operation of the product across the entire adsorption cycle.

In the context of the research, the evaluation of the need to produce 1 kg of PS–biochar from peanut shells is a fundamental step. These calculations provide valuable insights into the resources and processes required for manufacturing. Moreover, they serve as a critical reference point for estimating the production requirements for other adsorbents, including magnetic–biochar and the two types of alginate beads, as detailed in Table III.1.

In essence, this comprehensive approach to adsorbent design and production optimization is essential for achieving the desired results in adsorption processes and is integral to the success of our study.

Table III.1. Calculation of the required mass to produce 1 kilogram of PS–biochar.

Number of samples	PS Feed stock (g)	After pyrolysis (g) (700°C for 3 h)	Lose %	Yield %
1	69.44	17.66	74.57	25.43
2	68.00	18.05	73.46	26.54
3	89.96	23.33	74.07	25.93
4	84.01	21.44	74.48	25.52
Average	**77.85**	**20.12**	**74.15**	**25.86**
Ratios (1/x) (kg)		**3.87**		

As expected, the average yield of biochar production operation was approximately 25.9%, which means that to produce 1 kg of the black PS–biochar (Fig. III.1a), it was necessary to pyrolyze 3.87 kg of feedstock. The weight loss during the process of pyrolysis is under 75 % due to the nature of peanut shells, which are fragile and not solid. In *Chapter II*, it was reported that the preparation of the magnetic–biochar (MB) needs 4.6 g of biochar (besides 2.98 g of $FeCl_3$ and 1.52 g of $FeSO_4$) to produce approximately 9 g of dried magnetic–biochar with reddish brown colour (Fig. III.1b). The sieve size (in mm) of both PS–biochar and magnetic biochar (MB) in this study is in between 0.08 and 0.0125.

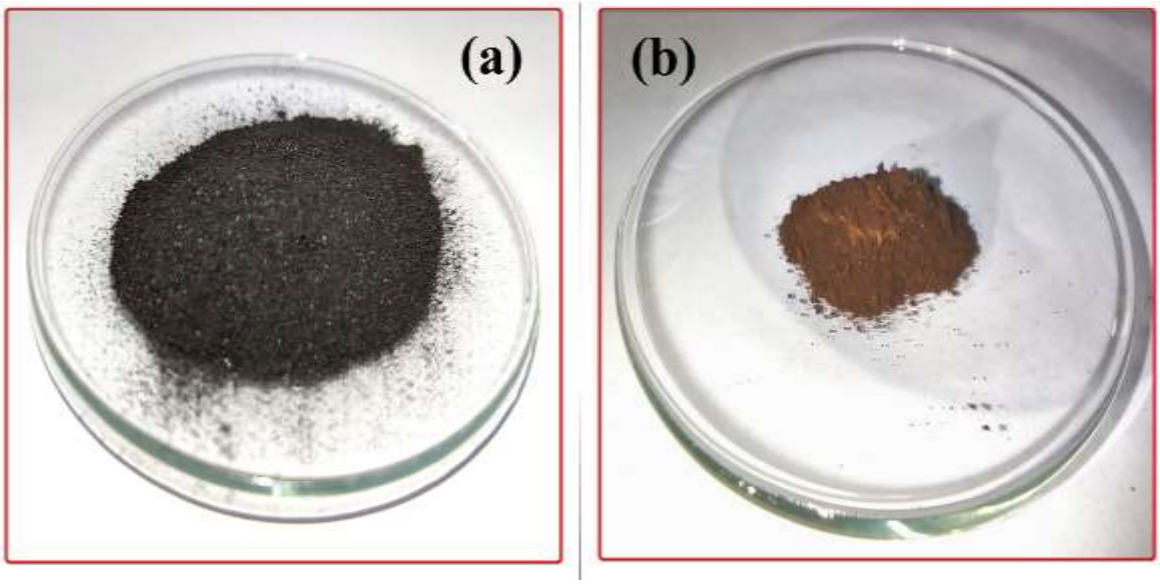

Fig. III.1. Powder of (**a**) PS–biochar and (**b**) Magnetic–biochar (MB)

In general, the alginate beads are mainly spherical and relatively uniform in size as shown in Fig. III.2. The colon black appearing in the B/A sample (Fig. III.2a) is due to the black carbon

of the incorporated PS–biochar and the reddish–brown colour is maintained in MB/A materials because of the contained magnetic–biochar (MB) (Fig. III.2b). In Fig. III.2b', the magnetic beads appear as they are strongly attracted to the magnetic field applied by the magnet. This means that the separation of particles could be better than the flotation method or other conventional methods.

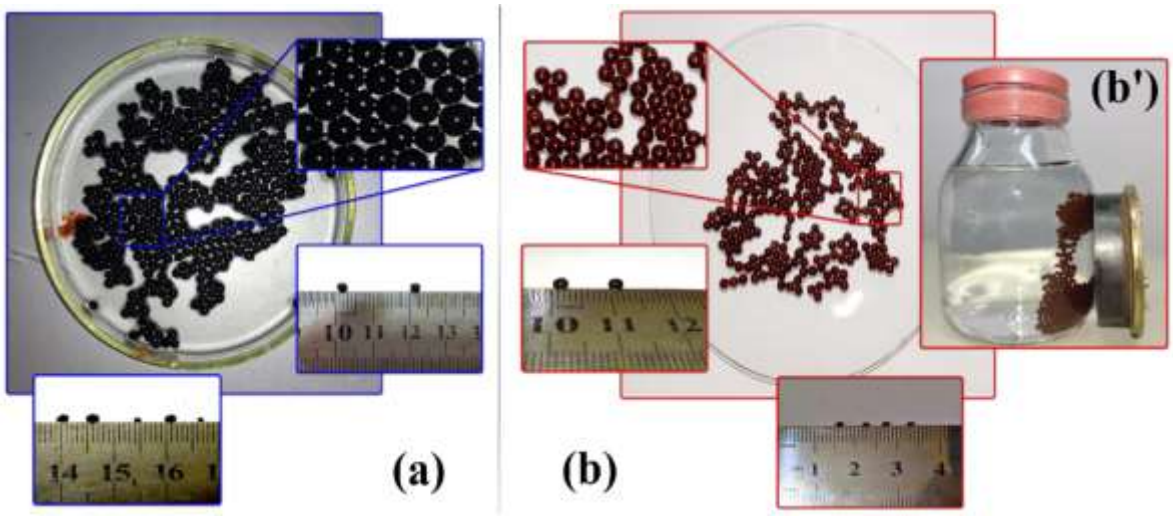

Fig. III.2. Digital images of: (**a**) B/A bead and (**b** and **b'**) MB/A bead

Studying the shape and size of the bead is very important to confirm the effectiveness of the entire design. The corresponding Table III.2 represents the different properties of alginate beads based on the initial biochar (B/A) and alginate beads based on magnetic biochar (MB/A). The size of B/A and MB/A beads in the wet state are around 3 mm, while in the dried form they are in the range of 1– 2 mm (for B/A) and 1–1.2 mm (for MB/A). The water content in B/A (93%) and MB/A (90%) indicates that the wet beads are soft materials. This explains why beads in both types (magnetic and non–magnetic beads) shrink by more than twice their initial size in the wet state.

The indirect reason for obtaining both types of materials (B/A and MB/A) with similar bead diameters in the wet state is due to manufacturing equipment with a fixed diameter (1.2 mm). Other reasons are the nature and characteristics of the materials involved in the composition (initial biochar and iron oxides of Fe_3O_4 nanoparticles). This is observed through the difference in the diameter of the B/A and MB/A beads after the drying process.

Biopolymer beads, including alginate beads, were used in many forms: hydrogel or dried beads. For example, Andreas et al., (2021) used hydrogel beads to eliminate methylene blue from

water. Dried beads have been likewise studied widely: alginate/biochar beads employed for the uptake of cadmium ions from solutions (Ayouch et al., 2020a). In our case, the beads were used in the dried state due to the possibility of storage for a long time until the adsorption experiments.

Table III.2. Design and properties of the hybrid adsorbents B/A and MB/A.

Sample	Wet bead size (mm)	Dried bead size (mm)	Wet beads (g)	After air drying (g)	Water content %	Colour
B/A	3	1 – 2	7.02	0.48	93	Black carbon
MB/A	3	1 – 1.2	5.016	0.574	90	Reddish brown

The reason for choosing the spherical shape of the beads used in our study is to facilitate their movement in solutions and their separation, in addition to preserving their relative mass during adsorption experiments. This design has been widely adopted in previous studies, with varying differences in bead size, components, and preparation protocols. Table III.3 shows previous studies in preparation of beads of spherical shape with different parameters. The water content and the size (diameter) of their prepared beads were very close to our fabricated spherical B/A and MB/A beads.

Table III.3. Previous studies in preparation of beads of spherical shape

Spherical bead	Wet bead diameter (mm)	Colour	Water content %	Separation technology	Study
Cu–alginate	3.2	Transparent	–	Flotation	(Wan et al., 2022)
TiO2@Cu–SA hydrogel	3.5	Light blue	–	Flotation	
Co–alginate	3.7	Pink	–	Flotation	
Biochar/Alginate	2.2	Black	95	Flotation	(Biswas, Sen, et al., 2019)
Magnetic–biochar/alginate	2	Black	–	Magnetically	(Prasannamedha et al., 2022)
Biochar/alginate	3	Black	–	Flotation	(Jain et al., 2013)
Clay/alginate samples	3	Clay colour	92–94	Flotation	(Chabane et al., 2017)
Empty Ca–alginate	1.51	Transparent	98	Flotation	(Rivas et al., 2019)

III.3. SEM micrographs and EDX analysis

III.3.1. SEM micrographs

Generally, biochars derived from lignocellulose material (obtained from agricultural waste, including peanut shells biomass) exhibit a typical porous structure shown by the fairly rough and irregular morphology of the biochar surface, which relies on the chosen temperature for the pyrolysis of feedstock materials (Tomul et al., 2020). Meanwhile, the modification of biochar with other materials (i.e., iron oxides and alginate hydrogel) to create a new composite leads to a change in the composite morphology (Qiao, Tian, Bai, Wang, et al., 2020; Zeng et al., 2021). The development can be observed on the surface of the material using the SEM image technique, while element composition measured using EDX equipment.

According to the depicted Fig. III.3, SEM micrographs of PS–biochar and MB materials were taken at 10 and 20 µm magnifications. PS–biochar exhibited many rough asymmetric pores Fig. III.3a and a'). This observation may be attributed to the impact of pyrolysis temperature (700 °C) on biochar morphology (Ahmad et al., 2012; Hadj-Otmane et al., 2022). In Fig. III.3b and b', the surface of the initial biochar almost changed after the modification with $FeCl_3$ and $FeSO_4$ salts. The resulting magnetic–biochar (MB) was a ragged and irregular structure explained by the iron oxide nanoparticles incorporation into the biochar, which covered its surface and assumed a place on their porous.

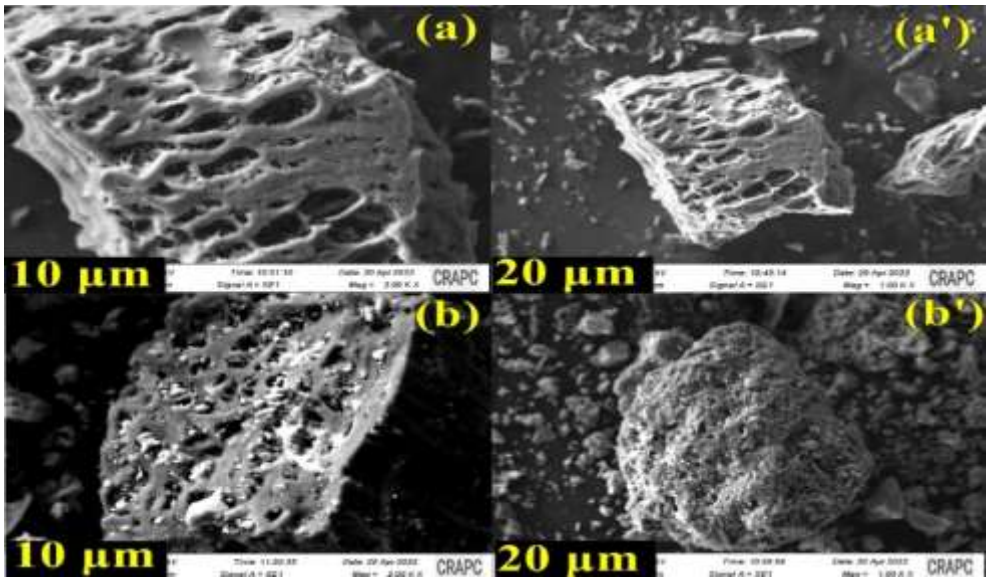

Fig. III.3. SEM micrographs: (**a** and **a'**) PS–biochar and (**b** and **b'**) MB

In general, hydrogel alginate beads (without further change) are known to have smooth surfaces because of the wet form (above 90% of water) (Biswas, Sen, et al., 2019; Wan et al., 2022). Based on Fig. III.4, the microscopic images of the dried beads B/A and MB/A samples revealed the rough external surface. For the B/A surface, the bulges and folds were caused by the initial biochar addition in the alginate hydrogel structure. Meanwhile, the MB/A surface is ragged due to the combination of the magnetic biochar.

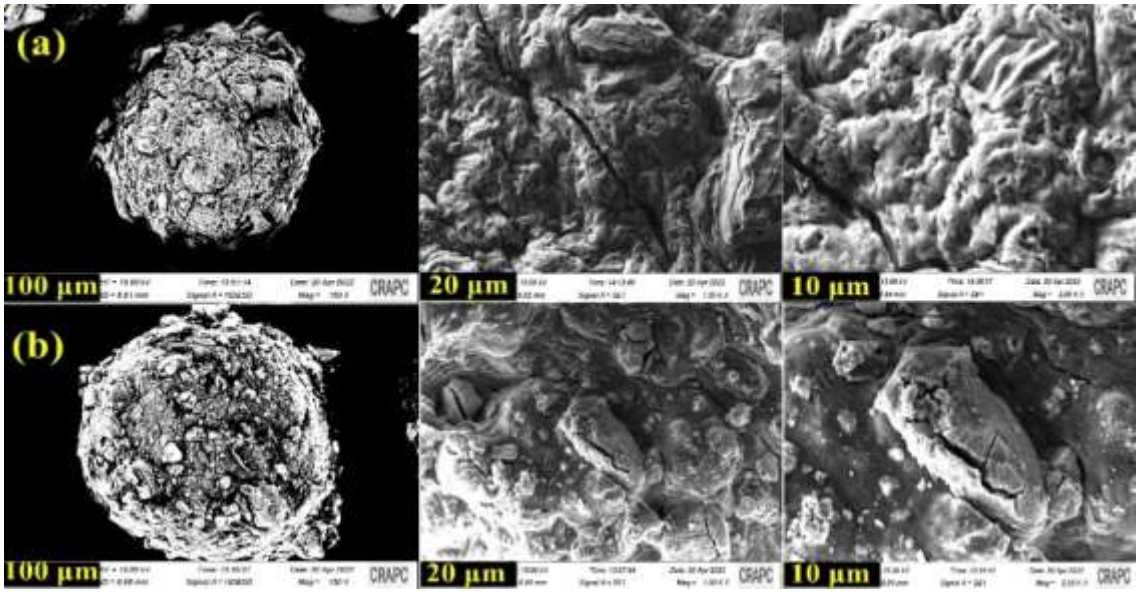

Fig. III.4. SEM micrographs: (**a**) B/A, and (**b**) MB/A.

III.3.2. EDX analysis of samples

The element composition of samples was measured using EDX equipment. In general, biochar was reported as black carbon having a composition of carbon and oxygen (Nouioua et al., 2023). The atomic ratios from the EDX analysis of the MB, B/A, and MB/A samples in the current study are summarized in Table III.4.

Table. III.4. Atomic percentage of MB, B/A, and MB/A samples.

Element % / Sample	C	O	Ca	Fe	S	Total
B/A	44.8	43.11	11.72	–	–	100
MB	34.17	36.11	–	27.54	2.2	100
MB/A	37.06	46.50	3.57	12.9	–	100

The proportional distribution of chemical elements, including oxygen, supports the hypothesis of the successful fabrication of Fe_3O_4 nanoparticles due to the divers O–containing functional groups (Li et al., 2022). This directs to the formation possibility of complexes with other metal ions, such as copper and cadmium (Li et al., 2022). The presence of a low atomic percentage of S (sulphur) in the MB sample (2.2%) and its absence in MB/A materials may be due to repeated operation washing of MB/A beads.

III.4. FTIR Spectroscopy of samples

III.4.1. Define IR spectra of the functional groups

In water chemistry, the different functionals of O–containing and aromatic rings groups existed on the surface of adsorbent materials have been widely recognized as active groups in binding with heavy metals such as copper and cadmium. Despite the availability of numerous technical research papers that have identified these functional groups discovered in the current study, it is challenging to distinguish them because of the similar structures of O–containing functional groups that could exist on the surface of the adsorbent materials. For example, lactones have an analogous structure to esters. Also, ketones and quinones have the same case (Qiu et al., 2023). Various functional groups are available on the surface of the four samples: PS–biochar, magnetic biochar (MB), biochar/alginate bead (B/A), and magnetic–biochar/alginate bead (MB/A). The results were recorded in their FTIR spectrum Fig. III.5.

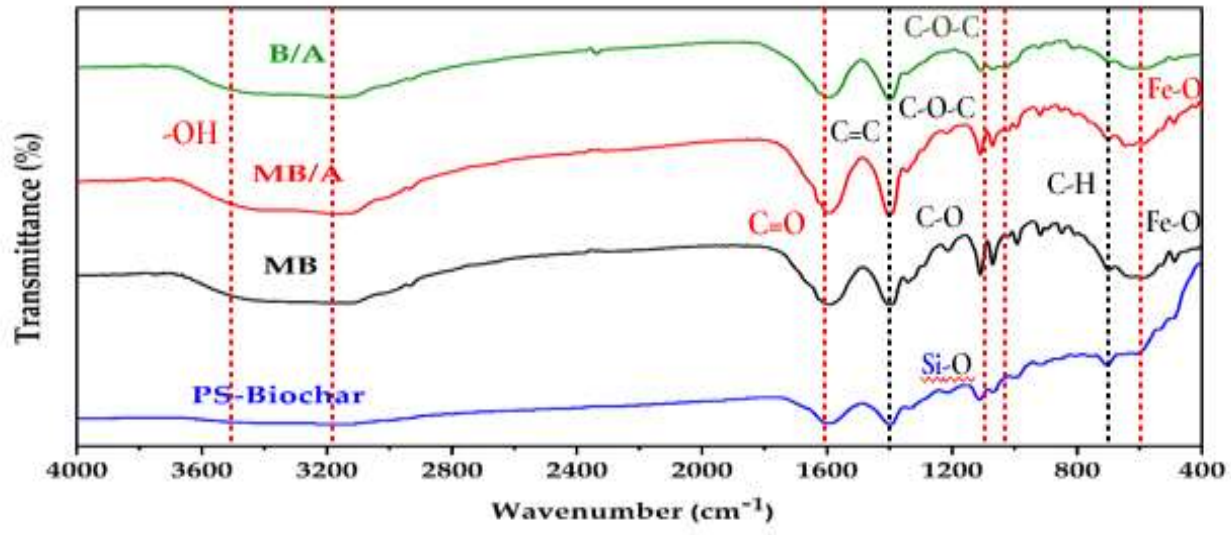

Fig. III.5. FTIR spectrum of PS–biochar, MB, B/A, and MB/A.

The data recoded in Fig. III.5 can be exemplified simply and straightforwardly for all the subjected samples:

a) The existence of oxygen (O)–containing groups

Hydroxyl groups (–OH) were identified at the band ≈ 3400 cm^{-1} in all samples. A similar finding was recorded in peanut shell biochars at 3398 cm^{-1} (Jin et al., 2022), magnetic peanut shell biochars at 3398 cm^{-1} (Jin et al., 2022), biochar/alginate beads in the range of 3200–3400 cm^{-1} (Park et al., 2022), and magnetic–biochar/alginate beads between 3300 and 3500 cm^{-1} (Qiao, Tian, Bai, Zhao, et al., 2020). Carbonyl groups (C=O) indicative of possible exploration at 1600 cm^{-1} band were repressed in ketones for PS–biochar (Albalasmeh et al., 2020) and overlapped with MB (Zeng et al., 2021), as well as in the carboxylates (COO^{-}) for both samples of alginate beads (B/A and MB/A) (Yadav et al., 2021). The 1100 and 1074 cm^{-1} bands have the potential for Si–O (silanol groups) (Ouakouak et al., 2020) and C–O (Azri et al., 2022) groups for PS–biochar and MB. However, the 1074 cm^{-1} spectrum also identifies C–O–C groups in B/A and MB/A samples (Yadav et al., 2021), and it overlaps with the C–O of the two biochars loaded in their bead composition (Alves et al., 2019). The band at 605 cm^{-1} present in the MB (composite combination of PS–biochar–Fe_3O_4) spectrum indicates the new band of Fe–O group (iron oxide) (Alves et al., 2019), resulting from the successful modification of the initial biochar with Fe_3O_4 nanoparticles (Li, Zimmerman, et al., 2020). This band is maintained in the IR spectrum of the MB/A bead. The FTIR data of Cd + B/A and Cu + MB/A samples after the adsorption were not plotted because there is no change or shift in their spectrum.

b) Characteristic aromatic rings

The bond at around 1400 cm^{-1} could represents the C=C bond (alkene) within aromatic rings (Tomul et al., 2020; Yadav et al., 2021), and it existed in all samples. Meanwhile, C–H bonds is described the aromatic carbons defined by the bond of 700 cm^{-1} in IR spectrum of all the analysed samples (Bouchelta et al., 2008).

III.4.2 Discussion in results

The existence of oxygen–containing functional groups in the examined samples, such as hydroxyl, carbonyl, Si–O, C–O, C–O–C, and Fe–O groups, could potentially react with metal ions (i.e., cadmium and copper) through coordination, complexation, chelation (including –COOH

groups) and ion exchange (Yu et al., 2017b). Likewise, aromatic rings (aromatics of alkenes and carbons) can contribute to metal binding through π–π interactions and enhanced surface area (Afzal et al., 2019; Tran, Lee, et al., 2017; Tran, You, et al., 2017). Based on previous research papers (Tran et al., 2016a; Tran, You, et al., 2017; Zhu et al., 2020) the chemical reactions (presence of the functional groups) and physical interactions (i.e., electrostatic interactions and Van der Waals) participate in the adsorption process as mechanisms in the existence of a specific kind of organic or inorganic element. These adsorption mechanisms could act as weak or as the main contributor to the uptake of metal ions.

III.5. XRD analysis of samples

Biochar based–biomass and alginate beads (biopolymer) materials without further modification are known as materials with amorphous structures, and this was reported in many previous papers, such as woody biochar (Wathukarage et al., 2019) and alginate beads (Vijayalakshmi et al., 2016). The crystalline structure describes the materials containing iron oxides, such as magnetic powder like Fe_3O_4 particles (Shafiee et al., 2019; X. Zhang et al., 2018). Results of Fig. III.6 showed two peaks recorded at 2–theta (θ) = 12.74°, 22.9° (002), and 42.9° (100) denote the amorphous state of the PS–biochar powder and B/A bead samples (Abdelwahab et al., 2022; Tomul et al., 2020). The findings are similar to other published papers that studied eco–friendly materials like biochars and biopolymers (Andreas et al., 2021; Biswas, Sen, et al., 2019).

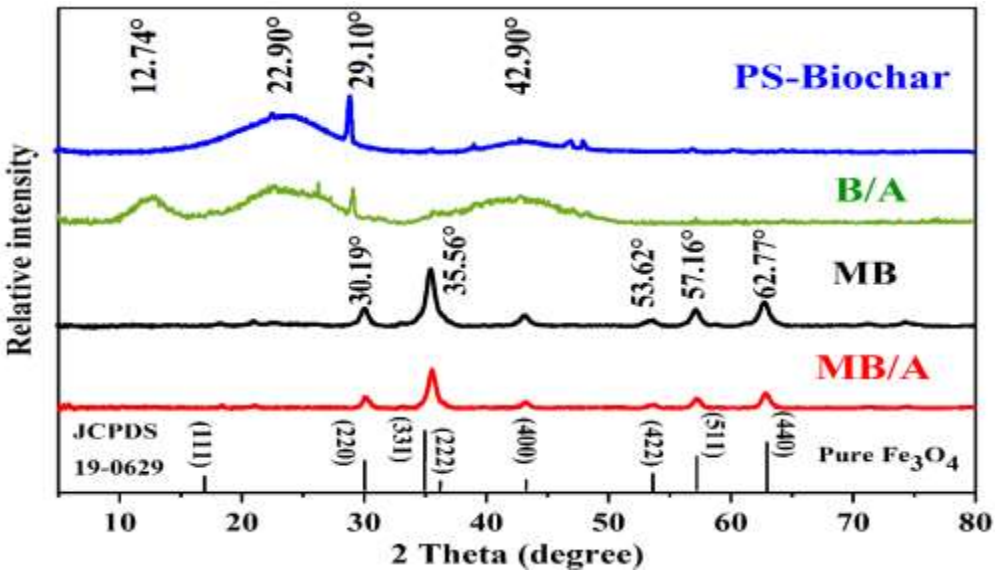

Fig. III.6. XRD diffraction of PS–biochar, MB, B/A, and MB/A.

After the PS–biochar modification by the iron oxide in their particles, using JCPDS n°19–0629 card, new peaks appeared in the fabricated MB materials at 2–θ (Degree) = 18.27, 30.19, 35.56, 43.2, 53.62, 57.16, 62.77, and other weak peaks at 71.4, and 74.5 assigned to Fe_3O_4 particles by the respective order of the following planes: 111, 220, 311, 400, 422, 511, 440, 620 and 533 (Abdelwahab et al., 2022; Yu et al., 2017b). Indeed, this development indicates the successful chemical protocol of co–precipitation to synthesize Fe_3O_4 in peanut shell biochar using the two iron $FeCl_3$ and $FeSO_4$ salts. The XRD diffraction of MB/A maintained the same diverse peaks found in the MB sample. It suggests the second incorporated operation in alginate hydrogel bead ended in successful. On the other hand, there is no interesting change in the XRD patterns of B/A or MB/A beads after the adsorption process of cadmium and copper, respectively. Thus, their data were not plotted in the Fig. III.6 Again, the successful preparation of the hybrid materials (B/A and MB/A) based on biochar or iron oxides is confirmed and the outcomes support the section of FTIR discussion.

III.6. TGA and DTG analysis

III.6.1 Presentation of TGA and DTG data and discussion

In general, the rise in temperature leads to the breaking of chemical bonds and the liberation of volatile components during the thermal degradation of materials. In the case of biochar–based materials, the degradation often leads to the loss of functional groups. Indeed, since the exposure of the alginate biopolymer beads containing biochar materials to extreme temperature variations such as heating or freezing in different experiences is knowledgeable, influential structural shifts or changes in the materials may occur. Hammoudi et al., (2020) mentioned a similar note for alginate films. As per the study of (Chakraborty et al., 2011), the thermal degradation of volatile material and polymers occurred under N_2 gas flow, while carbon material remained unaffected due to its inert nature in the presence of N_2 gas. Upon switching the gas flow to O_2, the carbon material underwent burn, resulting in the formation of inorganic residue or ash. In our case, the used two flows were: N_2 gas (1) and air (2) (mixture of O_2 and N_2 gases). However, using air flow (O_2+N_2) is also can identify inorganic and ash contents.

The TGA and DTG analyses were conducted on PS-biochar, B/A bead, MB, and MB/A bead samples under both N_2 gas and air flows. The abbreviation of the weight loss (Δm; %) is

represented as TGA % while the DTG % is used to represent the differential thermogravimetric analysis (see Fig. III.7 and 8). The collected thermal data was outlined in Table III.5.

Table III.5. TGA data for samples utilizing N_2 gas and airflow.

	***T* (°C)**	**30–200**	**200–400**	**400–800**	**30–750**	**30–800**
Δ*m* (%) N_2 gas	**PSB**	8.23	2.26	12.46	–	21.5
	B/A	14.82	31.37	35.71	–	62.4
	MB	4.51	1.68	9.77	–	16.40
	MB/A	10.46	20.81	18.74	–	50.65
Δ*m* (%) Air flow	**PSB**	9.97	3.39	95.23	96.0	96.0
	B/A	19.01	27.34	88.21	93.1	93.1
	MB	4.89	2.63	42.28	51.29	51.26
	MB/A	9.96	21.4	37.0	69.26	69.27

Note: PSB is the PS–biochar.

It was observed that increasing temperature led to thermal degradation in the materials. Based on DTG results, the samples went through degradation in three phases. The first phase occurred at $T < 200$°C under N_2 and air flows, which corresponded to the dehydration section (physically adsorbed water) (de Araújo et al., 2022; Hadj-Otmane et al., 2022).

The second phase was observed at 200−400°C for N_2 of both samples and air of B/A while PS-biochar and MB materials went beyond 400. This section represents the maximum reaction of materials and their strong decrease in mass with the breakdown of sodium alginate (Ayouch et al., 2020b).

The third phase began beyond 400°C for N_2 and air flows and indicated the decomposition of the carbonaceous materials. The thermal data of both PS-biochar and MB analysis under airflow have only two stages.

The negative ΔT and the shape of their DTG curves indicated the decomposition of the studied samples. Thus, the process is endothermic, meaning it absorbs energy, which is utilized in reactions like dehydration and the breakdown of functional groups (Hadj-Otmane et al., 2022).

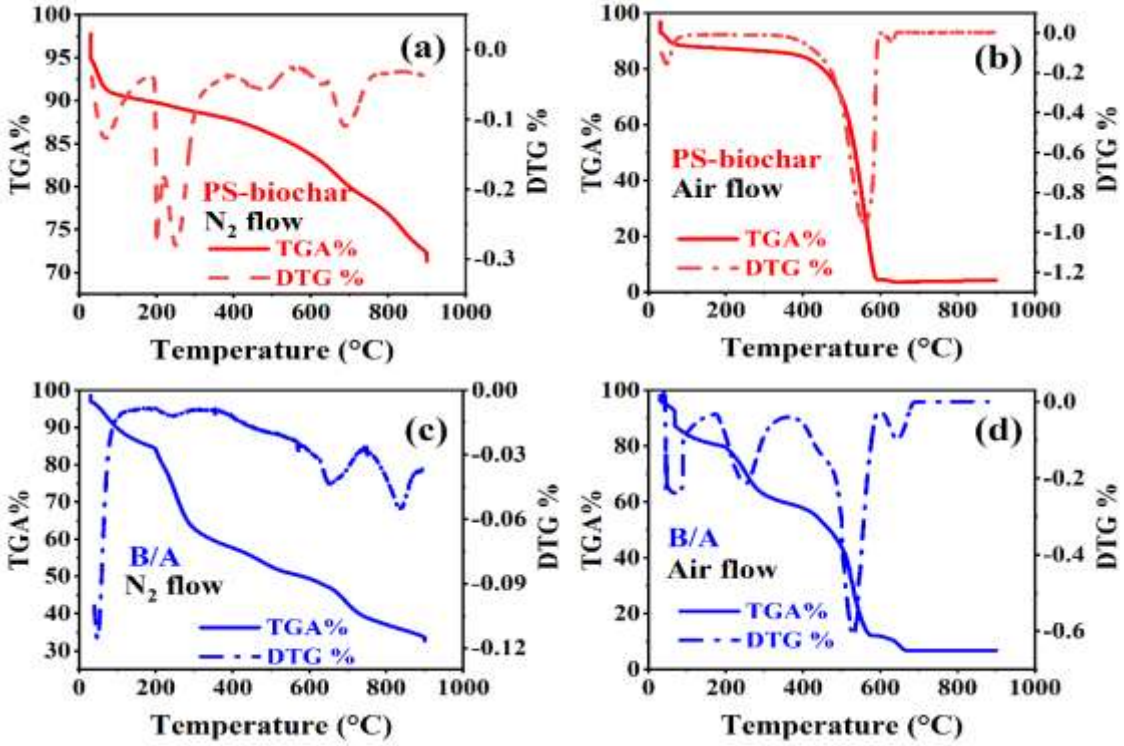

Fig. III.7. TGA and DTG analyses for: (**a** and **b**) PS-biochar, and (**b** and **c**) B/A bead.

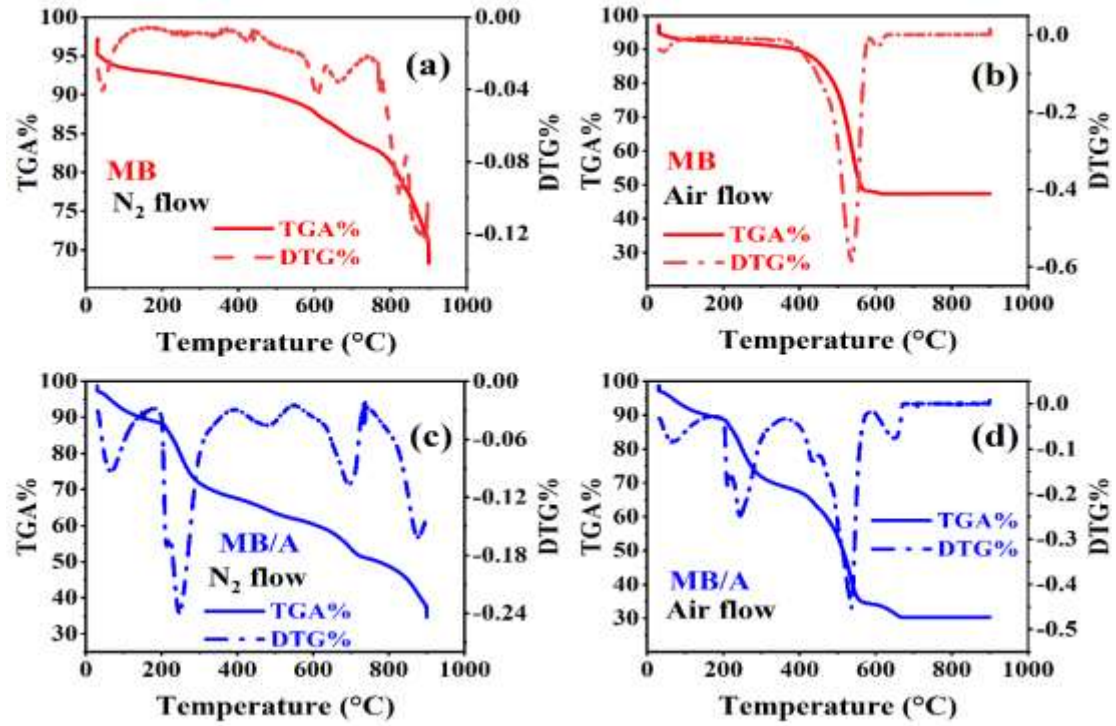

Fig. III.8. TGA and DTG analyses for: (**a** and **b**) MB, and (**b** and **c**) MB/A bead.

III.6.2 Implication and discussion on functional groups degradation

From the results, biochar powders (PS-Biochar, MB) undergo thermal decomposition of organic components. The addition of Fe_3O_4 particles and alginate influences the materials' thermal behaviour and may impact the thermal stability of the materials, especially in MB. As expected, the significant contribution of alginate to the degradation of composite materials appeared in samples B/A and MB/A beads through the appearance of successive decreasing thresholds of the weight loss with increasing temperature values, and this was recorded in both N_2 gas and air flow (Fig. III.7a and b). These outcomes explain that the alginate material has a weak structure and is quickly affected by heat, as mentioned in previous studies (Hammoudi et al., 2020).

Based on TGA and DTG analyses utilizing N_2 gas (Fig. III.7 and 8), the three observed types of weight loss in the materials serve to delineate and elucidate the degradation of functional groups. The initial stage of degradation reflects the initial loss attributed to the removal of moisture from the materials (30°C – 200°C). Subsequently, the second stage (200°C – 400°C) entails the degradation and elimination of hydroxyl groups (–OH) from organic compounds, accompanied by the decomposition of aliphatic structures such as C=C bonds (alkenes) and the liberation of constituent water from these structures, occurring within the temperature range of 200 °C to 400 °C. Potential decomposition of ketones and carboxylates may occur, resulting in the decline of carbonyl groups (C=O). This degradation, coupled with the decomposition of anhydride and ether functional groups (if present in the materials), leads to the release of CO and CO_2, transpiring between 200 °C and 400 °C. A potential degradation of Si–O and C–O groups, commencing at 400 °C. Beyond the 400 °C mark, the final phase of weight loss signifies the decomposition of aromatic compounds, releasing volatile materials (Hadj-Otmane et al., 2022).

III.7. Ash content analysis of samples

In general, the ash content could be calculated using the forenamed method *ASTM D1762* or obtained from the TGA analysis. In our case, ash content calculations were performed using the *ASTM D1762* method and then was compared with the results of the TGA method. However, the TGA equipment required a sample mass of very low weight to analyse the samples compared to the direct method *ASTM D1762*.

III.7.1. Calculation and results

Table III.6 shows the results of ash content analysis for four different samples: PS–biochar, B/A, MB, and MB/A. Ash content is a measure of the total mineral content in a material and is often used in various industries to provide insights into the purity and composition of a material The calculated results of the mentioned samples were heeded by the forenamed method (*ASTM D1762*).

To ensure accurate outcomes, the test was conducted using two samples for each type of material 1 and 2. The abbreviation of ‘’Total’’ represents the total weight of the crucible containing the materials of the sample.

The different calculation of the ash content % were obtained using the applied equation:

$$\frac{W_{before} - W_{after}}{W_{before}} \times 100 \qquad \text{(III.1)}$$

Table III.6. Ash content analysis for the four materials.

		PS–biochar	B/A	MB	MB/A
Weight before the test (g)	**Crucible empty 1**	25.83	25.70	30.53	31.10
	Material 1	0.30	0.30	0.31	0.30
	Total 1	26.13	26.00	30.83	31.41
	Crucible empty 2	14.31	14.32	14.37	14.98
	Material 2	0.30	0.30	0.30	0.30
	Total 2	14.61	14.62	14.67	15.29
Weight After the test (g)	**Total 1**	25.83	25.72	30.67	31.20
	Total 2	14.32	14.34	14.52	15.08
ASTM D1762	**Ash content 1 %**	**1.33**	**6.27**	**47.09**	**30.66**
	Ash content 2 %	**1.99**	**7.34**	**48.72**	**32.35**
	Average %	**1.66**	**6.81**	**47.90**	**31.51**
TGA method	**Ash content**	**4.01**	**6.92**	**48.71**	**30.74**

From the results, the ash content varies significantly among the different samples. Magnetic–biochar (MB) has the highest ash content (47.9%), followed by magnetic–biochar/alginate bead (MB/A) (31.51%), biochar/alginate bead (B/A) (6.81%), and the initial PS–biochar (1.66%).

III.7.2. Discussion in the results

Peanut shell biochar appears to have a relatively low ash content of 1.66%. This suggests that the biochar preparation process effectively removed most of the non–carbonaceous components, leaving behind a predominantly carbon–based material.

The ash content in the biochar/alginate bead (B/A) (6.81%) is higher compared to pure peanut shell biochar. This increase can be attributed to the addition of alginate, which may contain mineral impurities or ash.

The magnetic–biochar (MB) sample has a significantly higher ash content (47.9%) compared to pure PS–biochar and B/A. This substantial increase in ash content could be attributed to the incorporation of iron–based reagents ($FeCl_3$ and $FeSO_4$) during the preparation process. These reagents likely contributed to the higher ash content.

Similar to the magnetic–biochar/alginate bead (MB/A), the combination of alginate and magnetic–biochar also increased the ash content (31.51%). However, it is still lower than the ash content in the magnetic biochar itself. This suggests that while alginate contributed to the ash content, the iron–based reagents in the magnetic biochar have a more significant effect on increasing ash content.

The TGA technique provided similar result in the ash content values of samples However, PS–biochar sample showed a negligible difference between the results of the two ash content methods. This could be due to TGA method that required a very small quantity of sample's weight.

III.8. Textural property of samples

Fig. III.9 showcases the N_2 (nitrogen gas) adsorption and desorption isotherms for four dried materials: PS–biochar, magnetic–biochar, B/A bead, and MB/A bead. Following the classification prescribed by the *IUPAC* as articulated by Thommes et al., (2015), the isotherm profile for PS–biochar B/A, MB, and MB/A bead falls into *Type IV* (exhibiting hysteresis loops akin to *H3–type*. This classification signifies their characterization as mesoporous materials.

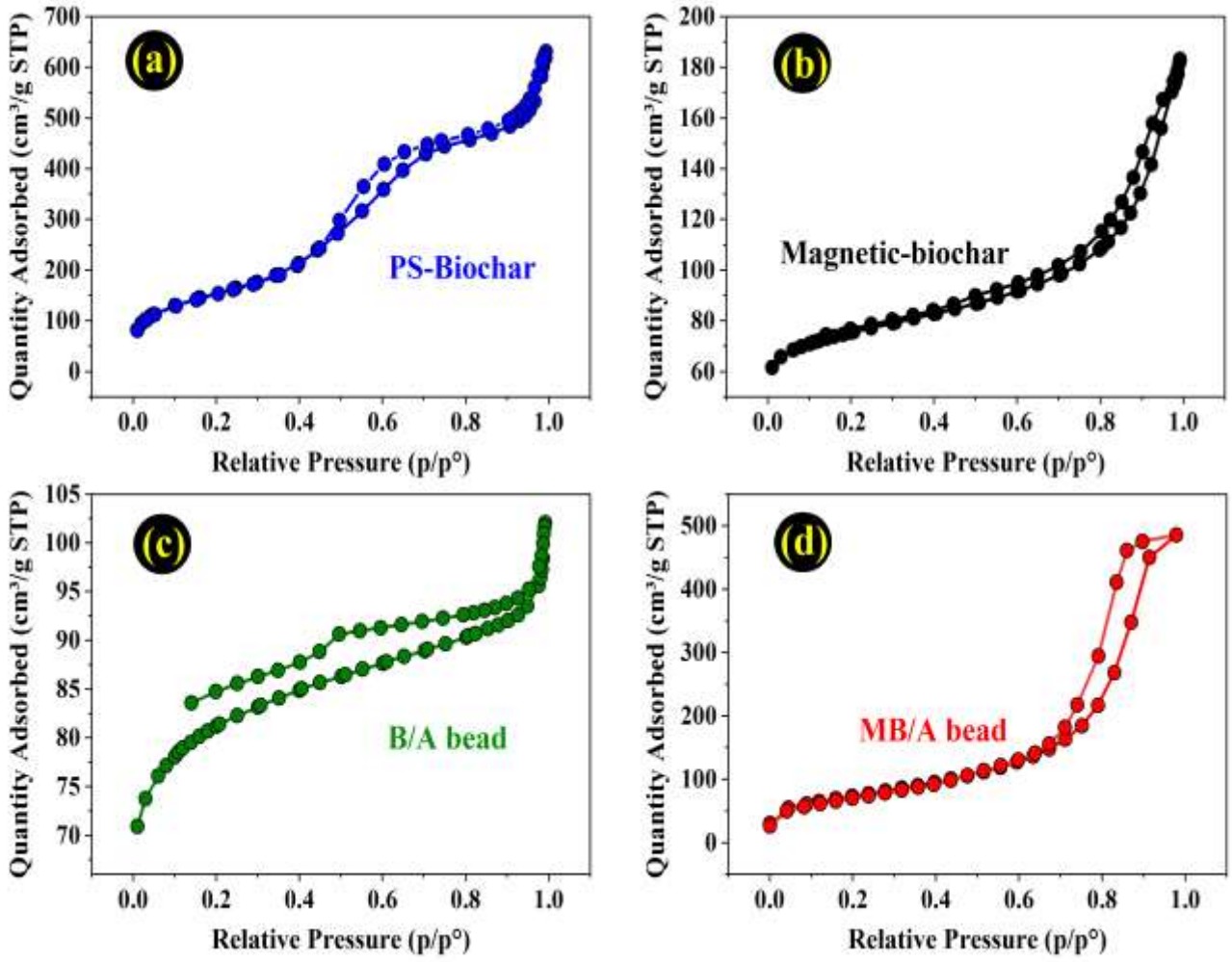

Fig. III.9. N_2 isotherm at 77K for (**a**) PS–biochar, (**b**) magnetic–biochar, (**c**) B/A bead, and (**d**) MB/A bead.

Intriguingly, the pore widths of these materials fall within the mesoporous range, spanning from 2 to 50 nm. Specifically, the initial peanut shells biochar showcases a pore width focalized at 4.24 nm, MB (18.5 nm), B/A bead (2.90 nm), and MB/A bead (18.2 nm). A noticeable distinction arises in the specific surface area (S_{BET}) and total pore volume (V_{Total}) values between the initial PS–biochar and the other developed samples, as elucidated in Table III.7. Remarkably, PS–biochar powder exhibits substantially elevated S_{BET} and V_{Total} values at 553.1 m^2/g and 0.975 cm^3/g, respectively, in stark contrast to the comparatively modest values of B/A bead (353.25 m^2/g; 0.929 cm^3/g), MB (282.5 m^2/g; 0.318 cm^3/g), and MB/A bead (262.4 m^2/g; 0.751 cm^3/g). This stark contrast arises from the significant diminution in particle size for the former material

where the initial biochar its impressive textural properties are attributed to the minuscule dimensions of its particles, as explained by Fig III.10.

Table III.7. Textural parameters of samples (N_2 adsorption isotherm at 77 K).

Textural parameters	Unit	Materials			
		PS–biochar	MB	B/A bead	MB/A
S_{BET}	m^2/g	553.1	282.5	353.25	262.4
S_{Ext}	m^2/g	—	—	—	248.9
S_{Micro}	m^2/g	—	—	—	13.47
V_{Total}	cm^3/g	0.975	0.318	0.929	0.751
V_{Micro}	cm^3/g	—	—	0.041	0.0051
L_o	nm	7.051	4.50	2.43	11.44

Generally, materials endowed with a considerable specific surface area typically manifest heightened adsorption capacity and enhanced solute diffusion rates compared with counterparts possessing a lowered S_{BET}. Nevertheless, it becomes apparent that the adsorption process for potentially hazardous metallic elements, such as copper ions, operates under a different mechanism than that for organic molecules. For example, Palm petiole biochar, boasting an S_{BET} of 640 m^2/g, V_{Total} of 0.430 cm^3/g, and L_o (average pore width) of 3.37 nm, proves effective in adsorbing crystal violet (CV) dye through mesopore–filling. This efficacy is attributed to the substantial molecular dimensions of the CV dye, measuring 1.34 by 1.28 nanometres, as expounded by Chahinez et al., (2020). In contrast, the endeavour to adsorb Cd^{2+} Cu^{2+} ions, characterized by a diminutive hydrated radius of 0.097 and 0.072 nm and a hydrated ionic radius of 0.263 and 0.295 nm, respectively, into the internal pore network of B/A or dried MB/A bead materials through pore–filling emerges as a nonviable proposition (Al-Zboon, 2023; Visa et al., 2010).

The adsorption of Cd^{2+} and Cu^{2+} ions entail the involvement of alternative mechanisms, encompassing ion exchange, coordination complexes, and electrostatic attraction (Li et al., 2010; Tran, Lee, et al., 2017; Zhang et al., 2015). These observations underscore the intricate interplay of material properties, surface area, and the nature of adsorbates, enriching our understanding of adsorption processes at the nanoscale (Ben Salem et al., 2023).

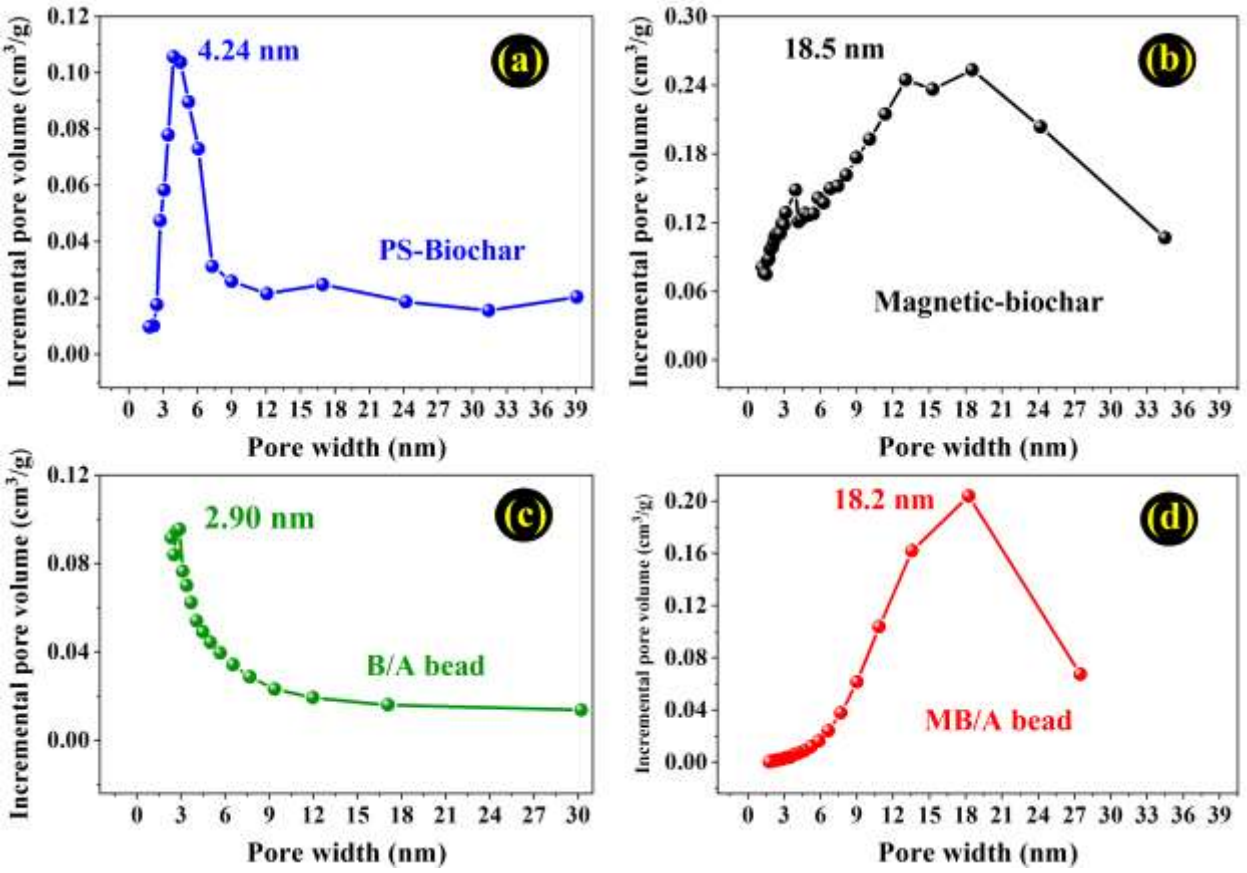

Fig. III.10. Pore distribution size obtained by BJH method for (**a**) PS–biochar, (**b**) magnetic–biochar, (**c**) B/A bead, and (**d**) MB/A bead.

III.9. The pH_{PZC} of samples

The isoelectric point, abbreviated as pH_{PZC}, signifies the pH at which a surface charge of the adsorbent becomes neutral. This point is a tipping scale, where the propensity of the adsorbent materials to attract or repel other molecules reaches equilibrium. Understanding the significance of pH in adsorption mechanisms is crucial in unravelling the behaviour of substances interacting with surfaces. At the heart of this phenomenon lies the concept of the pH_{PZC}, a pivotal juncture where the surface charge of substances shifts to a neutral state. The interplay between pH and pH_{PZC} governs whether a surface becomes anionic or cationic, greatly influencing adsorption.

In our case, the direct drift method was utilized to define the pH_{PZC} values of the different studied samples due to their ease and simplicity. Based on this technique, the obtained experimental data are plotted (Fig. III.11), and the diverse parameters along with the pH_{PZC} results are summarized in Table III.8.

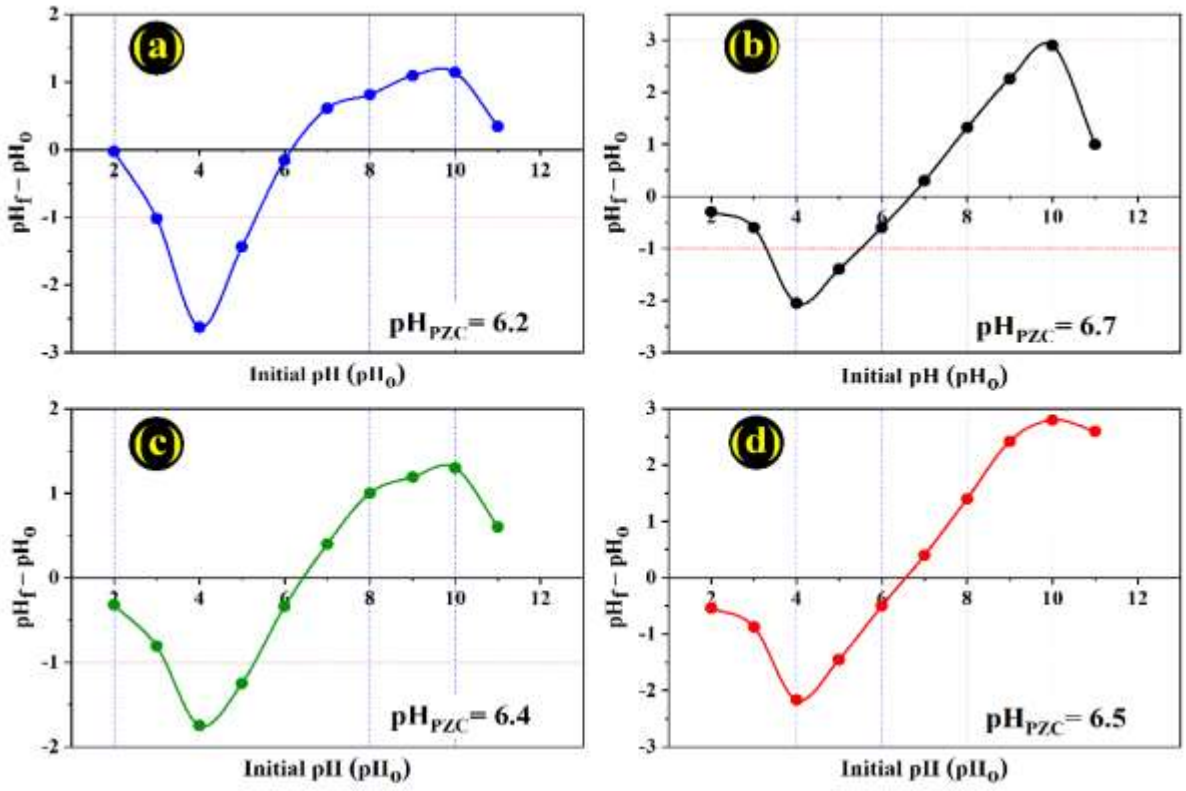

Fig. III.11. pH_{PZC} of: (**a**) PS–biochar, (**b**) MB, (**c**) B/A and (**d**) MB/A

From the results, the pH_{PZC} of the prepared samples ranges from 6.2 to 6.7, and this is due to the nature of the materials used in the preparation. In our case, for example, alginate and biochar are alkaline.

These materials (PS–biochar, MB, B/A, and MB/A adsorbents) will act as cationic (positive charge +) or anionic (negative charge –) exchangers depending on the solution pH. To grasp the significance of pH_{PZC}, envision the adsorbent surface charge as a dynamic entity. At pH values lower than the pH_{PZC}, the surface tends to be positively charged, while at pH levels higher than pH_{PZC}, the surface leans toward negativity. This dichotomy of surface charge becomes the linchpin of adsorption behaviours.

In other words, when the pH of the surrounding environment dips below the pH_{PZC} of the adsorbent, an abundance of H^+ ions take centre stage. These ions act as proverbial guests, binding to the available functional groups on the surface. Conversely, as the pH surpasses the pH_{PZC} adsorbent, the prevalence of OH– ions prompt deprotonation. This leads to shedding positively charged protons from the surface functional groups.

Table III.8. pH_{PZC} data of the samples PS-Biochar, MB, B/A, and MB/A.

pH_o	pH_f				$pH_o–pH_f$				pH_{PZC}			
Samples	**PSB**	**MB**	**B/A**	**MB/A**	**PSB**	**MB**	**B/A**	**MB/A**	**PSB**	**MB**	**B/A**	**MB/A**
2	2.03	2.30	2.32	2.54	–0.03	–0.30	–0.32	–0.54	**6.2**	**6.7**	**6.4**	**6.5**
3	4.02	3.60	3.81	3.87	–1.02	–0.60	–0.81	–0.87				
4	6.63	6.06	5.75	6.17	–2.63	–2.06	–1.75	–2.17				
5	6.44	6.40	6.25	6.45	–1.44	–1.40	–1.25	–1.45				
6	6.16	6.60	6.34	6.50	–0.16	–0.60	–0.34	–0.50				
7	6.39	6.70	6.60	6.60	0.61	0.30	0.40	0.40				
8	7.19	6.68	7.00	6.60	0.81	1.32	1.00	1.40				
9	7.91	6.74	7.81	6.58	1.09	2.26	1.19	2.42				
10	8.86	7.10	8.70	7.20	1.14	2.90	1.30	2.80				
11	10.66	10.00	10.40	8.40	0.34	1.00	0.60	2.60				

Note: PSB is PS–biochar

III.10. Techno–economic feasibility

The cost estimation of the prepared biochar, magnetic–biochar, biochar/alginate bead (B/A), and magnetic–biochar/alginate (MB/A) bead production involves various factors that significantly impact economic efficiency. Andreas et al., (2021) employed a *Direct Operating Cost* (*DOC*) method to approximate the synthesis cost of hydrogel beads–based composites. This method primarily focused on the cost of precursor materials, with reagents being the primary contributors.

In this research project, our previously published paper provided lower prices for the initial PS-biochar of 0.091 US$ based on the year 2021 prices (electricity prices 0.011 U$/kg; feedstock 0.015 U$/kg) compared to prices in the year 2024 (Ben Salem et al., 2023). This increase is not higher but could affect the prices when the quantity of materials increases for the industrial scale application.

To be updated, the cost calculation was adjusted to prices in 2024 (i.e., energy, chemicals, and feedstock prices). The supplier prices (chemicals) were not changed to refer. In essence, the calculation of the prepared adsorbents cost is summarized in Table III.9.

Table III.9. Calculation detail of the price for the prepared materials in this study.

Samples and materials	Mass used (kg)	Analytical laboratory grade				Industry grade	
		Suppliers (US$/kg)	China products (US $/kg)			China products (US $/kg)	
		Unit price	Total price	Unit price	Total price	Unit price	Total price
Peanut shells biochar			**0.248**				
Peanut Shells biomass	3.867	0.037	0.143	—	—	—	—
Energy consumption	3.010	0.035	0.11	—	—	—	—
Magnetic–biochar			**184.99**		**3.62**		**0.38–0.97**
PS–biochar	0.511	0.248	0.127	0.248	0.127	0.248	0.127
Iron (1): $FeCl_3$	0.331	17.28	5.722	2.00	0.662	0.60–0.80	0.199–0.265
Iron (2): $FeSO_4$–$7H_2O$	0.169	100.9	17.04	6.39	1.079	0.05–0.10	0.008–0.017
Sodium hydroxide (NaOH)	0.996	162.8	162.1	1.760	1.752	0.05–0.566	0.05–0.563
Biochar/alginate bead			**253.62**		**23.12–30.13**		**1.278–8.12**
Peanut shells biochar	0.515	0.248	0.128	0. 248	0.128	0. 248	0.128
Sodium alginate (SA)	0.515	177.7	91.60	42–45	21.63–23.18	2–15	1.03–7.73
$CaCl_2$	1.363	118.8	161.9	1–5	1.36–6.82	0.09–0.19	0.12–0.26
MB/Alginate bead			**348.8**		**24.85–31.86**		**1.348–8.49**
Magnetic–biochar	0.515	184.99	95.26	3.62	1.864	0.38–0.97	0.196–0.499
SA	0.515	177.7	91.60	42–45	21.63–23.18	2–15	1.03–7.73
$CaCl_2$	1.363	118.8	161.9	1–5	1.36–6.82	0.09–0.19	0.12–0.26

Note: The prices of Chinese products vary from one company to another and were obtained from Made-In-China's website. Energy consumption was used as Algeria prices in 2024 (for industry).

The chemicals were sourced from suppliers detailed in *Chapter II* (Materials and Methods), primarily relying on information from the *Trading China products* (website market). Our cost estimations for inputs, such as the feedstock (PS biomass) and energy consumption (grind, pyrolysis, dry), were based on Algerian local prices. During the experimentations, distilled water (DW) was accessible within the laboratory and was factored into the estimations for washing operations and solution preparation. However, the limited utilization of hydrochloric acid reagent

(HCl) for washing PS–biochar and MB materials was not considered a substantial component of our primary expenditure. The production process of adsorbent materials was designed on a laboratory scale, simplifying the cost estimation. Charges (costs) related to labour, taxes, equipment maintenance, and management were excluded. Additionally, expenses associated with collecting and transporting peanut shell wastes for biochar production were negligible. The other prices of chemical reagents, based on trading prices in China and different chemical suppliers, were the most critical input parameters, scaled up for one kilogram of dried materials.

The cost of producing peanut shells biochar was primarily based on feedstock material price (PS residuals), PS–biochar yield, and energy consumption. Energy and feedstock were deemed primary contributors, resulting in a cost feasibility of 0.248 US$/kg for PS–biochar production. Biochar is recognized as a low–cost material compared to activated carbon due to its chemical–free production process. Nematian et al., (2021) analysed biochar production costs under industrial scales, ranging from 0.449 US$/kg to 1.847 US$/kg.

The cost of magnetic biochar production was calculated based on PS–biochar and chemical prices, with negligible mass loss. The total production cost for dried magnetic biochar (0.38–184.99) was extremely dependent on chemical purity, trademark, and analytical grade. B/A (based on biochar) and MB/A (based on magnetic–biochar), exhibited variable costs, ranging from 1.278–8.12 US$/kg for B/A, and 1.348 – 8.49 US$/kg for MB/A (*industry–grade; China products*). The costs based on the analytical laboratory–grade provide 23.12–30.13 US$/kg for B/A and 24.85–31.86 US$/kg for MB/A. Supplier prices are the most expensive cost with 253.62 US$/kg for B/A and 348.8 US$/kg for MB/A. Thus, industry–grade prices are the most popular option for minimizing material production expenses in industrial applications (Ben Salem et al., 2023).

For industrial applications, cost considerations expand to factors like feedstock material, transportation, labour, taxes, maintenance, administration, energy, water, liquefied gas, and waste disposal, making the total cost for our adsorbents production sustainably higher than the calculated costs. However, the adsorbents designed in this study remain competitive in cost to previous studies, as shown in Table II.10.

Table III.10. Previous studies in techno–economic of adsorbent materials.

Adsorbent material	Total cost (US$/kg)	Study
Glutaraldehyde@alginate bead	3.17	Andreas et al., (2021)
Magnetic–biochar alginate bead	2850.25	Prasannamedha et al., (2022)
Commercial activated carbon	20 – 22	Babel & Kurniawan, (2003)
Market activated carbon	45.71	(http://hnhsty.com)
Pomelo peel biochar–KOH	9.82	Cheng et al., (2020)
Activated walnut shell biochar	6.97	Patel et al., (2022)
Magnetic rice biochar	116.2	Ajmal et al., (2020)
Rice biochar	108.2	Ajmal et al., (2020)

III.11. Conclusion

In this chapter, the properties of the prepared hybrid adsorbents (B/A and MB/A beads) based on the carbon, peanut shells biochar were demonstrated. The different samples were characterized using physicochemical, spectroscopic, and microscopic methods.

The characterization results confirmed the successful synthesis of all materials, especially the hybrid adsorbents B/A and MB/A beads that will be used for the adsorption of cadmium and copper ions, respectively. In addition, the design of B/A MB/A materials is applicable in the adsorption operations and even for other activities based on the obtained spherical and relatively uniform–sized beads with flotation and magnetic properties. The surface area obtained from the BET method was calculated to be 553.1 m^2/g (PS–biochar), 282.5 m^2/g (MB), 353.25 m^2/g (B/A bead), and 262.4 m^2/g (MB/A bead).

The techno–economic of our materials was studied in detail. The cost estimations US$/kg in the year 2024 of the initial PS–biochar (0.248), MB (0.38–184.99), B/A bead (1.278– 253.62), and MB/A bead (1.348–348.8) were technically comparable and could be used as cost–effective adsorbent.

Chapter IV

Adsorption of cadmium and copper onto the hybrid adsorbents

Chapter IV: Adsorption of cadmium and copper onto the hybrid adsorbents

IV.1. Introduction

This chapter is divided into two large parts. The study was focused on the adsorption of cadmium and copper solutions using two different hybrid adsorbents in the batch system:

- ❖ Adsorption of Cd ions onto biochar/alginate B/A bead.
- ❖ Removal of Cu ions using magnetic–biochar/alginate MB/A bead.

The two parts of our research begin by studying the effect of pH solution to choose the pH corresponding to the absorption of metal ions (Cd^{2+} or Cu^{2+}). The second section is the effect of time on the adsorption process for each bio–adsorbent to determine the stirring time required to reach the adsorbent/adsorbate equilibrium. Exploring the equilibrium time led us to investigate the influence of the cadmium or copper initial concentration on its adsorption onto the adsorbents in detail (third section). The fourth section will be concerned with the temperature effect on the metal ion adsorption at varied initial concentrations. By studying overall, modelling the experimental data to examine the kinetic and isotherm using multiple selected models along with the thermodynamic model allows us to explain and discuss the results and go through the suitability of the adsorption process. The investigated results allow us to know the mechanism involved in each system for the mentioned experiments, calculate the maximum quantity of metal ions eliminated by our materials, and understand the behaviour of the adsorption processes.

In the last section, the reusability of the developed hybrid adsorbents was studied to confirm their efficiency and cost–effective as eco–friendly materials.

IV.2. Cadmium adsorption onto the biochar/alginate (B/A) bead

IV.2.1. Adsorption study

IV.2.1.1. Influence of solution pH and adsorption mechanism

To comprehend the adsorption behaviour of Cd metal ions, it must first grasp the importance of solution pH. pH, a measure of the acidity or alkalinity of a solution, plays a pivotal role in determining the mechanisms behind adsorbent/adsorbate interactions. It acts as a silent orchestrator, guiding the entire process.

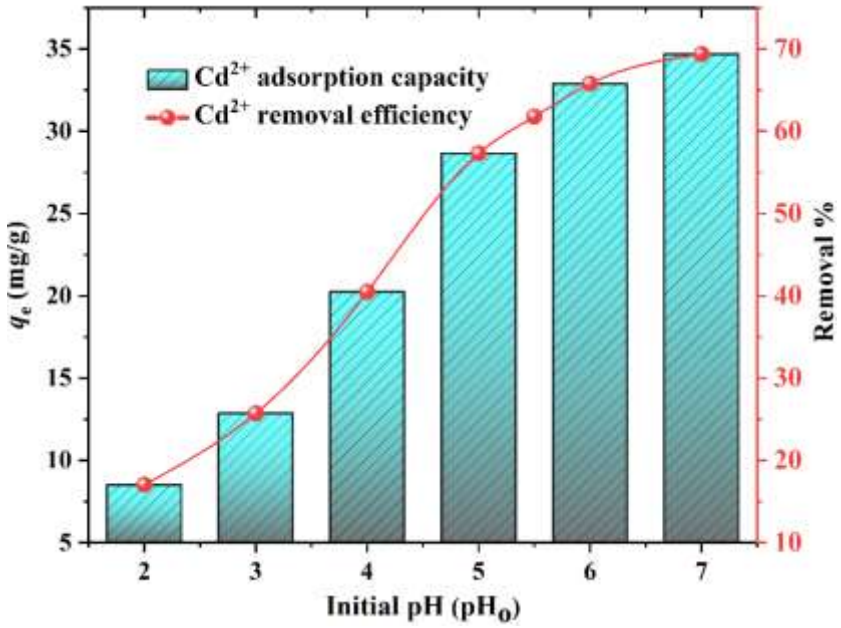

Fig. IV.1. pH effect (C_o = 50 mg/L, t = 240 min at 200 rpm, pH = 2 – 7.0, m/V = 1g/L, and at T = 15°C).

As expected, the results from Fig. IV.1 shows that the pH of the solution effectively impacts the adsorption of Cd^{2+} ions onto the B/A bead. As the pH increases from 2.0 to 7.0, the adsorption capacity (q_e) and the removal efficiency (R%) of the B/A beads are enhanced by q_e = 8.52 to 44.94 mg/L and 17% to 69%, respectively. This trend is consistent with the findings of other studies (Alves et al., 2019; Kataria & Garg, 2018). The pH_{PZC} of the B/A bead is 6.4, which means that the surface of the bead is positively charged at pH values below 6.4, and negatively charged at pH values above 6.4. When B/A surface is the positive state (protonation of the carboxylic acid groups), the metal ions are repulsed which reduced the adsorption capacity (electrostatic repulsion). These carboxylic acid groups are more protonated at lower pH values, which makes them less negatively charged and more likely to form a bond with the Cd^{2+} ions. The negative charge (–) attracts the positively charged (+) Cd^{2+} ions, which supports the formation of electrostatic bonds (electrostatic attraction) (Tran et al., 2016a). This is because the cadmium ions are also attracted to the carboxylic acid groups on the surface of the adsorbent. This trend leads to improve the adsorption capacity. However, the increase in adsorption with increasing pH levels was maintained at pH values above the pH_{PZC}. The reason for the improvement in adsorption capacity at pH < pH_{PZC} is the complexation mechanism by forming a soluble complex between the cadmium ions and the functional groups on the surface of the B/A adsorbent (Yadav et al., 2021).

In addition to the electrostatic interaction and complexation, the adsorption of cadmium ions onto biochar/alginate beads may also involves other mechanisms: the limited contribution of pore–filling (mainly found in the biochar) and the high contribution of ion exchange (characterised by the alginate). The ion exchange mechanism is the exchange of the cadmium ions for other ions already present on the surface of the adsorbent (i.e., Ca^{2+}) (Aichour, 2019; Aichour et al., 2019). In general, cadmium hydroxide is existed in different species including Cd^{2+}, $Cd(OH)_2$, $Cd(OH)^-_3$, and $Cd(OH)^+$ and their percentage (%) is controlled by the solution pH as depicted in Fig. IV.2 (Farooq et al., 2010). However, the optimal pH for Cd^{2+} uptake in our study is around 5.0 because at this pH value there is no precipitation phenomenon in the adsorption process (Farooq et al., 2010; Sočo & Kalembkiewicz, 2016). Further studies were used pH 5.0 to adsorb Cd^{2+}, such as alginate beads prepared by Ayouch et al., (2020b, 2020a), and magnetic alginate beads (Alves et al., 2019). It can be concluded from the results that the relative importance of these different mechanisms will depend on the pH of the solution and the properties of the B/A adsorbent. Thus, the prepared B/A bead adsorbent can be a promising material for the uptake of Cd^{2+} ions from water.

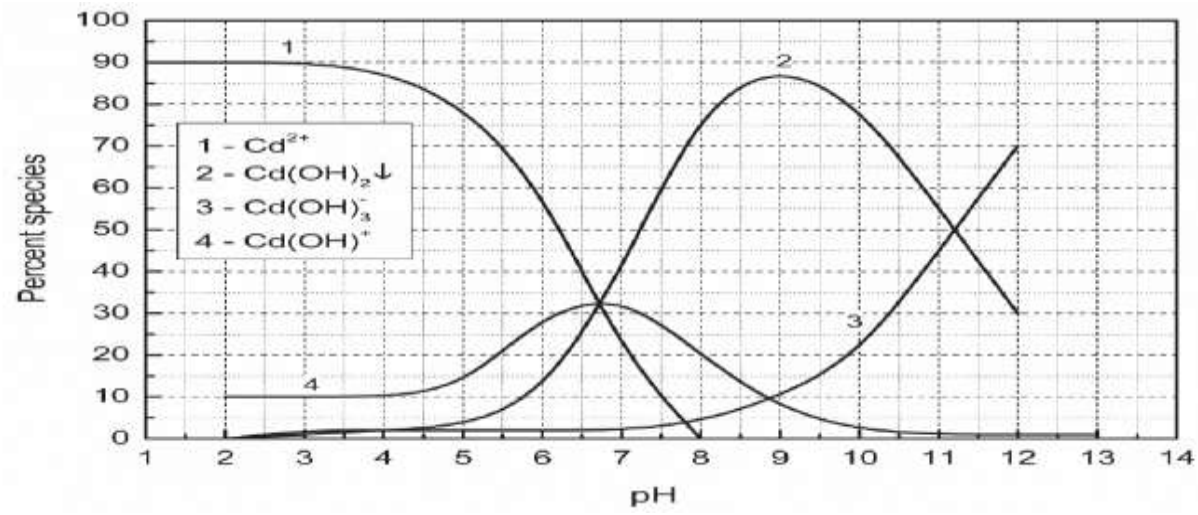

Fig. IV.2. Cadmium species distributed at pH of different values (Farooq et al., 2010).

Other mechanisms were reported in previous studies as further contributors to the adsorption of Cd ions onto different adsorbents. Tran et al., (2016b) mentioned in their paper that cadmium ions–π interactions could provide a further mechanism (π–donor), and similar conclusions were published elsewhere (Teng et al., 2020; H. Wang et al., 2015).

IV.2.1.2. Contact time effect and equilibrium

This section aims to investigate how the contact time of the adsorption operation influences the uptake of Cd^{2+} ions from a solution by the B/A adsorbent. The results of our adsorption study involving Cd^{2+} ions onto biochar/alginate B/A bead at an initial concentration of 50 mg/L and varying contact times provide valuable insights into the efficiency of this adsorption system (Fig. IV.3). Over 360 minutes, the adsorption capacity (q_e; mg/g) steadily increased from an initial value of 1.04 mg/g at 5 min to a maximum of 34.40 mg/g at the equilibrium time of 300 min. Thus, the optimum stirring time for the adsorption of Cd^{2+} ions onto the B/A bead is 300 min. Concurrently, the removal efficiency (R%) also showed a notable rise with increasing contact time. Starting at 2.07% (at 5 min), it reached a remarkable 68.81% (at 300 min), defining the equilibrium state. This is because the cadmium ions have more time to diffuse to the surface of the B/A bead and interact with the binding sites.

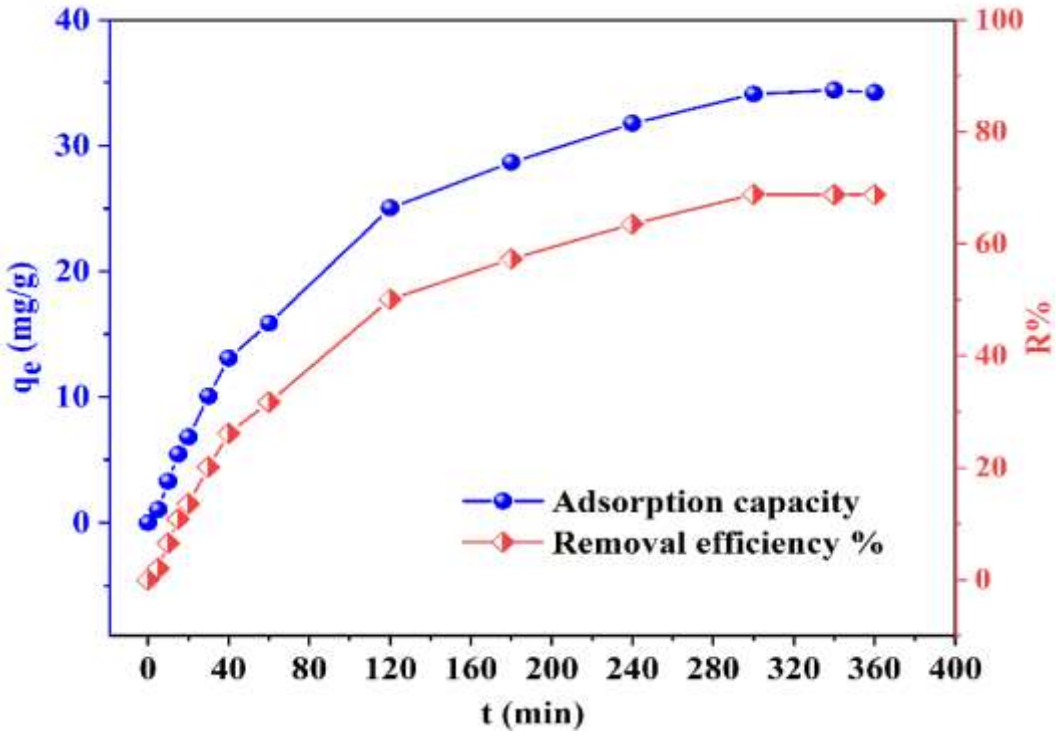

Fig. IV.3. Time effect on the adsorption of Cd^{2+} ions on B/A adsorbent (C_o = 50 mg/L, t = 0 – 360 min at 200 rpm, pH = 5.0, m/V = 1g/L and at T = 15°C).

The progressive increase in q_e and R% indicates that the adsorption process is time–dependent and acquired its equilibrium over an extended period, underlining the effectiveness of

biochar/alginate bead in removing cadmium ions from the solution. This trend suggests that longer contact times result in higher removal percentages, highlighting the importance of allowing sufficient time for the adsorption process to reach its highest potential.

IV.2.1.3. Effect of initial Cd^{2+} concentration

In this section, the influence of the initial Cd^{2+} amount on its adsorption process onto the B/A bead was investigated by varying the initial cadmium concentration from 2 to 200 mg/L at pH 5.0, temperature of 15°C, and solid/liquid ratio of 1 g/L ($m_{B/A}$ = 50 mg) (Fig. IV.4).

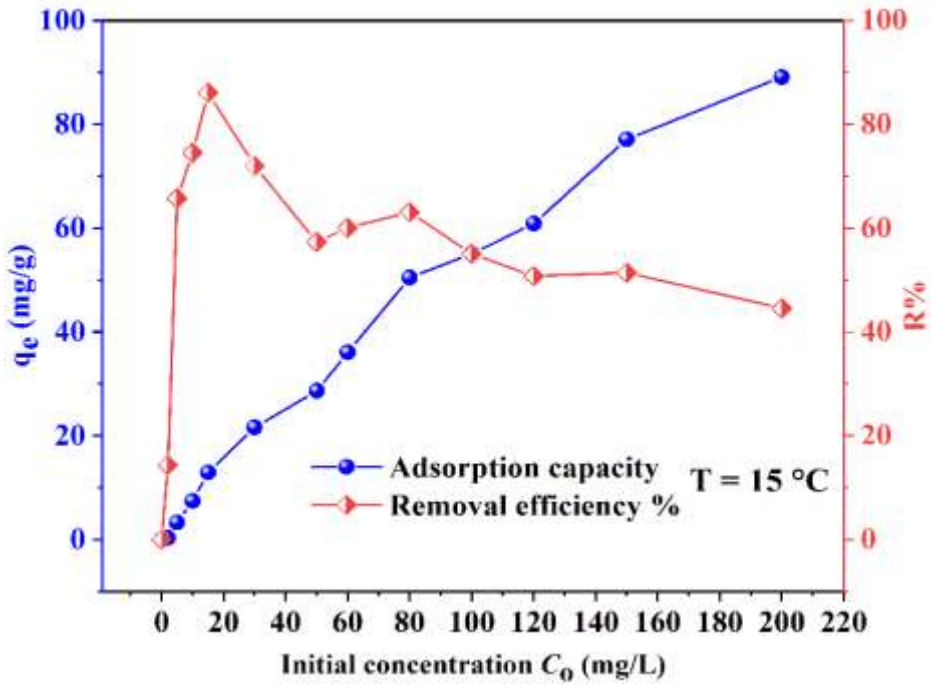

Fig. IV.4. Initial concentration effect on the uptake of Cd^{2+} ions by the B/A adsorbent (C_o = 2 – 200 mg/L, t = 240 min at 200 rpm, pH = 5.0, m/V = 1g/L and at T = 15°C).

The results indicate a clear correlation between the initial concentration (C_o) of cadmium ions and the adsorption capacity (q_e), along with the removal efficiency (R%) of the beads. As the initial concentration increases from 2 to 200 mg/L, q_e and R% show a consistent trend.

At weak initial concentrations, the adsorption capacity (q_e; mg/g) is relatively low, with q_e values ranging from 0.29 mg/g at C_o = 2 mg/L to 12.91 mg/g at C_o = 15 mg/L. However, as the initial concentration increases beyond 15 mg/L, q_e experiences a significant boost, reaching 89.09 mg/g at C_o = 200 mg/L. This suggests that the adsorption capacity of the beads is highly dependent

on the initial concentration of cadmium ions. R% follows a similar pattern with a gradual augmentation from 14.33% at C_o = 2 mg/L to 86.07% at C_o = 15 mg/L. It then stabilizes around 50 – 60% for higher initial concentrations.

The decrease in q_e and R% at higher initial concentrations is due to the saturation of the B/A bead with cadmium ions. The bead has a limited capacity to adsorb Cd ions, and once this capacity is reached, the additional Cd^{2+} ions will not be able to be fixed on the adsorbent surface.

IV.2.1.4 Effect of the change in temperature

The clear temperature–dependent impact on the Cd adsorption capacity of the B/A bead was confirmed in this study. The Cd^{2+} initial concentrations in the chosen temperatures (15, 30, and 45°C) were varied from 5 to 200 mg/L as depicted in Fig. IV.5.

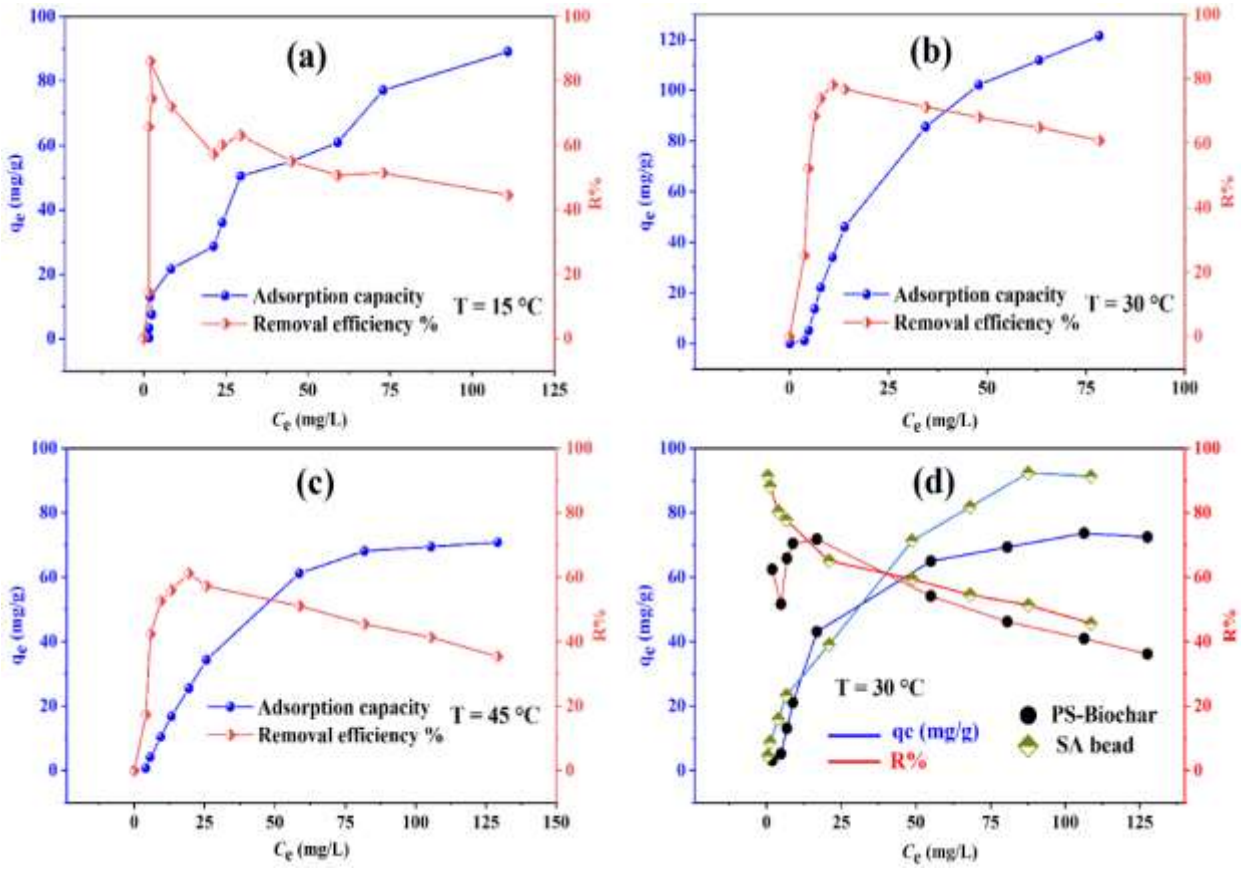

Fig. IV.5. Temperature effect on the uptake of Cd^{2+} by: B/A adsorbent (**a**) at 15°C, (**b**) at 30°C, (**c**) at 45°C, and (**d**) at 30°C for PS-Biochar and SA bead (C_o = 5 – 200 mg/L, t = 240 min at 200 rpm, at pH = 5.0, and m/V = 1g/L).

The results indicate that the Cd adsorption capacity (q_e) of the B/A bead rises with increasing temperature. Its removal efficiency (R%) in the three selected temperatures developed positively at the low initial concentration in the 30 – 50 mg/L range with the highest value of 80% and then decreased with percentages between 35% and 61%. At 15°C, as the initial concentration (C_o) of cadmium ions in the solution increases, the concentration at equilibrium (C_e) and the adsorbed quantity (q_e) also increase.

However, the removal efficiency (R%) of the metal ions shows a height of 74.5 % at initial concentrations of 10 mg/L and then declines with higher initial concentrations to 44.6% (200 mg/L), suggesting that the beads are most effective at lower Cd^{2+} ion concentrations at this temperature.

As temperature increases from 15 to 30°C, the diffusion of Cd^{2+} on the B/A adsorbent is expected to escalate. Similar conclusion was mentioned by (Kavand et al., 2020). This suggests that higher temperatures may lead to a more efficient adsorption process (Kataria & Garg, 2018). At 30°C, the q_e value of the beads toward Cd ions is significantly enhanced.

C_e and q_e values increase across all initial concentrations, indicating higher adsorption efficiency at 30°C for B/A, SA bead, and PS-biochar. R% also exhibits an increasing that the beads perform better at higher temperatures, especially at higher initial concentrations.

At 45°C, the adsorption capacity of the B/A bead declined compared to 15°C and 30°C. Also, it observed that R% reduced at this temperature for higher initial concentrations, suggesting the existence of Van der Waals force during the process (Chen et al., 2020).

Another reason for the lowering in the adsorption improvement could be attributed to the properties of the alginate biopolymer (Zhang et al., 2019). It can conclude that the best temperature to adsorb Cd^{2+} ions from water is at 30°C.

IV.2.2 Modelling of Cd^{2+} adsorption data

IV.2.2.1 Kinetic models

Fig. IV.6 showed the simulation of the plotted experimental kinetic data. The employed models were PFO, PSO, PNO, Avrami, Elovich and IP diffusion and their salient parameters are summed in Table IV.1.

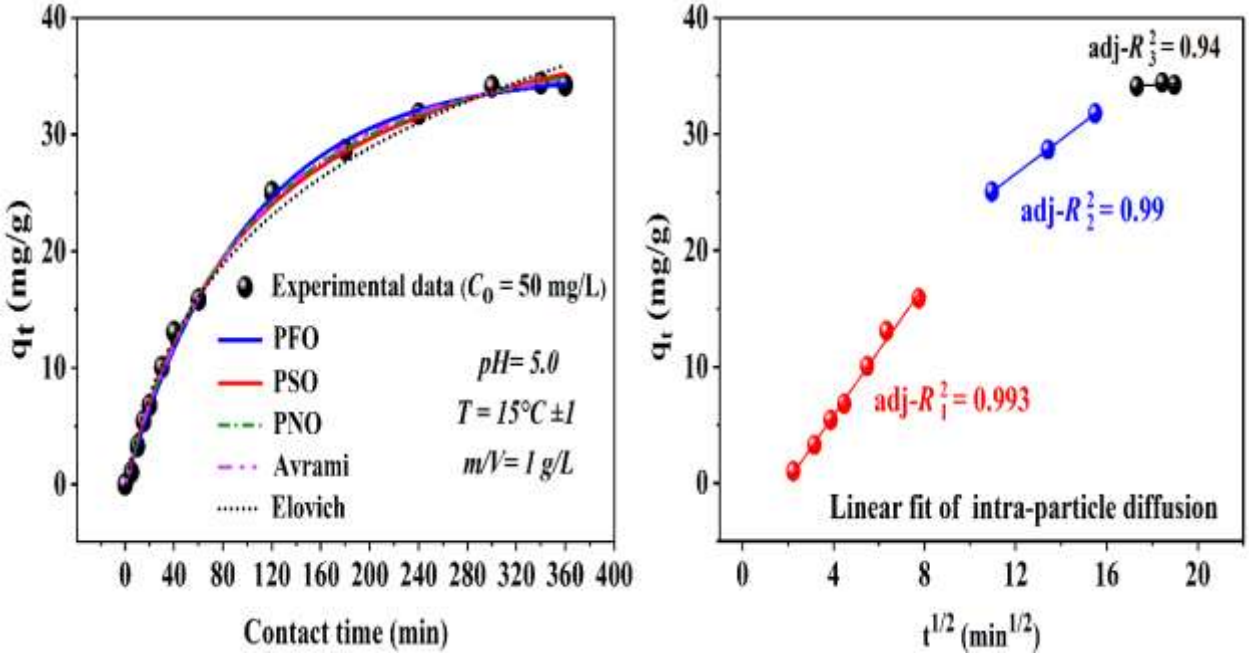

Fig. IV.6. Kinetic modelling using contact time data of Cd^{2+} + B/A (C_o = 50 mg/L, t = 0 – 360 min at 200 rpm, pH = 5.0, m/V = 1g/L and T = 15°C).

Reaching thermodynamic equilibrium between the liquid phase adsorbent and metal ions depends on various factors. The speed of diffusion of the constituents in the adsorbent and the contaminant solution with the different interactions in the solid/liquid can determine the nature of the process. The study of adsorption kinetics is crucial in understanding the underlying mechanisms involved. This provides valuable information that can help in gaining insight into the process.

The suitability metrics denoting a high adj–R^2, along with lower values of *SD* and reduced Chi–square (χ^2), indicate the conforming nature of kinetic data modelling. The sequential order observed in the modelling (t in minutes) was as follows: the pseudo–2nd–order, PNO, and Avrami.

The values of their parameters are significantly close to each other except in the Elovich model. The pseudo–1st–order model follows closely behind with an adj–R^2 of 0.996, *SD* at 0.78, and $\chi 2$ at 0.61, while the Elovich model takes a place as the last appreciate model because of its lower parameters.

However, the modelling of adsorption data exhibit the highest adj–R^2 at 0.997, lowest *SD* at 0.70 and with $\chi 2$ between 0.48–0.50. Thus, the adsorption process aligns admirably with all four non–linear kinetic models.

Furthermore, the adsorption capacity of the B/A bead, as determined by the pseudo–1st–order model at equilibrium ($q_{e,PFO}$ = 35.28 mg/g), demonstrates remarkable consistency with the experimental data ($q_{e,exp}$ = 34.40 mg/g). In contrast, the pseudo–2nd–order model yields a $q_{e,PSO}$ value of 45.97 mg/g, which surpasses $q_{e,exp}$. This observation suggests that the pseudo–first–order model is also the plausible description for the adsorption process of Cd^{2+} ions onto the B/A bead.

On the other hand, multiple factors influence the adsorption process, including the diffusion of Cd ions onto the B/A bead. Based on the experimental data and specifically on the plot of the adsorbed quantity (q_e) with $t^{1/2}$, a linear curve is observed where this line passes through the origin, indicating that IP diffusion is involved in the fixation of the adsorbed metal ions. Thus, the process of Cd adsorption onto the B/A bead involves three steps: film diffusion (1), intraparticle diffusion (2), and the equilibrium state (3) (Fig. IV.6b).

Furthermore, the suitability of the IPD model revealed by its parameters (Table IV.1) supports the discussed observation where R^2 is between 0.94 and 0.999 and *SD* in the range of 0.02 – 0.43. Overall, these findings furnish valuable insights into the adsorption process, which can be utilized to develop efficient and effective adsorption systems.

Table IV.1. Fitted parameters of the selected kinetic models for experimental data of the cadmium adsorption onto B/A bead.

Experiment and Model equation	Model Parameter	Parameter Unit	Cd + B/A value
Experimental data	$q_{e,exp}$	mg/g	34.40
1. PFO equation $q_t = q_e(1-e^{-k_1 t})$ (VI.1)	$q_{e,PFO}$	mg/g	35.25
	k_1	1/min	9.99
	adj–R^2	—	0.996
	SD	—	0.78
	χ^2	—	0.61
2. PSO equation $q_t = \frac{q_e^2.k_2.t}{1+q_e.k_2.t}$ (VI.2)	$q_{e,PSO}$	mg/g	45.97
	k_2	g/(mg × min)	0.197
	adj–R^2	—	0.997
	SD	—	0.70
	χ^2	—	0.49
3. PNO equation $q_t = q_{e,PNO} \times \left[1-\left[\frac{1}{(1+(m-1)\times(q_{e,PNO}{}^{(m-1)})\times k_{pno}\times t)}\right]^{\frac{1}{m-1}}\right]$ (VI.3)	$q_{e,PNO}$	mg/g	40.17
	k_{PNO}	g^{m-1}/(min × mg^{m-1})	0.0015
	m	—	1.501
	adj–R^2	—	0.997
	SD	—	0.699
	χ^2	—	0.489
4. Avrami equation $q_t = q_e(1-e^{-(K_{Av}t)^{n_{Av}}})$ (VI.4)	$q_{e,Av}$	mg/g	36.55
	k_{Av}	1/min	0.009
	n_{Av}	—	0.919
	adj–R^2	—	0.997
	SD	—	0.707
	χ^2	—	0.500
5. Elovich equation $q_t = \frac{1}{\beta}\ln(\alpha.\beta.t+1)$ (VI.5)	a	mg/(g × min)	0.5235
	β	g/mg	0.0759
	adj–R^2	—	0.993
	SD	—	1.082
	χ^2	—	1.169
5. IP diffusion equation $q_t = k_{ipd}t^{(1/2)} + C$ (VI.6)	$k_{IPD,1}$	(mg/g.$min^{1/2}$)	2.79
	C_1	(mg/g)	5.76
	adj–R^2	—	0.993
	SD	—	0.43
	$k_{IPD,2}$	(mg/g.$min^{1/2}$)	1.47
	C_1	(mg/g)	8.82
	adj–R^2	—	0.999
	SD	—	0.02
	$k_{IPD,3}$	(mg/g.$min^{1/2}$)	0.03
	C_1	(mg/g)	32.40
	adj–R^2	—	0.940
	SD	—	0.17

Note: All equations were mentioned before in detail in Chapter II.

IV.2.2.2 Equilibrium models

To assess the adsorption capacity of materials, isotherm modelling is a crucial analytical technique. This study employed non–linear plots to fit experimental data to four prominent isotherm models: Langmuir, Freundlich, Sips, and Redlich–Peterson. These models are well–regarded for their ability to describe adsorption phenomenon accurately (Fig. IV.7).

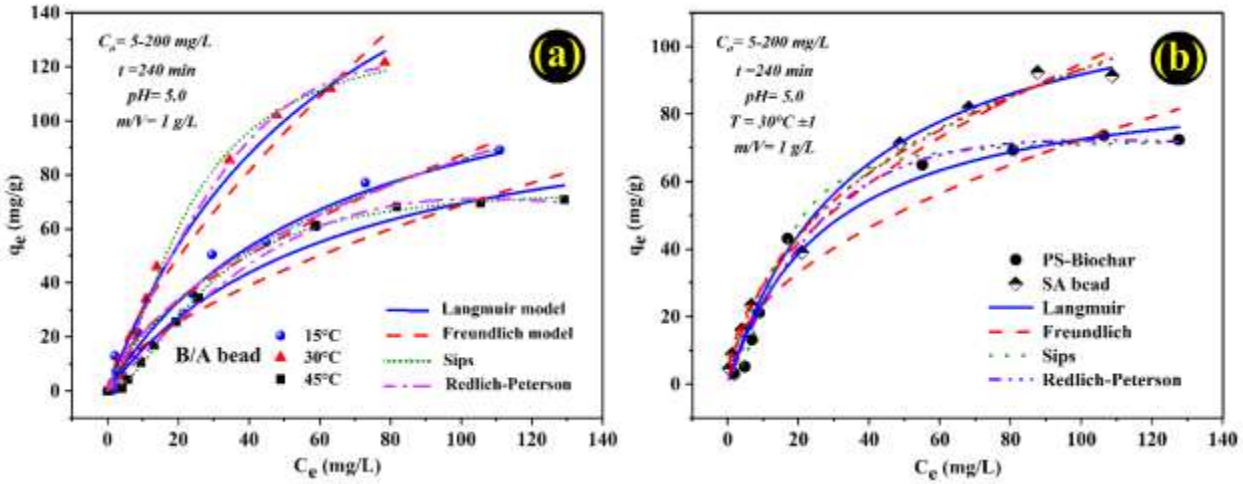

Fig. IV.7. Isotherm modelling for data of Cd–adsorption onto B/A, PS–biochar, and SA bead (C_o = 5 – 200 mg/L, t = 240 min at 200 rpm, at pH = 5.0, and m/V = 1g/L).

The findings summarized in Table IV.2 present a comprehensive view of the parameters obtained from the isotherm modelling. The goodness–of–fit indicators, including adjusted R^2, *SD*, and χ^2, and, all demonstrated favourable values, ranging from 0.91 to 0.998 1.058 to 9.62, and 1.12 to 92.7, respectively. These results suggest that the chosen models effectively captured the adsorption data at various temperatures. Among the four models, the Sips isotherm exhibited superior data fitting compared to them.

This finding points towards a heterogeneous adsorption system, where the Sips model better represents the complex adsorption dynamics. In line with the Langmuir model, it identified that B/A bead adsorption capacity for Cd^{2+} ions reached its maximum at 30°C, boasting an impressive Q_{max} of 230 mg/g. Notably, even at a relatively lower temperature of 15°C, the Q_{max} remained substantial at 139 mg/g. The Q_{max} values of PS-biochar and sodium alginate bead at 30°C were found to be lower compared to the B/A bead adsorbent, showcasing its superior performance in metal ions uptake over both the PS-biochar and SA bead.

Table IV.2. Fitted parameters of Langmuir, Freundlich, Sips and Redlich–Peterson (R–P) models for experimental data of the cadmium adsorption onto B/A bead, PS–biochar, and SA bead.

Model and its equation	**Model Parameters**	**Unit**	**B/A bead**			**30°C**	
			15°C	**30°C**	**45°C**	**PSB**	**SA**
1. Langmuir equation	Q_{max}	mg/g	139.0	230.0	114.1	92.9	125.6
	K_L	L/mg	1.553	1.537	1.553	0.035	0.027
$q_e = \frac{Q_{max}.K_L.C_e}{1+K_L.C_e}$ (VI.7)	adj–R^2	—	0.974	0.980	0.975	0.91	0.985
	SD	—	4.77	6.62	4.53	9.28	4.33
	χ^2	—	22.82	43.90	20.60	28.35	18.73
2. Freundlich equation	n_F	—	1.66	1.38	1.61	1.96	9.06
	K_F	$mg^{1-1/n}.L^{1/n}.g^{-1}$	5.46	5.71	3.95	2.053	7.69
$q_e = K_F.C_e^{(1/n)}$ (VI.8)	adj–R^2	—	0.974	0.958	0.937	0.906	0.985
	SD	—	4.80	9.62	7.33	9.28	4.26
	χ^2	—	23.01	92.70	53.78	86.28	19.92
3. Sips equation							
	Q_{max}	mg/g	222.95	134.62	76.09	72.57	185.75
	K_{Sips}	$(mg/L)^{-1/n_{Sips}}$	0.017	0.006	0.002	0.005	0.033
$q_e = \frac{Q_{max}.K_{Sips}.C_e^{n_{Sips}}}{1+K_{Sips}.C_e^{n_{Sips}}}$ (VI.9)	n_{Sips}	—	0.781	1.611	1.821	1.98	0.736
	adj–R^2	—	0.976	0.993	0.998	0.995	0.989
	SD	—	4.66	3.68	1.058	2.11	3.73
	χ^2	—	21.71	13.55	1.121	4.42	13.97
4. R–P equation							
	K_{r-p}	L/g	4.12	2.93	1.33	2.63	6.47
	a_{r-p}	$(mg/L)^{-g_{r-p}}$	0.229	2.87	7.86	0.005	0.241
$q_e = \frac{K_{r-p}.C_e}{1+a_{r-p}.C_e^{g_{r-p}}}$ (VI.10)	g_{r-p}	must be ≤1	0.610	1.85	2.02	1.35	0.69
	adj–R^2	—	0.975	0.985	0.994	0.977	0.986
	SD	—	4.67	5.68	2.43	4.57	4.20
	χ^2	—	21.83	32.22	5.91	20.89	17.71

Note: PSB is PS–biochar and all equations were mentioned before in detail in Chapter II.

It is important to highlight that the Q_{max} value dipped to 114.1 mg/g at 45°C, albeit still demonstrating considerable adsorption capacity. To underscore the exceptional performance of B/A bead as a cadmium ion adsorbent, the Table IV.3 compared the theoretical adsorption capacity (Q_{max}), as predicted by the Langmuir model, with data from other materials documented in the existing literature. A glance at Table IV.3 reveals that the B/A adsorbent prepared in this study outshines other materials previously investigated in Q_{max} in m/g: biochars (37.6 – 114.7), different activated carbonaceous materials (75.6 and 117.9), and alginate composites (24.2 – 94.3) previously investigated. Thus, B/A bead could be used as an effective material for water treatment.

Table IV.3. Different studies compared with our study in the Cd^{2+} adsorption capacity (Q_{max}).

Study	**Conditions of experiment**					**Q_{max} (mg/g)**	**Developed materials**
	***m/V* (g/L)**	**pH_{eq}**	**C_{Cd} (mg/L)**	***T* (°C)**	***t* (h)**		
Jeon, (2018)	1.0	4.0	10 – 100	25	3	37.6	Peanut shells biochar
Teng et al., (2020)	1.0	6.0	10 – 600	25	5	92.7	Pinecone biochar
Tran et al., (2016a)	2.0	7.0	50 – 600	25	6	114.7	Orange peel biochar
Kavand et al., (2020)	5.0	7.0	0 – 800	30	2.5	117.9	Granular– AC
Sardella et al., (2015)	0.6	6.0	10 – 200	20	2	75.6	Grape pomace–AC
Alves et al., (2019)	0.7	6.0	10 – 250	25	1	94.3	Magnetic SA
Ayouch et al., (2020)	1.0	7.0	10 – 100	25	4	53.2	Bentonite/SA
	1.0	7.0	10 – 100	25	4	54.3	Sludge/SA
Liu et al., (2020)	2.0	6.0	25 – 200	24	24	24.2	Water hyacinth biochar/SA
	2.0	6.0	25 – 200	24	24	46.0	Magnetic–biochar/alginate
This study	1.0	5.0	5–200	15		139.0	B/A bead
				30		230.0	
				45		114.1	
				30		92.9	PS–biochar
				30		125.6	SA bead

Note: AC is activated carbon and SA is sodium alginate.

IV.2.2.3 Thermodynamic model

The standard parameters of thermodynamics (given in kJ/mol) concerning the Gibbs free energy (also known as available energy) ($\Delta G°$) associated in terms of both enthalpy ($\Delta H°$) and entropy ($\Delta S°$) were used to recognize the temperature change impact on the cadmium adsorption operation. The Cd adsorption process was performed under different temperatures T_1 = 15°C, T_2 = 30°C, and T_3 = 45°C (transformed for the calculations to the Kelvin unit). To investigate the effect of temperature, some computations were applied using the and Van't Hoff and Gibbs equations as explained in the next example of calculation as mentioned by Tran, (2022).

Example for the calculation of thermodynamic parameters

- Calculation of K_C value:

$$K_C \approx K_L\left(L/mg\right) \times M_{element}\left(mg/mol\right) \times C°\ \left(mol/L\right) \quad \text{(VI.11)}$$

K_C (15°C) = 0.0155 * (112.411*1000) * 1 = 1742 => ln K_C = 7.46

The same operation was used for the calculation of K_C values at 30°C and 45°C. After that, by plotting ln K_C versus 1/T values, the Van't Hoff equation were generated as dipected in Fig. IV.8.

The generated Van't Hoff equation: Y = −91.94x + 7.77

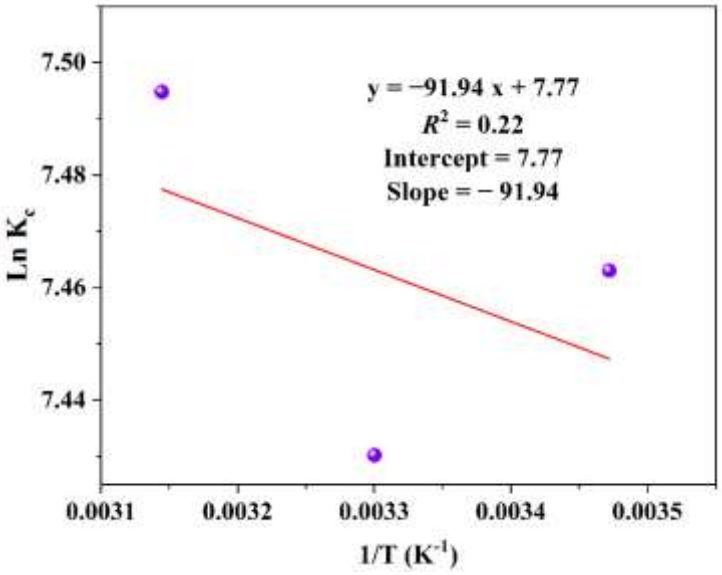

Fig. IV.8. Van't Hoff graph for Cd^{2+} adsorption onto B/A bead (linear equation and detail).

- Calculation of Gibbs parameters: the Gibbs parameters values were obtained using Van't Hoff equation detail (slope and intercept):

Standard Van't Hoff equation: $$Ln\ K_c = -\frac{\Delta H^\circ}{R} \times \frac{1}{T} + \frac{\Delta S^\circ}{R} \quad \text{(VI.12)}$$

Y = –91.94x + 7.77

Slope = −91.94 = $-\frac{\Delta H^\circ}{R}$ => $\Delta H° = -91.94 * \frac{8.314}{1000} = 0.764$ kJ/mol

Intercept = 7.77 = $\frac{\Delta S^\circ}{R}$ => $\Delta S° = 7.77 * \frac{8.314}{1000} = 64.6$ J/mol

For the calculation of $\Delta G°$ values at the different temperatures (15, 30, and 45C°), there are two helpful methods as the following:

Standard Gibbs equation: $$\Delta G° = -RT\ ln\ K_L \quad \text{(VI.13)}$$

$\Delta G°$ (15°C) = $-\frac{8.314}{1000}$ * ln (0.0155) = –17.87 kJ/mol

Direct calculation: $$\Delta G° = \Delta H° - T\Delta S° \quad \text{(VI.14)}$$

$\Delta G°$ (15°C) = 0.764 – (288 * 0.0646) ≈ –17.84 kJ/mol

The calculated parameters values of the thermodynamic model for Cd^{2+} uptake onto B/A bead are summed in Table IV.4. The adsorption process shows remarkable energetic favourability. This conclusion stems from the negative values of $\Delta G°$, which are –17.87 kJ/mol (15°C), –18.72 kJ/mol (30°C), and –19.82 kJ/mol (45°C). These negative values signify that the process is spontaneous adsorption as a natural and self–driven phenomenon. $\Delta H°$ is a positive 0.764 kJ/mol. This positive value implies the endothermic adsorption process. $\Delta S°$ stands at a positive 64.6 J/mol, suggesting that the adsorption process increases the disorder or randomness of the system.

Table IV.4. Van't Hoff detail and Gibbs parameters of cadmium adsorption onto B/A bead.

Temperature	***K*C value**	**Van't Hoff detail**	**Thermodynamic parameters**		
			$\Delta G°$(kJ/mol)	$\Delta H°$(kJ/mol)	$\Delta S°$(J/mol)
T_1 = 288 K	1742	y = −91.94x + 7.77	−17.87	0.764	64.6
T_2 = 303 K	1686	R^2 = 0.22	−18.72		
T_3 = 318 K	1799	Intercept = 7.77	−19.82		
		Slope = −91.94			

However, the R^2 (~0.22) recorded in the van't Hoff equation is quite low. This makes the analysis operation for $\Delta H°$ and $\Delta S°$ parameters insufficient. Also, the recorded Q_{max} and K_L values do not match the expected order (15°C < 30°C < 45°C) (Nguyen et al., 2020).

Accordingly, $\Delta H°$ and $\Delta S°$ parameters were computed in two operations (Nguyen et al., 2020). The first process was at 288–303K, and the second was at 303–318K. The $\Delta H°$ parameter was computed by Eq. VI.15. $\Delta S°$ was obtained based on Eq. VI.15. $\Delta G°$ and $\Delta S°$ parameters were obtained from their respective equations (Eq. 13 and Eq. 14).

$$\Delta H° = R\left(\frac{T_2 \times T_1}{T_2 - T_1}\right)\ln\left(\frac{K_{T_2}}{K_{T_1}}\right) \quad \text{(VI.15)}$$

where T_2 and T_1 (with $T_2 > T_1$) denote temperatures for two process; K_{T1} and K_{T2} represent the constant K_C at their respective process T_2 and T_1, respectively.

According to Table IV5, a negative $\Delta H°$ value (−1.6 kJ/mol) was recorded in the first process, accompanied by an increase in the Q_{max} value from 139.0 to 230.0 mg/g. Conversely, a positive $\Delta H°$ value (3.5 kJ/mol) in the second process was followed by a decline in the Q_{max} value to 114.1 mg/g. This indicates the role of the van der Waals force in reaction to temperature increases (Chen et al., 2020). $\Delta S°$ values were positive. Nguyen et al., (2020) reported that this finding was due to the desorption/adsorption phenomenon. This process occurs first by desorption of the water content in the adsorbent and then the adsorption of the pollutant.

Table IV.5. Values of $\Delta H°$ and $\Delta S°$ parameters for Cd^{2+} uptake onto BAB (calculated at two process temperatures).

***T* (K)**	**$\Delta H°$ (kJ/mol)**	**$\Delta S°$ (J/mol×K)**
288−303	−1.6	57
303−318	3.5	73

IV.2.3 Regeneration of the loaded B/A beads

The reusability of adsorbents bears substantial pragmatic implications across various industries, owing to several pivotal factors encompassing cost–efficiency, sustainability, and operational efficacy (Azri et al., 2022). Moreover, the recyclability of adsorbents constitutes a key criterion in their selection and utilization. Nevertheless, it is imperative to acknowledge that certain

materials may undergo degradation or experience diminished effectiveness following repeated deployment, thereby necessitating the exploration of novel adsorbent materials to enhance the efficiency of the adsorption process. In light of this, the present study subjected the stable B/A beads to a series of rigorous tests involving exposure to 50 mg/L Cd^{2+} solutions through multiple adsorption cycles, followed by subsequent regeneration through desorption procedures (as depicted in Fig. IV.9).

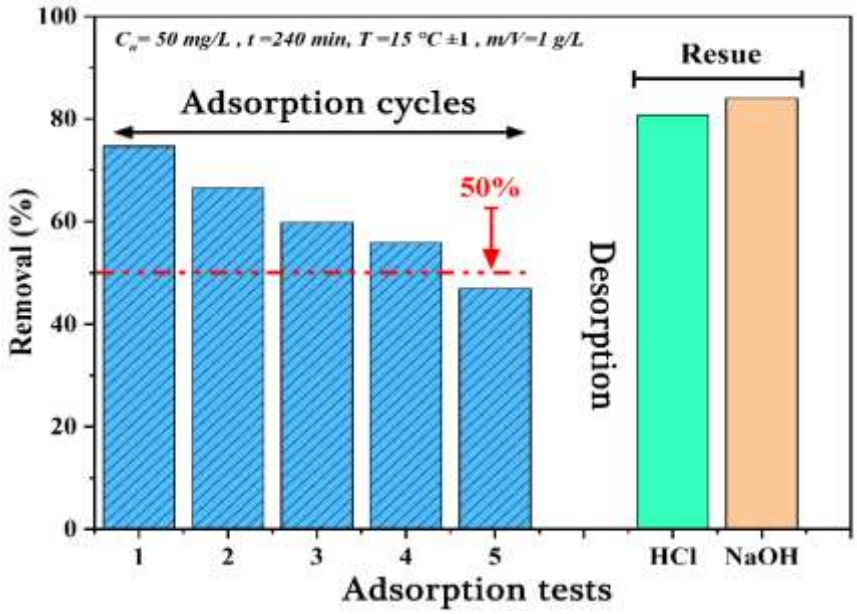

Fig. IV.9. Cd-adsorption cycles and reusability (after desorption) of MB/A bead (C_o = 50 mg/L, t = 240 min, pH = 5.0, m/V = 1g/L at T = 20°C).

The empirical findings unveiled a gradual reduction in the removal efficiency of cadmium ions over successive adsorption cycles, dwindling from an initial 75% in the inaugural cycle (Cycle 1) to a diminished 47% by the fifth iteration (Cycle 5). This decrement in the ion uptake rate can be ascribed to the depletion of active adsorption sites on the B/A material matrix. Conversely, the diminution in bead mass remained marginal, registering at less than 2% across five consecutive cycles. This minimal mass loss can be attributed to the intrinsic hardness and robust physical–chemical stability characterized by the B/A beads. Intriguingly, during the reusability evaluation, the beads showcased a notable uptick in their capacity, effecting an approximately 81% removal of metal ions from the aqueous medium—an increment of about 9% when juxtaposed against the initial deployment. It is noteworthy that the utilization of HCl emerged as a pivotal regenerative agent for B/A beads. The cumulative outcomes from this comprehensive analysis lend credence to

the conceivable deployment of B/A adsorbent as an indispensable solution within various industrial applications, thereby underscoring their potential significance in addressing contemporary environmental and sustainability challenges.

IV.3. Copper adsorption onto magnetic–biochar/alginate (MB/A) bead

IV.3.1. Adsorption study

IV.3.1.1. Influence of solution pH

In chemistry and materials science, understanding the behaviour of metal ions in solutions is a topic of immense implication. One crucial factor that significantly influences this behaviour is the level of the solution pH. One metal that exhibits intriguing pH–dependent adsorption behaviour is copper. The current research by shed light on this phenomenon, subjecting the MB/A bead. The results depicted in Fig. IV.10, reveal a compelling story: the number of copper ions adsorbed increases significantly as the pH of the working solution rises from 2.0 to 6.0.

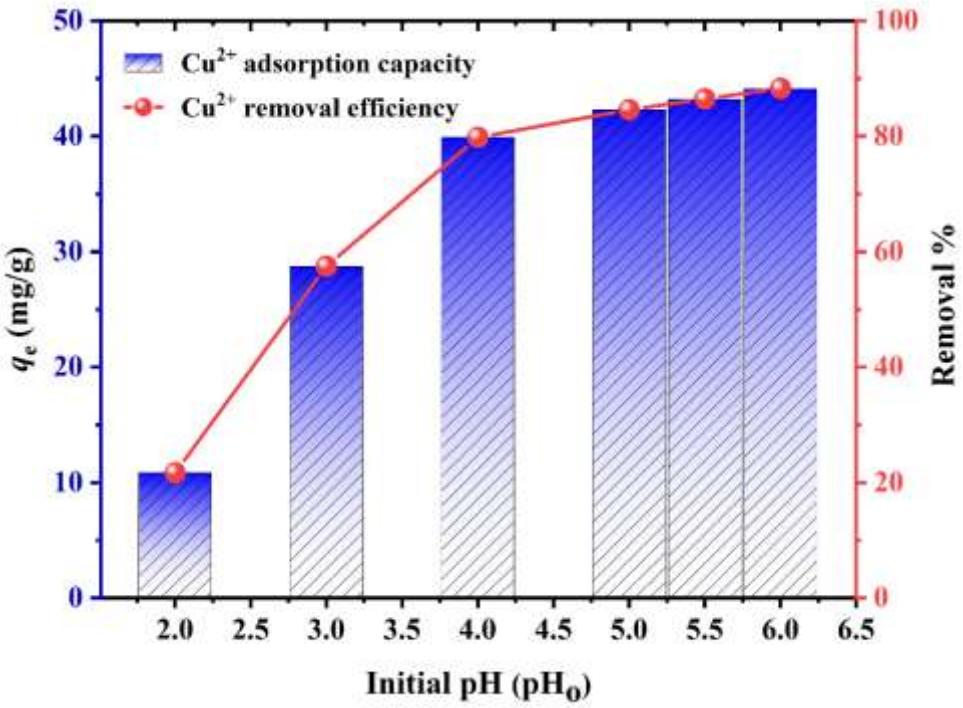

Fig. IV.10. pH effect (C_o = 50 mg/L, t = 240 min at 200 rpm, pH = 2– 6.0, m/V = 1g/L, and at T = 20°C).

At pH 2.0, the adsorption encounters a negative situation, and the process becomes chaotic. The culprit behind this unfavourable adsorption is the protonation of carboxylic groups in the

presence of excess H^+ ions, as explained by Ayouch et al., (2020a). This protonation hinders the copper ions from binding effectively due to the electrostatic repulsion. Instead, physical mechanisms like pore–filling, as elucidated by Hassan et al., (2022), come into play. This protonation creates a hostile environment for copper ions looking for a spot to settle.

In the rising stage of pH, moving from 2 to the pH < pH_{PZC} 6.5 (pH 6.0), the electrostatic competition between H^+ ions and Cu^{2+} for carboxylic groups starts to ease up. This easing of tension leads to a remarkable improvement in the adsorption efficiency, resulting in well adsorbing of copper ions, as reported by Tran et al., (2016a, 2017). The development indicates the existence of the surface complex force is more decisive than the electrostatic repulsion force during the adsorption process. Coordination usually existed between copper ions and –OH and –COOH chelating groups on the adsorbent surface (Yu et al., 2017a).

Fig. IV.11 illustrates the distribution of copper species with the change in the initial pH solution synthesized from the same salt used in our study ($CuSO_4$•$5H_2O$). Across a range of pH values from 1 to 14, as described by (Yang et al., 2016), it was observed that when the pH of the solution exceeded the 5.0 value, copper inherently transformed, converting into $Cu(OH)^+$ ions and precipitating as $Cu(OH)_2$ solids. For instance, at a pH of 7.0, the copper species in the solution consisted of approximately 70% Cu^{2+} ions, about 15% Cu $(OH)^+$ ions, and another 15% $Cu(OH)_2$ solids. Consequently, to maintain the presence of Cu^{2+} ions, adsorption experiments (kinetic and isotherm) were conducted at a pH equal to 5.0. Park et al., (2022) and Tran et al., (2017) also found similar patterns in their research. This consistency reinforces the validity of these findings and the significance of pH in metal ion adsorption.

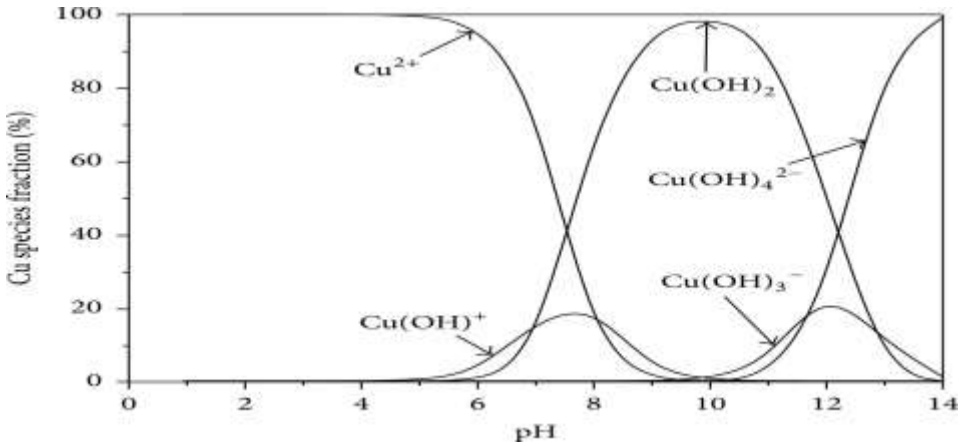

Fig. IV.11. Copper species variation (distributed) at different pH values (Yang et al., 2016)

IV.3.1.2. Contact time effect and equilibrium

The study aims to investigate how the contact time influences the removal of copper ions from a solution using MB/A adsorbent.

results show that the adsorption of Cu^{2+} increases with contact time (Fig. IV.12). The initial increase in the adsorption rate is rapid, with the amount of the adsorbed copper (q_e) improving from 27.3 mg/g to 46.19 mg/g in the first 40 minutes. After 60 minutes, the adsorption rate of the process slows down, and the amount of copper adsorbed reaches equilibrium at 48 mg/g (92%) at 180 minutes. The removal efficiency of copper (R%) also increases with contact time, reaching 98.81% after 360 minutes.

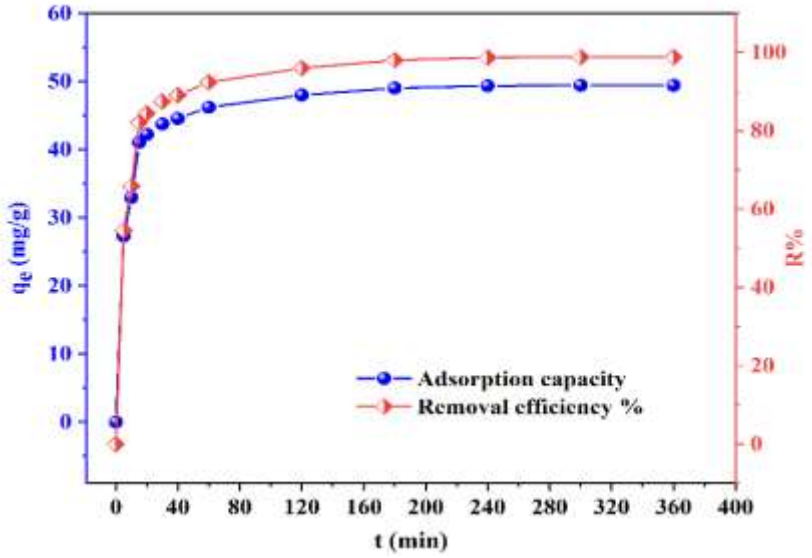

Fig. IV.12. Time effect on the adsorption of Cu^{2+} ions on MB/A adsorbent (C_o = 50 mg/L, t = 0 – 360 min at 200 rpm, pH = 5.0, m/V = 1g/L, and at T = 20°C).

The rapid initial increase in the adsorption rate is likely due to the rapid diffusion of copper ions to the surface of the beads. As the surface of the beads becomes saturated with copper ions, the diffusion rate slows down while the adsorption rate reaches equilibrium. The equilibrium adsorption capacity of the beads is 48 mg/g, which is a relatively high value. This suggests that magnetic–biochar/alginate bead is a promising adsorbent to treat copper water.

IV.3.1.3. Effect of initial Cu^{2+} concentration in single– and binary–metal systems

In single–metal (Cu ions only) and competitive (binary–metal of Cu + Cd ions in the solution) systems (Fig. IV.13), the effect of the initial copper amount on its adsorption process

onto the MB/A bead surface was investigated by varying the initial Cu^{2+} concentration from 5 to 200 mg/L and additional presence of Cd^{2+} ions (50 mg/L) for the binary–metal system at pH 5.0, 20°C (293 K) and solid/liquid ratio of 1 g/L ($m_{MB/A}$= 30 mg).

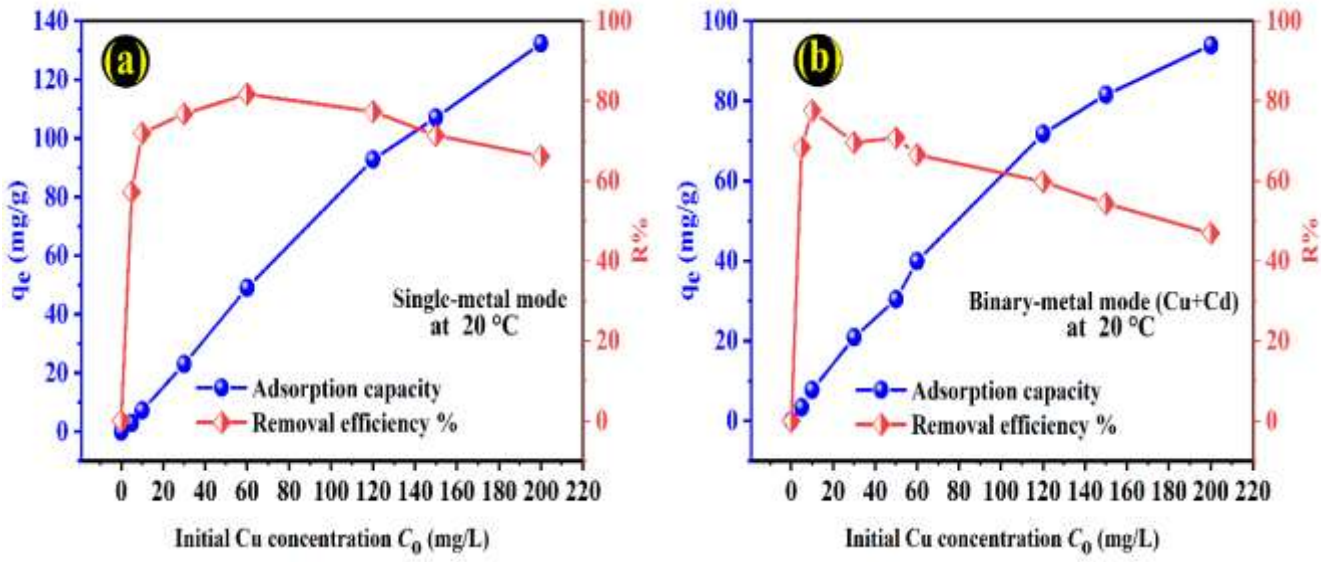

Fig. IV.13. Initial Cu^{2+} concentration effect on MB/A bead adsorption capacity in: (**a**) the Cu single mode and (**b**) the Cu + Cd ions binary system ($C_{o,\,Cu}$ = 2 – 200 mg/L, $C_{o,\,Cd}$ = 50 mg/L for binary–metal system, t = 240 min at 200 rpm, pH = 5.0, m/V = 1g/L, and at T = 20°C).

The results show that the initial concentration of Cu has a consequential influence on its adsorption onto magnetic–biochar/alginate beads (MB/A). In the single–metal system, the adsorption capacity (q_e) increased from 2.86 mg/g at an initial concentration of 5 mg/L to 132.31 mg/g at C_o = 200 mg/L. The removal efficiency (R%) also increased from 57.23% to 66.16% over the same range of initial concentrations.

The removal efficiency then plateaued at around 81% for initial concentrations of 60 mg/L and above. The saturation point of the adsorption isotherm is the maximum amount of adsorbate that can be adsorbed onto an adsorbent. The saturation point was acquired at an initial concentration of nearly 150 mg/L. This is because the higher the initial concentration of copper, the more copper ions are available to be adsorbed onto the beads.

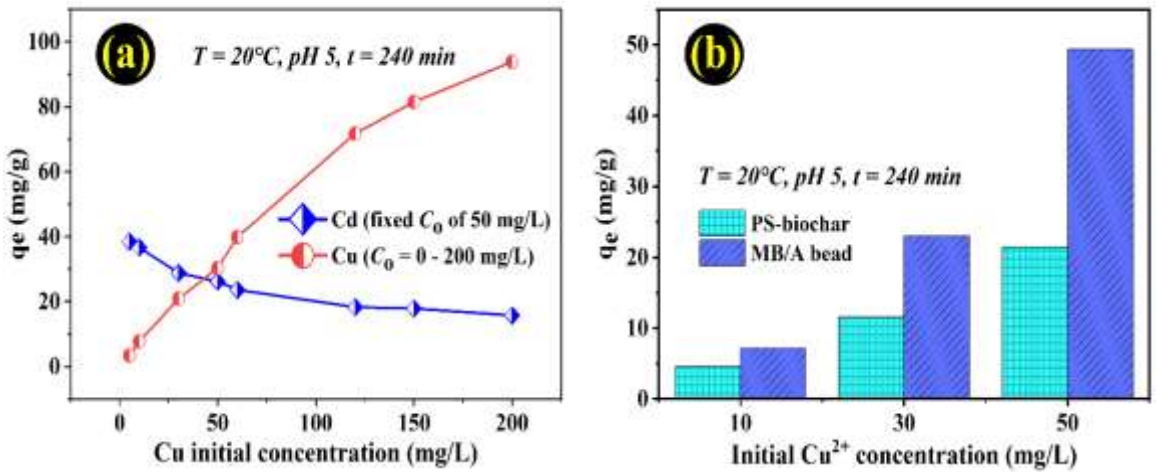

Fig. IV.14. (**a**) Cd^{2+} effect on Cu^{2+} adsorption onto MB/A bead, and (**b**) Comparison between PS–biochar and MB/A bead in Cu^{2+} adsorption capacity (C_o = 10, 30, and 50 mg/L, t =240 min at 200 rpm, pH = 5.0, m/V = 1g/L, and at T = 20°C).

In the binary–metal system, the additional cadmium (Cd^{2+}) ions inhibited the adsorption of Cu ions in solution. The q_e values were lower than those in the single–metal system, and the R% values were also lower. For example, at an initial concentration of 50 mg/L of copper, the q_e value was 7.75 mg/g in the binary–metal system, compared to 23.03 mg/g in the single–metal system. The R% value was 77.53% in the binary–metal system, compared to 81% in the single–metal system. This is because cadmium ions compete with copper ions for adsorption sites on the beads. The higher the concentration of cadmium ions, the more competitive they become, and the lower the adsorption capacity of the MB/A bead for copper ions. However, at the initial Cu concentration of 50 mg/L, the adsorbed quantities of copper and cadmium are close by 30.39 mg/g and 26.21 mg/g, respectively. Thus, the adsorbed quantity of both metal ions Cu and Cd onto MB/A is valuable even with the decline in maximum Cu–adsorption quantity.

Copper's higher affinity to oxygen-containing functional groups in adsorbents compared to cadmium is attributed to its transition metal properties (Tran et al., 2017; Yadav et al., 2021). If the adsorption mechanism only involves complexation, the adsorption capacity of MBA-beads for Cu^{2+} ions is unlikely to decline in the presence of Cd^{2+} ions. A decline in adsorption capacity may be due to the co-existence of other mechanisms like ion exchange. Cd^{2+} ions are more readily exchanged with Ca^{2+} in MBA-beads than Cu^{2+} ions. This suggests that ion exchange played a crucial role in the mechanism of Cu^{2+} adsorption. The cation exchange between Ca^{2+} in the Fe_3O_4-biochar/hydrogel bead and Cu^{2+}ion solution has been previously documented (Yu et al., 2017).

To confirm the superiority in the Cu^{2+} adsorption capacity (in the single–metal system) of the prepared MB/A bead over the pristine PS–biochar, a comparison test was conducted under varied initial concentrations of 10, 30, and 50 mg/L at 25 °C and pH 5.0. As expected, The MB/A bead showed an adsorption capacity twice what was recorded for the initial PS–biochar (Fig. IV.14).

IV.3.1.4. Effect of temperature

Energy consumption is an essential factor in the economic component of wastewater treatment on the industrial scale when considering the temperature that may affect the adsorption efficiency. The adsorption temperature in the single–metal was altered at different degrees (20, 30 and 40°C), while the other parameters were maintained at fixed values, such as contact time, pH (5.0) and dose of the MB/A bead (1 g/L) (Fig. IV.15).

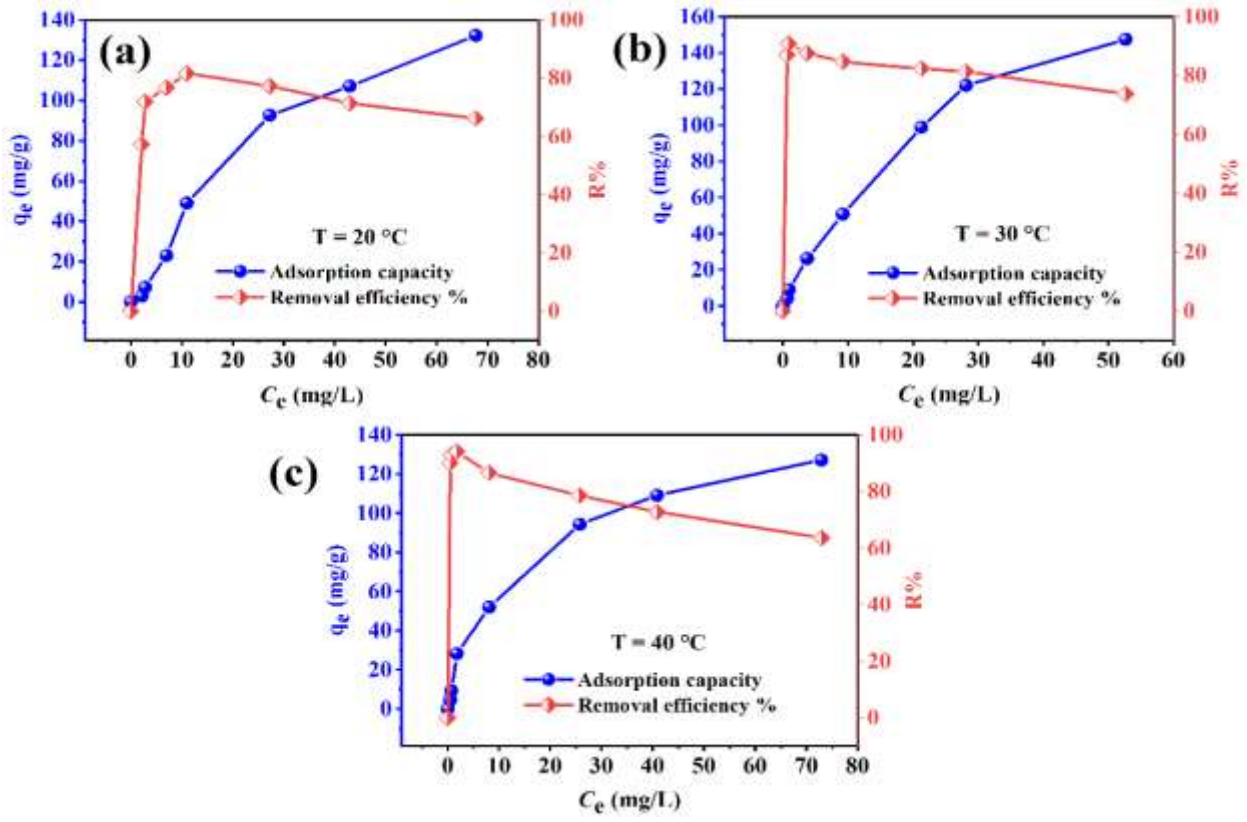

Fig. IV.15. Temperature effect on the Cu^{2+} adsorption by the B/A adsorbent: (**a**) at 20°C, at 30°C (**b**) and (**c**) at 40°C (C_o = 5 – 200 mg/L, t = 240 min at 200 rpm, at pH = 5.0, and m/V = 1g/L).

The results show that the adsorption of copper ions onto MB/A bead increases with increasing temperature. The temperature highly affected the adsorption of the low Cd initial concentration in the range of 5 to 30 mg/L onto the MB/A adsorbent (with a positive impact).

At 20°C, the removal efficiency (R%) of Cu^{2+} from water is 57.23%, 86.93%, and 89.94% for initial concentrations of 5, 10, and 30 mg/L, respectively. At 30°C, the R% is 86.9%, 90.74%, and 92.88% for the same initial concentrations. At 40°C, the R% is 89.94%, 92.88%, and 94.01%. This trend is consistent with the findings of other studies, which have shown that the adsorption of metal ions onto adsorbents is typically enhanced by increasing temperature. For example, Weng et al., (2007) studied the influence of the change in temperature on the uptake of copper ions using activated clay. The isothermal conditions were selected to be 4, 27, and 50°C. Their conclusions were identical to our investigation. Biswas, Meikap, et al., (2019) reported the same conclusion. They investigated the isothermal condition in the temperature range of 25–45 for copper and nickel removal using pine cone biochar filled in alginate beads.

The increase in adsorption with increasing temperature can be attributed to the fact that the kinetic energy of the molecules increases with temperature. This allows the molecules to move more freely and collide with the surface of the adsorbent more often, increasing the chances of adsorption. Likewise, the increased temperature can also cause the water molecules to become more disordered, creating more free sites on the surface of the adsorbent for the metal ions to bind to. For the three temperatures, the decrease in the removal efficiency (R%) above the initial concentration of 60 mg/L may be due to the possibility of reducing the adsorption sites into MB/A materials, which supports the outcomes mentioned before in *Section IV.3.1.3*.

On the other hand, the decrease in adsorption capacity (q_e; mg/g) at 40°C compared to 20 and 30°C is due to several factors. One possibility is that the increased temperature causes the water molecules to become more mobile, making it more difficult for the copper ions to bind to the surface of the adsorbent. Furthermore, the increased temperature can also cause the adsorbent to undergo structural changes, reducing its adsorption capacity. This finding was also observed for the adsorption of Cd^{2+} onto biochar–alginate bead (B/A) in our research. However, the adsorbed quantity of copper ions remained elevated even at this temperature (40°C), which make the MB/A bead a stable and effective adsorbent in different condition of temperatures.

IV.3.2. Modelling of Cu^{2+} adsorption data

IV.3.2.1. Kinetic models

The results of the kinetic data of the five selected models (PFO, PSO, PNO, Avrami, and Elovich) were estimated using the modelling method. The simulation curves of the models are depicted in Fig. IV.16 and their different parameters are summed in Table IV.6.

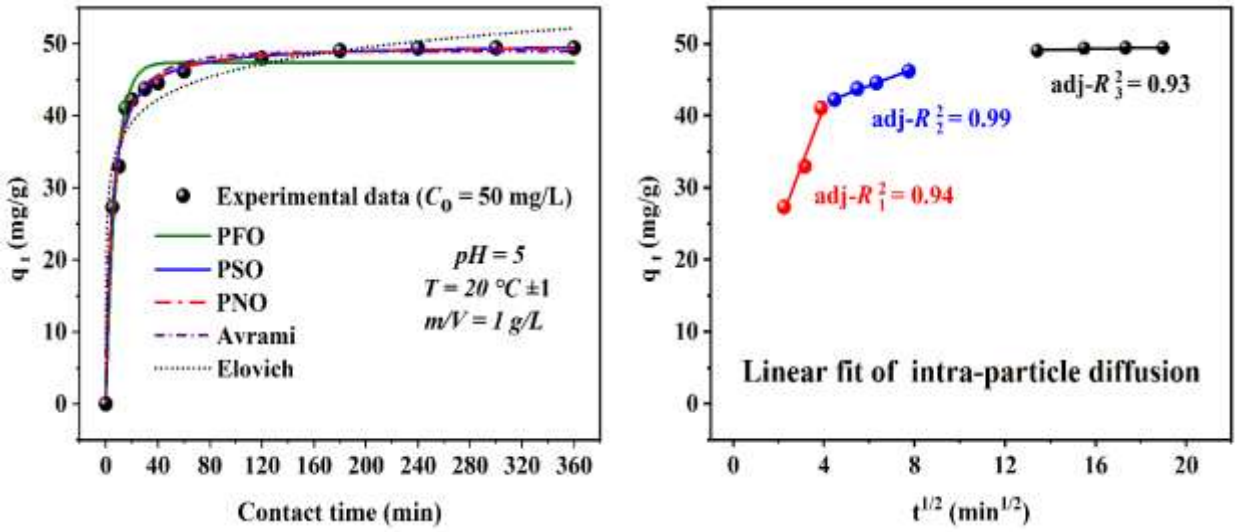

Fig. IV.16. Kinetic modelling using contact time data of Cu^{2+} + MB/A (C_o = 50 mg/L, t = 0 – 360 min at 200 rpm, pH = 5.0, m/V = 1g/L, and T = 20°C).

Adsorption kinetics were well–fitted to the equilibrium data by the chosen models, with adj–R^2 values of at least 0.96. The percentage (%) of dissimilarity in the adsorption capacity values obtained from the experimental ($q_{e,exp}$) and the model ($q_{e,mod}$) was significantly low where the lowest was for the Avrami model by 0.93% then the PSO model by 1.25% and PNO model by 1.26%, and the highest was for PFO model by 4.1%. The PSO model had the highest adj–R^2 value and lowest *SD* and reduced chi–squared ($\chi 2$) value, indicating the best fit to the experimental data compared to the rest of the selected models. Meanwhile, the exponent of PNO model (m_{PNO}) is near to 2. This value is consistent with the PSO model being a good fit for the data.

In general, the adsorption process is influenced by various factors like Cu ions diffusion and interactions with the particles of MB/A adsorbent. According to the intra–particle diffusion parameters (Table IV.6), the adsorption of Cu onto the MB/A bead involves three steps: film diffusion (1), intraparticle diffusion (2), and equilibrium plateau (3).

Table IV.6. Fitted parameters of the selected kinetic models for experimental data of the copper adsorption onto MB/A bead.

Experiment and models	Parameters	Unit	Value
Experimental data	$q_{e,exp}$	mg/g	49.39
1. PFO	$q_{e,\ PFO}$	mg/g	47.41
	k_1	1/min	0.1346
	adj–R^2	—	0.973
	SD	—	2.023
	χ^2	—	5.114
2. PSO	$q_{e,\ PSO}$	mg/g	50.01
	k_2	g/(mg × min)	0.0047
	adj–R^2	—	0.994
	SD	—	0.989
	χ^2	—	0.979
3. PNO	$q_{e,PNO}$	mg/g	49.87
	k_{PNO}	$g^{m-1}/(min \times mg^{m-1})$	0.0055
	m	—	1.956
	adj–R^2	—	0.994
	SD	—	1.036
	χ^2	—	1.073
4. Avrami	$q_{e,\ Av}$	mg/g	48.93
	k_{Av}	1/min	0.1441
	n_{Av}	—	0.5710
	adj–R^2	—	0.992
	SD	—	
	χ^2	—	1.419
5. Elovich	*a*	mg/(g × min)	1350
	β	g/mg	0.2223
	adj–R^2	—	0.957
	SD	—	2.871
	χ^2	—	8.244
6. IP diffusion	$k_{IPD,1}$	$(mg/g.min^{1/2})$	8.27
	C_1	(mg/g)	8.18
	adj–R^2	—	0.937
	SD	—	1.73
	$k_{IPD,2}$	$(mg/g.min^{1/2})$	1.19
	C_1	(mg/g)	37.02
	adj–R^2	—	0.990
	SD	—	0.15
	$k_{IPD,3}$	$(mg/g.min^{1/2})$	0.06
	C_1	(mg/g)	48.2
	adj–R^2	—	0.930
	SD	—	0.11

IV.3.2.2. Equilibrium models

The plotted data (curves) in Fig. IV.17 and parameters grouped in Table IV.7 of copper adsorption onto MB/A bead were obtained by fitting data to the Langmuir, Freundlich, and Sips equations.

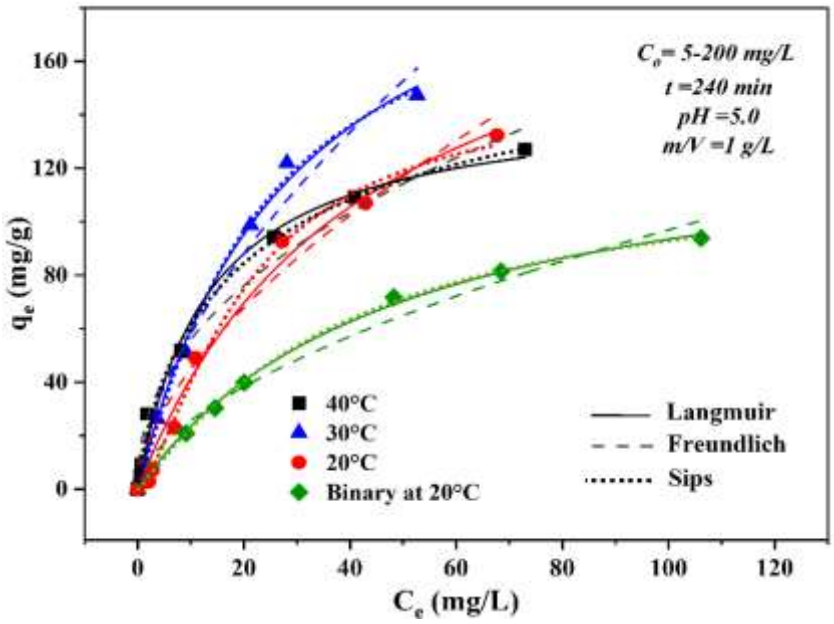

Fig. IV.17. Isotherm modelling for data of Cu^{2+} + MB/A adsorption system (C_o = 5 – 200 mg/L, t = 240 min at 200 rpm, at pH = 5.0, and m/V = 1g/L).

From the results, the values of the adj–R^2 (ranging between 0.965 and 0.996), *SD* (1.42 – 10.54) and χ^2 (2.026 – 111.1) suggested that the equilibrium data are well–fitted by all stated adsorption isotherm models. However, the Langmuir model was the best fit for the equilibrium data compared to the rest of models (Freundlich and Sips models). As expected from the Langmuir model calculations, the maximum adsorption capacity (Q_{max}) of MB/A bead at 20 °C showed the superiority of the single mode over the binary system, and they were estimated to be 218.72 and 139.37 mg/g, respectively. These values of Q_{max} demonstrated that the adsorbent had a greater adsorption affinity toward Cu^{2+} ions in the single mode, and there is a competition between Cu^{2+} and Cd^{2+} ions for adsorption sites of M/BA bead which decreased the adsorption capacity of copper. Moreover, the hybrid adsorbent exhibited a high Q_{max} value at 30 °C (234.1 mg/g). On the contrary, the Q_{max} value decreased to 146.76 mg/g at 40 °C.

Table IV.7. Fitted parameters of Langmuir, Freundlich, and Sips models for experimental data of the copper adsorption onto MB/A bead.

Model	**Model Parameters**	**Unit**	**Cu–Single mode**			**Binary mode**
			20°C	**30°C**	**40°C**	**at 20°C**
1. Langmuir	Q_{max}	mg/g	218.72	234.1	146.76	139.37
	K_L	L/mg	0.023	0.034	0.074	0.020
	adj–R^2	—	0.985	0.995	0.990	0.998
	SD	—	6.32	3.94	4.99	1.54
	χ^2	—	40.04	15.57	24.95	2.383
2. Freundlich	n	—	1.51	1.66	2.25	1.73
	K_F	$mg^{1-1/n}.L^{1/n}.g^{-1}$	8.73	14.55	20.13	6.77
	adj–R^2	—	0.965	0.976	0.977	0.979
	SD	—	10.54	8.88	7.60	5.02
	χ^2	—	111.1	78.86	57.80	25.21
3. Sips	Q_{max}	mg/g	151.14	205.77	180.55	125.92
	K_{sips}	$(mg/L)^{-1/n_{Sips}}$	0.012	0.029	0.086	0.017
	n_{sips}	—	1.450	1.133	0.773	1.105
	adj–R^2	—	0.992	0.995	0.994	0.998
	SD	—	4.37	3.91	3.86	1.42
	χ^2	—	19.17	15.30	14.91	2.026

These findings revealed a very high superiority for copper adsorption onto the hybrid MB/A bead compared to other previous works, such as modified corn straw biochar (64.9 mg/g) (Zhou et al., 2018), magnetic–biochar beads produced from coconut shell (40.42 mg/g) (Yu et al., 2017a), pine cone–derived biochar–alginate (112 mg/g) (Biswas, Sen, et al., 2019), banana peel biochar (142.86 mg/g) (Amin et al., 2018), and modified cellulose beads (153.6 mg/g) (Maaloul et al., 2021). Overall, the results showed the synthesized MB/A beads are effective adsorbents for Cu^{2+} elimination in both metal systems.

IV.3.2.3. Thermodynamic model

The thermodynamic study is crucial to understand whether the process is energetically favourable. To decipher this, Fig. IV.18 represents the Van't Hoff graph of the linear equation and Table IV.8 presents the thermodynamics parameters for 20°C (T_1), 30°C (T_2), and 40°C (T_3) transformed to the K unit.

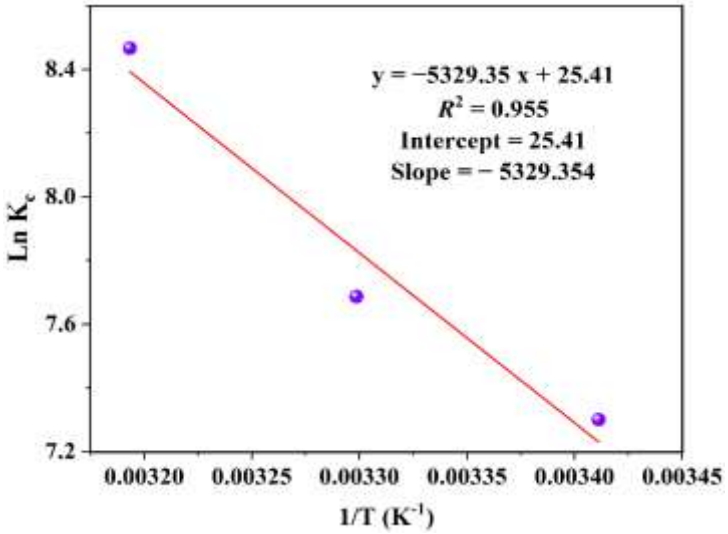

Fig. IV.18. Van't Hoff graph for thermodynamics parameters of Cu^{2+} adsorption onto MB/A bead.

The results outlined in Table IV.8 demonstrated that both $\Delta G°$ was with negative (−) values, whereas $\Delta H°$ and $\Delta S°$ were in positive (+) value. These developments imply that the nature of the system is spontaneous, endothermic ($\Delta H°$ = 44.26 kJ/mol), and has a physical and chemical characteristic. Likewise, numerous studies found matching consequences (Eltaweil et al., 2021).

Table IV.8. Van't Hoff detail and Gibbs parameters of cadmium adsorption onto MB/A bead.

Temperature	***K*C value**	**Van't Hoff detail**	**Thermodynamic parameters (kJ/mol)**		
			$\Delta G°$	**$\Delta H°$**	**$\Delta S°$**
T_1 = 293 K	1480.62	y = −5329.35x + 25.41	−17.79	44.34	0.211
T_2 = 303 K	2178.35	R^2 = 0.955	−19.37		
T_3 = 313 K	8403.84	Intercept = 25.41	−22.04		
	4750.70	Slope = − 5329.354			

IV.3.3. Insights and mechanisms of copper adsorption

IV.3.3.1. pH factor

One intriguing aspect that our study unveils is the influence of pH on the adsorption process. At a pH value lower than 5.0, the surface of the M/BA adsorbent is positively charged (+). This rules out weak electrostatic attraction (physisorption) as the dominant force governing the adsorption process of copper ions. While the pore filling is observed, its contribution remains negligible. Instead, the primary adsorption mechanisms of Cu^{2+} ions into MB/A bead are considered as complexation (1), ion exchange (2), and the forces of Van–der–Waals (3) concluded from temperature effect.

IV.3.3.2. Interaction role by MB/A properties

Intriguingly, the FTIR spectrum of the MB/A bead recorded after the copper ions adsorption represented in *Section III.6* did not reveal significant transformations or shifts in wavenumbers. This observation implies the presence of weak forces governing the interaction between Cu^{2+} ions and MB/A bead (Yu et al., 2017a). Li & Bai, (2005) performed a comprehensive investigation into copper adsorption by chitosan/cellulose beads employing the XPS technique. Their findings are in harmony with our conclusions, as they found no remarkable differences in the XPS analysis of the beads before and after the adsorption process. This indicates the physical adsorption of copper ions onto MB/A bead, characterized by electrostatic attraction or existing of weak chemical interactions.

IV.3.3.3. Decoding the thermodynamics

Chemisorption, characterized by the covalent bond formation via electron interaction (i.e., sharing or exchange), is a key for Cu^{2+} ion adsorption onto adsorbents. Studies have revealed that this process often results in remarkably high values of $\Delta H°$, typically ranging from 200 to 800 kJ/mol (Chang & Thoman Jr, 2014). Notably, the magnitude of $\Delta H°$ in our study stands at 44.26 kJ/mol, a critical indicator that physically dominant adsorption mechanisms are at play (Tran, 2022). Our findings align with the research conducted by others and support that physisorption plays a significant role in the adsorption process. Zhang et al., (2019) and Chen et al., (2020) have reported low $\Delta H°$ values for copper ions adsorption using soft bead materials with 9.76 kJ/mol and 10.34 kJ/mol, respectively.

IV.3.3.4. Discussed mechanisms in literature

Tran et al., (2017) examined Cu^{2+} and Pb^{2+} ions adsorption onto spherical biochar. They reported the contribution of π–π interaction as one of the stronger interactions in addition to the electrostatic attraction when the temperature of solid/liquid increased. Fe–O coordination reaction was reported in a previous study by (Jin et al., 2022), they synthesized Fe_3O_4 in peanut shells biochar and subjected it to adsorb Pb^{2+} ions. This reaction could contribute as a further mechanism to adsorb metal ions. Accordingly, Fe–O functional groups were recorded in our FTIR data, where they possibly make Fe–O coordination reactions in solution and adsorb copper ions on the MB/A surface. Like copper ions, the contribution of the precipitation mechanism for Cd ions uptake was detected in previous studies. Deng et al., (2019) and Tran et al., (2017) analysed the XRD and EDX data before and after Cd adsorption. Their results confirmed the presence of cadmium in different forms Cd_3CO_3 and $(Cd,Ca)CO_3$ in the XRD patterns, meanwhile, the EDX identified the loaded cadmium forms on their adsorbent surface.

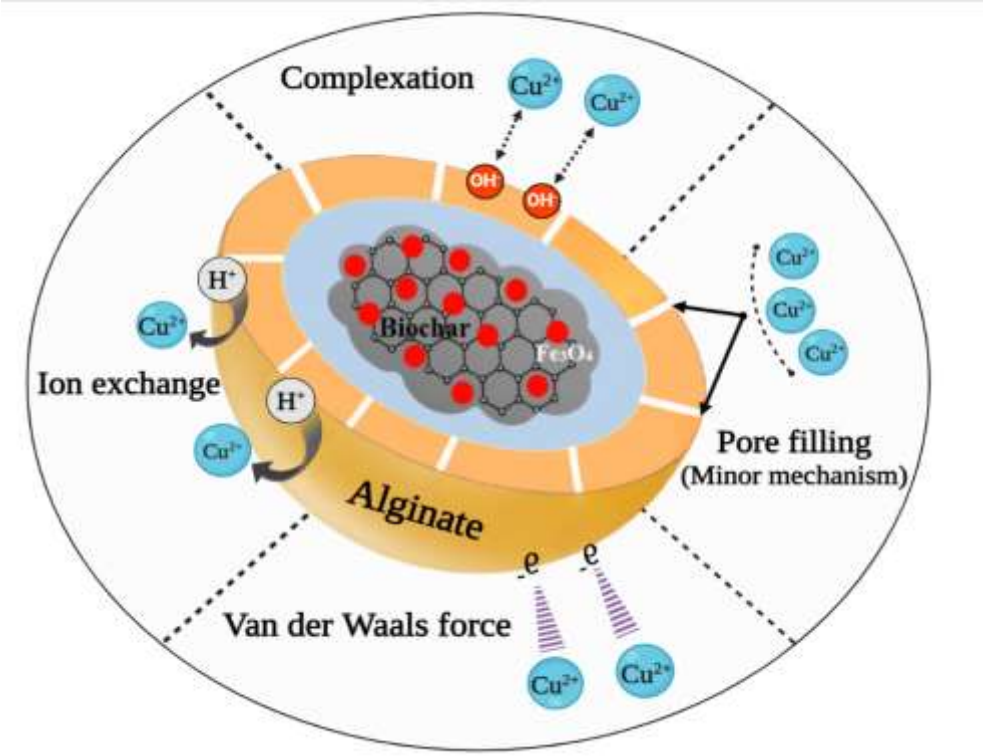

Fig. IV.19. The principal adsorption mechanisms for the Cu adsorption onto MB/A bead (Ben Salem et al., 2023)

IV.3.4. Regeneration of the loaded MB/A beads

Extending the lifespan of adsorbent materials curtails operational expenses and diminishes the volume of waste generated. This section delves into the remarkable case of MB/A bead, which underwent rigorous testing under high copper initial concentration of 200 mg/L through multiple adsorption cycles (Fig. IV.20). Results from this intensive experiment unveiled the true potential of M/BA beads. Initially, with their undying commitment to adsorption, the beads achieved an excellent Cu^{2+} removal rate of 66.6%. However, as the cycles wore on, the removal rate experienced a gradual decline, settling at 55.3% by the third cycle. This decline is inevitable, showcasing the enduring capacity of M/BA beads. After the last adsorption cycle, the beads were regenerated by subjecting them to the Cu^{2+} desorption test with 0.1 M NaOH or HCl. The beads treated with NaOH demonstrated a remarkable Cu^{2+} removal rate of 60.01%, while their counterparts treated with HCl were not far behind, achieving an acceptable 54.50% removal rate. These results showcased the adaptability of MB/A beads under varying desorption conditions. This experiment reinforces the adsorption/desorption capability of the magnetic biochar combined with alginate biopolymer as a compelling recyclable and easily separable adsorbent for heavy metal removal in our environment. The reusability of M/BA adsorbent offers a ray of hope as a promising material.

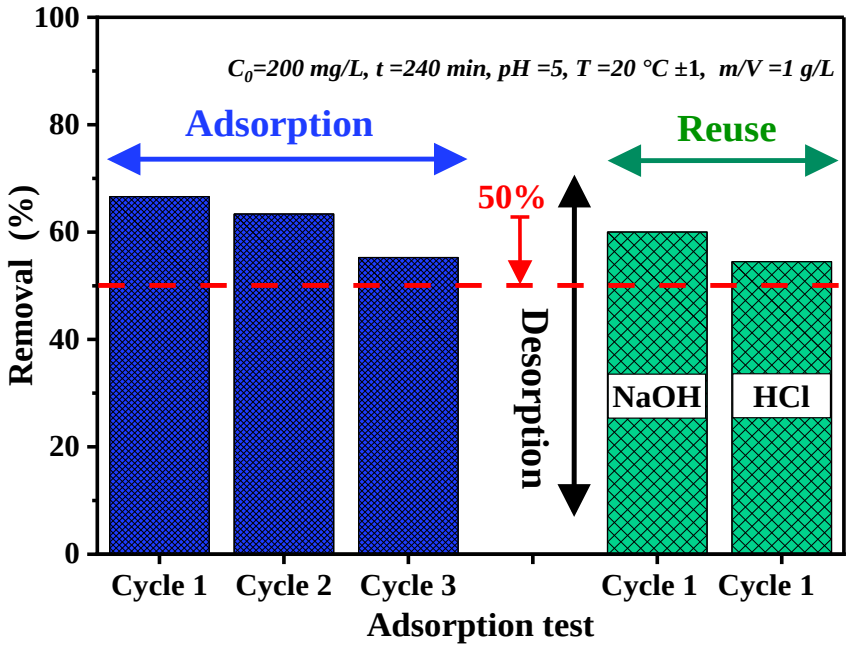

Fig. IV.20. Cd-adsorption cycles and reusability (after desorption) of MB/A bead (C_o = 200 mg/L, t = 240 min, pH = 5.0, m/V = 1g/L at T = 20°C).

IV.4. Conclusion

In this chapter, the adsorption of cadmium and copper ions onto the prepared hybrid adsorbents was studied successfully. The first part was concerned with the adsorption of cadmium ions onto the biochar/alginate (B/A) bead, and the second part was assigned to study the uptake of copper ions from liquids using magnetic–biochar/alginate (MB/A) bead. The studies performed were based on the solution pH, contact time, initial concentration, change in temperature, and regeneration of the adsorbent materials.

In the two parts of this chapter, results show that the solution pH highly affected the adsorption operation of the selected metal ions (Cu^{2+} and Cd^{2+}), and the recommended pH value was stated to be 5.0. Reaching the equilibrium state for the cadmium adsorption consumed 300 min, while only 180 min was recorded for the copper uptake, making the stirring time a key factor in their adsorption process. Isothermal condition (temperature change) was expressed as a critical parameter to identify the suitable environment to adsorb cadmium and copper, where 30°C is the favourable temperature to adsorb their ions. The data modelling of the two studies demonstrated the suitability of pseudo–2nd–order (2) (PSO) to fit the kinetic data, and the equilibrium data was suited to the Sips and Langmuir isotherm models. The highest adsorption capacity was recorded at 30°C from Langmuir Q_{max} calculations, which were 230 mg/g for Cd^{2+} adsorption onto B/A bead and 234.06 mg/g for Cu^{2+} adsorption on MB/A bead. The adsorption of Cu^{2+} in competition with Cd ions onto MB/A bead also gives a remarkable adsorption capacity (139 mg/g). The adsorption process of the two metals was controlled by different mechanisms: electrostatic interactions (repulsion and attraction), surface complexation, ion exchange, the Van der Waals force, and the minor contribution of pore–filling.

In terms of regeneration and reusability, the adsorbent performed well. B/A bead withstands 05 continuous adsorption cycles of 50 mg/L cadmium ions and 03 cycles for copper ions adsorption onto MB/A bead at a high initial concentration of 200 mg/L before the regeneration. B/A and MB/A adsorbents are prospective composite materials for successfully removing heavy metals (i.e., cadmium and copper) from waters in large industrial–scale purifications since it is environmentally safe and recyclable with smooth solid–liquid separation after adsorption operation.

General conclusion

General conclusion

The objective of this thesis was the production of innovative and original hybrid materials allowing the removal of elevated concentrations of toxic metal ions (cadmium and copper) in water with remarkable ease and high efficiency. To comply with the requirements of the environment for sustainable development, a developed protocol was performed for the synthesis of two composite materials and without magnetic properties consisting of the alginate biopolymer beads simultaneously encapsulating particles from biochar and magnetic biochar derived from the started material: peanut shells biomass obtained from agricultural waste. Thus, subjecting renewable, low–cost natural resources available in large quantities to developing new adsorbent materials positively impacts the environment and declines pollution.

Alginate biopolymer is a polysaccharide extracted from brown algae. Alginate is a linear binary copolymer: mannuronate and guluronate monomers are organized in blocks. The carboxylate functions carried by monomers give alginate the ability to form a gel in the presence of divalent cations like calcium ions. Biochar and magnetic biochar are widely used to adsorb organic or inorganic pollutants in water due to their properties: cation exchange capacity, porosity, specific surface area, and various surface functions found in them. The recovery of the laden materials after the adsorption process proves difficult due to their dispersion in the effluents during the treatment operation. Encapsulating these materials in alginate beads not only improves the adsorption capacity of pollutants but also overcomes a significant drawback related to their usage. Thus, taking out these beads, especially the magnetic beads from the aqueous solutions to be decontaminated makes it easy to recover all the used adsorbent materials and avoids the formation of further waste.

The used initial biochar was fabricated at 700°C by the so–called method “direct pyrolysis process” of the started biomass for 4 hours. Iron oxide materials were used for the synthesis of the magnetic biochar. Sodium alginate (SA) was used to encapsulate the biochars in the form of beads. The preparation of biochar/alginate B/A bead and magnetic–biochar/alginate MB/A bead was accomplished by applying the extrusion synthesis protocol mentioned in the literature. This straightforward and swift method will streamline the evolution to the larger–scale production of beads where it is controlled.

In our investigations, we extensively characterized the composite beads. In their wet state, the beads exhibited a spherical form with minimal polydispersity in size, maintaining a diameter of 3 mm. Upon drying, they underwent a shrinkage process and took on a smaller shape with diameters ranging from 1 to 1.2 mm. SEM images revealed a porous internal structure for PS–biochar, with MB, B/A bead, and MB/A bead showing less porosity due to their coating with iron oxide and alginate. Incorporating magnetic nanoparticles (Fe_3O_4) within the biochar and the beads was successfully confirmed by EDS, FTIR and XRD analysis. Temperature, material composition, and particle size are the essential factors that must be considered to accurately describe the degradation kinetics and ash formation of PS–biochar, magnetic–biochar, biochar/alginate beads, and magnetic-biochar alginate beads. Our analysis of these materials using TGA and DTG methods, coupled with the ASTM D1762 method, has provided us with a thorough understanding of their behaviour. The N_2 adsorption measurements at 77K conducted on the dried samples unveiled a noteworthy specific surface area for PS–biochar of 553 m^2/g, 282.5 m^2/g for MB, 275 m^2/g for B/A bead, and 262 m^2/g for MB/A bead.

The techno–economic analysis of our materials was conducted in great detail. The cost estimates in US dollars per kilogram for the year 2024 of the initial PS–biochar (0.248), MB (0.38–184.99), B/A bead (1.278–253.62), and MB/A bead (1.348–348.8) were found to be technically comparable. These materials could be used as cost-effective adsorbents.

The investigation into the adsorption characteristics of the subjected beads involved an analysis of adsorption isotherms at various temperatures for two cationic metals, specifically cadmium and copper, selected as representative models for heavy metal pollutants. B/A bead was evaluated as a potential candidate for cadmium removal, while MB/A bead was employed for the uptake of copper ions from solutions.

Optimal temperature conditions for the recovery of Cd and Cu ions from water using B/A and MB/A beads were identified as 30°C, demonstrating higher maximum adsorption capacities calculated from the Langmuir model, namely 230 mg/g and 234.1 mg/g, respectively. The adsorption capacity of MB/A beads for Cu^{2+} in competition with Cd ions is noteworthy, reaching a substantial value of 139 mg/g.

Comparing these isotherms with those obtained using non–encapsulated bio–adsorbents PS–biochar and SA bead at 30°C for cadmium removal facilitated the proposal of adsorption mechanisms. Notably, unmodified SA bead exhibited superior results compared to PS–biochar and inferior results compared to B/A bead in Cd adsorption. Additionally, the composite beads exhibited stronger adsorption of Cd and Cu ions, as they not only adsorbed on the bio–adsorbents but also underwent ionic exchange with the counterions of the carboxylate sites originating from the alginate. This was corroborated by the comparison between SA bead and PS–biochar in the uptake of Cd ions. The modelling of the adsorption isotherm data indicated that the Langmuir model aptly described the experimental results.

The adsorption mechanism's validity was further underscored by examining the impact of pH on metal ions adsorption. Specifically, at acidic pH levels, ion exchange–driven adsorption diminished, primarily due to the protonation of the carboxylate sites. In general, the adsorption process of the two metals Cd and Cu was controlled by different mechanisms: electrostatic interactions (repulsion and attraction), surface complexation, ion exchange, the Van der Waals force, and the minor contribution of pore–filling.

The adsorption kinetics of two metals by the two types of adsorbents B/A and MB/A beads were studied for the same initial metal concentration of 50 mg/L. The time required to reach equilibrium depends on the metal/adsorbent system. The hybrid adsorbents can adsorb the two metal ions with a short equilibrium time. The B/A bead was adsorbed Cd ions within 5 h while the MB/A bead was loaded with copper ions in 3 h. In kinetic modelling, the experimental curves are generally well described by the pseudo–2nd–order equation. Using the intraparticle diffusion model, the diffusion of metals within the hybrid beads is the step determining the speed at short times. In the context of regeneration and reusability, the adsorbent demonstrated commendable performance. The B/A bead exhibited resilience through 05 consecutive adsorption cycles of 50 mg/L cadmium ions, whereas the MB/A adsorbent demonstrated robustness with 03 cycles for adsorption of copper ions at a high initial concentration of 200 mg/L before the regeneration process by HCl or NaOH solution. This underscores the potential of B/A and MB/A adsorbents as promising composite materials for effectively removing heavy metals, specifically cadmium and copper, from water in large–scale industrial purification processes. Regeneration of the materials for reuse in successive cycles is crucial, and the research suggests exploring non–destructive

methods like ultrasound for efficient desorption. Notably, the prepared adsorbents are environmentally safe and exhibit recyclability, coupled with seamless solid–liquid separation post–adsorption operations, further enhancing their practical utility in industrial settings.

The research on hybrid beads for metal adsorption presents promising outcomes, showcasing materials with significant adsorbent properties for efficient pollutant extraction. The design features not only facilitate easy separation of solid–liquid but also allow for effective regeneration, minimizing costs and secondary waste generation. Utilizing biopolymer and biochar–derived materials contribute to cost reduction and enhances the process's overall appeal.

Although magnetic–biochar alginate beads were more practical during the recovery of the loaded beads from the water after adsorption operations compared to non–magnetic adsorbents, certain challenges remain for the industrial–scale application of magnetic alginate beads in pollution control. Incorporating magnetic nanoparticles within the beads opens avenues for magnetic separation, streamlining the recovery process and eliminating the need for complex decantation–flocculation and filtration procedures. Future research will focus on optimizing these treatments and evaluating the feasibility of magnetic separation to enhance the practical application of these innovative biomaterial beads in pollution remediation systems. Key areas for further exploration include a deeper understanding of adsorption kinetics and a detailed examination of the internal structure of the beads. The effectiveness observed in aqueous solutions necessitates testing in more complex environments resembling real effluents, addressing issues like resistance to microorganisms, stability against salinity and acidity, and potential modifications to the bead formulation. Therefore, the study emphasizes the importance of maintaining compatibility with eco–design principles while modifying bead formulations to meet specific effluent requirements.

For future research endeavours, our study recommends advancing the development of hybrid composite materials tailored for the treatment of water contaminated with heavy metal pollutants under diverse environmental conditions. This involves the creation of a multifunctional industrial semi–pilot capable of designing beads, effectively adsorbing pollutants, and regenerating loaded beads. This holistic approach leverages the expertise and skills of researchers at the laboratories, aiming to establish a robust framework for sustainable and efficient heavy metals remediation.

References

References

Abd El-Monaem, E. M., Omer, A. M., Khalifa, R. E., & Eltaweil, A. S. (2022). Floatable cellulose acetate beads embedded with flower-like zwitterionic binary MOF/PDA for efficient removal of tetracycline. *Journal of Colloid and Interface Science*, *620*, 333–345. https://doi.org/10.1016/j.jcis.2022.04.010

Abdelwahab, M. S., El Halfawy, N. M., & El-Naggar, M. Y. (2022). Lead adsorption and antibacterial activity using modified magnetic biochar/sodium alginate nanocomposite. *International Journal of Biological Macromolecules*, *206*(February), 730–739. https://doi.org/10.1016/j.ijbiomac.2022.03.053

Afzal, M. Z., Yue, R., Sun, X. F., Song, C., & Wang, S. G. (2019). Enhanced removal of ciprofloxacin using humic acid modified hydrogel beads. *Journal of Colloid and Interface Science*, *543*(May), 76–83. https://doi.org/10.1016/j.jcis.2019.01.083

Ahmad, M., Lee, S. S., Dou, X., Mohan, D., Sung, J. K., Yang, J. E., & Ok, Y. S. (2012). Effects of pyrolysis temperature on soybean stover- and peanut shell-derived biochar properties and TCE adsorption in water. *Bioresource Technology*, *118*, 536–544. https://doi.org/10.1016/j.biortech.2012.05.042

Ahmad, M., Rajapaksha, A. U., Lim, J. E., Zhang, M., Bolan, N., Mohan, D., Vithanage, M., Lee, S. S., & Ok, Y. S. (2014). Biochar as a sorbent for contaminant management in soil and water: A review. *Chemosphere*, *99*, 19–33. https://doi.org/10.1016/j.chemosphere.2013.10.071

Ahmed, M. J., & Dhedan, S. K. (2012). Equilibrium isotherms and kinetics modeling of methylene blue adsorption on agricultural wastes-based activated carbons. *Fluid Phase Equilibria*, *317*, 9–14. https://doi.org/10.1016/j.fluid.2011.12.026

Aichour, A. (2019). *Synthèse et propriétés de bioadsorbants encapsulés dans l'alginate : application à l'élimination des colorants du milieu aqueux*. These de Doctorat (Génie des Procédés), UNIVERSITÉ FERHAT ABBAS - SETIF1.

Aichour, A., Zaghouane-Boudiaf, H., Iborra, C. V., & Polo, M. S. (2018). Bioadsorbent beads prepared from activated biomass/alginate for enhanced removal of cationic dye from water medium: Kinetics, equilibrium and thermodynamic studies. *Journal of Molecular Liquids*, *256*, 533–540. https://doi.org/10.1016/j.molliq.2018.02.073

Aichour, A., Zaghouane-Boudiaf, H., Mohamed Zuki, F. B., Kheireddine Aroua, M., & Ibbora, C. V. (2019). Low-cost, biodegradable and highly effective adsorbents for batch and column fixed bed adsorption processes of methylene blue. *Journal of Environmental Chemical Engineering*, *7*(5), 103409. https://doi.org/10.1016/j.jece.2019.103409

Ajmal, Z., Muhmood, A., Dong, R., & Wu, S. (2020). Probing the efficiency of magnetically modified biomass-derived biochar for effective phosphate removal. *Journal of Environmental Management*, *253*(September 2019), 109730. https://doi.org/10.1016/j.jenvman.2019.109730

AL-Othman, Z. A., Ali, R., & Naushad, M. (2012). Hexavalent chromium removal from aqueous medium by activated carbon prepared from peanut shell: Adsorption kinetics, equilibrium and thermodynamic studies. *Chemical Engineering Journal*, *184*, 238–247. https://doi.org/10.1016/j.cej.2012.01.048

Al-Zboon, K. K. (2023). Single and Ternary Removal of Heavy Metals from Aqueous Solution Using Fe3O4 Magnetic Nano-particles. *Jordan Journal of Civil Engineering*, *17*(2). https://doi.org/10.14525/JJCE.v17i2.13

Albalasmeh, A., Gharaibeh, M. A., Mohawesh, O., Alajlouni, M., Quzaih, M., Masad, M., & El Hanandeh, A. (2020). Characterization and Artificial Neural Networks Modelling of methylene blue adsorption of biochar derived from agricultural residues: Effect of biomass type, pyrolysis temperature, particle size. *Journal of Saudi Chemical Society*, *24*(11), 811–823. https://doi.org/10.1016/j.jscs.2020.07.005

Alhashimi, H. A., & Aktas, C. B. (2017). Life cycle environmental and economic performance of biochar compared with activated carbon: A meta-analysis. *Resources, Conservation and Recycling*, *118*, 13–26. https://doi.org/10.1016/j.resconrec.2016.11.016

Ali, A., Shah, T., Ullah, R., Zhou, P., Guo, M., Ovais, M., Tan, Z., & Rui, Y. K. (2021). Review on Recent Progress in Magnetic Nanoparticles: Synthesis, Characterization, and Diverse Applications. *Frontiers in Chemistry*, *9*(July), 1–25. https://doi.org/10.3389/fchem.2021.629054

Ali, I., & Gupta, V. K. (2007). Advances in water treatment by adsorption technology. *Nature Protocols*, *1*(6), 2661–2667. https://doi.org/10.1038/nprot.2006.370

Allen, S. J., Mckay, G., & Khader, K. Y. H. (1989). Intraparticle diffusion of a basic dye during adsorption onto sphagnum peat. *Environmental Pollution*, *56*(1), 39–50.

Alslaibi, T. M., Abustan, I., Ahmad, M. A., & Foul, A. A. (2013). Cadmium removal from aqueous solution using microwaved olive stone activated carbon. *Journal of Environmental Chemical Engineering*, *1*(3), 589–599. https://doi.org/10.1016/j.jece.2013.06.028

Alves, L. de C., Yáñez-Vilar, S., Piñeiro-Redondo, Y., & Rivas, J. (2019). Novel magnetic nanostructured beads for cadmium(II) removal. *Nanomaterials*, *9*(3). https://doi.org/10.3390/nano9030356

Ambaye, T. G., Vaccari, M., van Hullebusch, E. D., Amrane, A., & Rtimi, S. (2021). Mechanisms and adsorption capacities of biochar for the removal of organic and inorganic pollutants from industrial wastewater. *International Journal of Environmental Science and Technology*, *18*(10), 3273–3294. https://doi.org/10.1007/s13762-020-03060-w

Amin, M. T., Alazba, A. A., & Shafiq, M. (2018). Removal of Copper and Lead using Banana Biochar in Batch Adsorption Systems: Isotherms and Kinetic Studies. *Arabian Journal for Science and Engineering*, *43*(11), 5711–5722. https://doi.org/10.1007/s13369-017-2934-z

Andreas, A., Winata, Z. G., Santoso, S. P., Angkawijaya, A. E., Yuliana, M., Soetaredjo, F. E., Ismadji, S., Hsu, H. Y., Go, A. W., & Ju, Y. H. (2021). Biocomposite hydrogel beads from glutaraldehyde-crosslinked phytochemicals in alginate for effective removal of methylene blue. *Journal of Molecular Liquids*, *329*, 115579. https://doi.org/10.1016/j.molliq.2021.115579

Arab, L. H., Boutaleb, A., & Berdous, D. (2021). Environmental assessment of heavy metal pollution in the polymetallic district of Kef Oum Teboul (El Kala, Northeast Algeria). *Environmental Earth Sciences*, *80*(7), 1–13. https://doi.org/10.1007/s12665-021-09570-1

Ayouch, I., Barrak, I., Kassab, Z., El Achaby, M., Barhoun, A., & Draoui, K. (2020a). Impact of the drying process on the efficiency of alginate beads for cadmium removal from water: Kinetic, isotherm and thermodynamic study. *Environmental Technology and Innovation*, *20*, 101157. https://doi.org/10.1016/j.eti.2020.101157

Ayouch, I., Barrak, I., Kassab, Z., El Achaby, M., Barhoun, A., & Draoui, K. (2020b). Improved recovery of cadmium from aqueous medium by alginate composite beads filled by bentonite and phosphate washing sludge. *Colloids and Surfaces A: Physicochemical and Engineering Aspects*, *604*(May), 125305. https://doi.org/10.1016/j.colsurfa.2020.125305

Azri, N., Ammar, F., Abdelkader, O., Rachid, C., Lynda, H., Syafiuddin, A., & Boopathy, R. (2022). Development of a novel and efficient biochar produced from pepper stem for

effective ibuprofen removal. *Bioresource Technology*, *347*(November 2021), 126685. https://doi.org/10.1016/j.biortech.2022.126685

Babel, S., & Kurniawan, T. A. (2003). Low-cost adsorbents for heavy metals uptake from contaminated water: A review. *Journal of Hazardous Materials*, *97*(1–3), 219–243. https://doi.org/10.1016/S0304-3894(02)00263-7

Bakhtiari, S., Shahrashoub, M., & Keyhanpour, A. (2022). A comprehensive study on single and competitive adsorption-desorption of copper and cadmium using eco-friendly magnetite (Fe3O4) nanoparticles. *Korean Journal of Chemical Engineering*, *39*(9), 2379–2393. https://doi.org/10.1007/s11814-022-1148-6

Ben Salem, D., Ouakouak, A., Touahra, F., Hamdi, N., Eltaweil, A. S., Syed, A., Boopathy, R., & Tran, H. N. (2023). Easy separable, floatable, and recyclable magnetic-biochar/alginate bead as super-adsorbent for adsorbing copper ions in water media. *Bioresource Technology*, *383*, 129225. https://doi.org/10.1016/j.biortech.2023.129225

Benettayeb, A., Guibal, E., Morsli, A., & Kessas, R. (2017). Chemical modification of alginate for enhanced sorption of Cd(II), Cu(II) and Pb(II). *Chemical Engineering Journal*, *316*, 704–714. https://doi.org/10.1016/j.cej.2017.01.131

Benhaddya, M. L., Halis, Y., & Hamdi-Aïssa, B. (2020). Assessment of heavy metals pollution in surface and groundwater systems in Oued Righ region (Algeria) using pollution indices and multivariate statistical techniques. *African Journal of Aquatic Science*, *45*(3), 269–284. https://doi.org/10.2989/16085914.2019.1703635

Benhaddya, M. L., Halis, Y., & Lahcini, A. (2019). Concentration, Distribution, and Potential Aquatic Risk Assessment of Metals in Water from Chott Merouane (Ramsar Site), Algeria. *Archives of Environmental Contamination and Toxicology*, *77*(1), 127–143. https://doi.org/10.1007/s00244-019-00631-y

Benmostefa, S., Dali Youcef, N., & Hadjel, M. (2022). Monitoring and evaluation of heavy metal pollution in surface water of Tafna wadi (Algeria). *Arabian Journal of Geosciences*, *15*(17). https://doi.org/10.1007/s12517-022-10692-4

Berndes, G., Hoogwijk, M., & Van Den Broek, R. (2003). The contribution of biomass in the future global energy supply: A review of 17 studies. *Biomass and Bioenergy*, *25*(1), 1–28. https://doi.org/10.1016/S0961-9534(02)00185-X

Bhatnagar, A., Hogland, W., Marques, M., & Sillanpää, M. (2013). An overview of the

modification methods of activated carbon for its water treatment applications. *CHEMICAL ENGINEERING JOURNAL*, *219*, 499–511. https://doi.org/10.1016/j.cej.2012.12.038

Bhatnagar, A., Sillanpää, M., & Witek-Krowiak, A. (2015). Agricultural waste peels as versatile biomass for water purification - A review. *Chemical Engineering Journal*, *270*, 244–271. https://doi.org/10.1016/j.cej.2015.01.135

Bilal, M., Shah, J. A., Ashfaq, T., Gardazi, S. M. H., Tahir, A. A., Pervez, A., Haroon, H., & Mahmood, Q. (2013). Waste biomass adsorbents for copper removal from industrial wastewater-A review. *Journal of Hazardous Materials*, *263*, 322–333. https://doi.org/10.1016/j.jhazmat.2013.07.071

Biswas, S., Meikap, B. C., & Sen, T. K. (2019). Adsorptive Removal of Aqueous Phase Copper (Cu2+) and Nickel (Ni2+) Metal Ions by Synthesized Biochar–Biopolymeric Hybrid Adsorbents and Process Optimization by Response Surface Methodology (RSM). *Water, Air, and Soil Pollution*, *230*(8). https://doi.org/10.1007/s11270-019-4258-y

Biswas, S., Sen, T. K., Yeneneh, A. M., & Meikap, B. C. (2019). Synthesis and characterization of a novel Ca-alginate-biochar composite as efficient zinc (Zn 2+) adsorbent: Thermodynamics, process design, mass transfer and isotherm modeling. *Separation Science and Technology (Philadelphia)*, *54*(7), 1106–1124. https://doi.org/10.1080/01496395.2018.1527353

Blanchard, G., Maunaye, M., & Martin, G. (1984). Removal of heavy metals from waters by means of natural zeolites. *Water Research*, *18*(12), 1501–1507. https://doi.org/10.1016/0043-1354(84)90124-6

Bouchelta, C., Medjram, M. S., Bertrand, O., & Bellat, J. P. (2008). Preparation and characterization of activated carbon from date stones by physical activation with steam. *Journal of Analytical and Applied Pyrolysis*, *82*(1), 70–77. https://doi.org/10.1016/j.jaap.2007.12.009

Bouhamed, F., Elouear, Z., & Bouzid, J. (2012). Adsorptive removal of copper(II) from aqueous solutions on activated carbon prepared from Tunisian date stones: Equilibrium, kinetics and thermodynamics. *Journal of the Taiwan Institute of Chemical Engineers*, *43*(5), 741–749. https://doi.org/10.1016/j.jtice.2012.02.011

Boukhalfa, N. (2019). *Etude de l'élimination des polluants émergents par des matériaux composites*. These de Doctorat (Génie Chimique), Université Ferhat Abbas - Setif1.

Boukhalfa, N., Boutahala, M., Djebri, N., & Idris, A. (2019). Maghemite/alginate/functionalized multiwalled carbon nanotubes beads for methylene blue removal: Adsorption and desorption studies. *Journal of Molecular Liquids*, *275*, 431–440. https://doi.org/10.1016/j.molliq.2018.11.064

Bouziane, N., & Zertal, A. (2007). *Elimination du 2-mercaptobenzothiazole par voie photochimique et par adsorption sur la bentonite et le charbon actif en poudre*.

Brunauer, S. (1943). *Adsorption of gases and vapors*.

Chabane, L., Cheknane, B., Zermane, F., Bouras, O., & Baudu, M. (2017). Synthesis and characterization of reinforced hybrid porous beads: Application to the adsorption of malachite green in aqueous solution. *Chemical Engineering Research and Design*, *120*(December 2017), 291–302. https://doi.org/10.1016/j.cherd.2016.12.014

Chahinez, H.-O. O., Abdelkader, O., Leila, Y., & Tran, H. N. (2020). One-stage preparation of palm petiole-derived biochar: Characterization and application for adsorption of crystal violet dye in water [Research-article]. *Environmental Technology and Innovation*, *19*(1), 100872. https://doi.org/10.1016/j.eti.2020.100872

Chakraborty, S., Roy, P., Pathak, A., Debnath, M., Dasgupta, S., Mukhopadhyay, R., & Bandyopadhyay, S. (2011). Composition analysis of carbon black-filled polychloroprene rubber compound by thermo-oxidative degradation of the compound. *Journal of Elastomers and Plastics*, *43*(5), 499–508. https://doi.org/10.1177/0095244311413442

Chang, R., & Thoman Jr, J. W. (2014). Intermolecular forces. *Physical Chemistry for the Chemical Sciences. University Science Books*, 792.

Chen, B., Zhou, D., & Zhu, L. (2008). Transitional adsorption and partition of nonpolar and polar aromatic contaminants by biochars of pine needles with different pyrolytic temperatures. *Environmental Science and Technology*, *42*(14), 5137–5143. https://doi.org/10.1021/es8002684

Chen, L., Hao, H., Zhang, W., & Shao, Z. (2020). Adsorption mechanism of copper ions in aqueous solution by chitosan–carboxymethyl starch composites. *Journal of Applied Polymer Science*, *137*(18), 48636. https://doi.org/10.1002/app.48636

Chen, M., He, F., Hu, D., Bao, C., & Huang, Q. (2020). Broadened operating pH range for adsorption/reduction of aqueous Cr(VI) using biochar from directly treated jute (Corchorus capsularis L.) fibers by H3PO4. *Chemical Engineering Journal*, *381*(September 2019).

https://doi.org/10.1016/j.cej.2019.122739

Chen, X., Yu, G., Chen, Y., Tang, S., & Su, Y. (2022). Cow Dung-Based Biochar Materials Prepared via Mixed Base and Its Application in the Removal of Organic Pollutants. *International Journal of Molecular Sciences*, *23*(17), 10094. https://doi.org/10.3390/ijms231710094

Cheng, D., Ngo, H. H., Guo, W., Chang, S. W., Nguyen, D. D., Zhang, X., Varjani, S., & Liu, Y. (2020). Feasibility study on a new pomelo peel derived biochar for tetracycline antibiotics removal in swine wastewater. *Science of the Total Environment*, *720*, 137662. https://doi.org/10.1016/j.scitotenv.2020.137662

Claude Cardot. (2010). *Les traitements de l'eau pour l'ingénieur* (Ellipses (Ed.); Ellipses). Ellipses.

Dąbrowski, A. (2001). Adsorption — from theory to practice. *Advances in Colloid and Interface Science*, *93*(1–3), 135–224. https://doi.org/10.1016/S0001-8686(00)00082-8

Dai, Y., Zhang, N., Xing, C., Cui, Q., & Sun, Q. (2019). The adsorption, regeneration and engineering applications of biochar for removal organic pollutants: A review. *Chemosphere*, *223*, 12–27. https://doi.org/10.1016/j.chemosphere.2019.01.161

de Araújo, T. P., Quesada, H. B., dos Santos, D. F., da Silva Fonseca, B. C., Barbieri, J. Z., Bergamasco, R., & de Barros, M. A. S. D. (2022). Acetaminophen removal by calcium alginate/activated hydrochar composite beads: Batch and fixed-bed studies. *International Journal of Biological Macromolecules*, *203*(January), 553–562. https://doi.org/10.1016/j.ijbiomac.2022.01.177

Deng, W., Feng, Y., Fu, J., Guo, H., Guo, Y., Han, B., Jiang, Z., Kong, L., Li, C., Liu, H., Nguyen, P. T. T., Ren, P., Wang, F., Wang, S., Wang, Y., Wang, Y., Wong, S. S., Yan, K., Yan, N., … Zhou, H. (2023). Catalytic conversion of lignocellulosic biomass into chemicals and fuels. *Green Energy & Environment*, *8*(1), 10–114. https://doi.org/10.1016/j.gee.2022.07.003

Deng, Y., Huang, S., Laird, D. A., Wang, X., & Meng, Z. (2019). Adsorption behaviour and mechanisms of cadmium and nickel on rice straw biochars in single- and binary-metal systems. *Chemosphere*, *218*, 308–318. https://doi.org/10.1016/j.chemosphere.2018.11.081

Derafa, G. (2021). Synthèse et caractérisation des billes composites pour l ' élimination de polluants organiques en milieu aqueux. In *these de doctorat,UNIVERSITÉ FERHAT ABBAS*

- *SETIF1 FACULTÉ DE TECHNOLOGIE*. These de Doctorat (Génie des Procédés), UNIVERSITÉ FERHAT ABBAS - SETIF1.

Djorfi, S., Foufou, A., Majour, H., Belloulou, L., Hani, A., & Djabri, L. (2010). *Impact de la decharge publique de annaba sur la qualite des eaux de la plaine de l'oued zied 1*. *June 2015*, 5–9.

Doğan, M., Alkan, M., Demirbaş, Ö., Özdemir, Y., & Özmetin, C. (2006). Adsorption kinetics of maxilon blue GRL onto sepiolite from aqueous solutions. *Chemical Engineering Journal*, *124*(1–3), 89–101.

Dudchenko, N., Pawar, S., Perelshtein, I., & Fixler, D. (2022). Magnetite Nanoparticles: Synthesis and Applications in Optics and Nanophotonics. *Materials*, *15*(7), 2601. https://doi.org/10.3390/ma15072601

Elovich, S. Y., & Larionov, O. G. (1962). Theory of adsorption from nonelectrolyte solutions on solid adsorbents. *Bulletin of the Academy of Sciences of the USSR Division of Chemical Science*, *11*(2), 198–203. https://doi.org/10.1007/BF00908017

Elovich, S. Y., & Zhabrova, G. M. (1939). Mechanism of the catalytic hydrogenation of ethylene on nickel. I. Kinetics of the process. *Journal of Physical Chemistry*, *13*, 1761.

Eltaweil, A. S., Mamdouh, I. M., Abd El-Monaem, E. M., & El-Subruiti, G. M. (2021). Highly Efficient Removal for Methylene Blue and Cu2+onto UiO-66 Metal-Organic Framework/Carboxylated Graphene Oxide-Incorporated Sodium Alginate Beads. *ACS Omega*, *6*(36), 23528–23541. https://doi.org/10.1021/acsomega.1c03479

Fan, C., Li, K., He, Y., Wang, Y., Qian, X., & Jia, J. (2018). Evaluation of magnetic chitosan beads for adsorption of heavy metal ions. *Science of the Total Environment*, *627*, 1396–1403. https://doi.org/10.1016/j.scitotenv.2018.02.033

Fares, R., Naim, H., & Bouadi, A. (2021). Groundwater pollution in the region of Relizane, Algeria with focus on the physical–chemical and bacteriological characteristics. *International Journal of Energy and Water Resources*, *5*(3), 247–257. https://doi.org/10.1007/s42108-021-00124-6

Farooq, U., Kozinski, J. A., Khan, M. A., & Athar, M. (2010). Biosorption of heavy metal ions using wheat based biosorbents - A review of the recent literature. *Bioresource Technology*, *101*(14), 5043–5053. https://doi.org/10.1016/j.biortech.2010.02.030

Feng, N., Guo, X., & Liang, S. (2009). Adsorption study of copper (II) by chemically modified

orange peel. *Journal of Hazardous Materials*, *164*(2–3), 1286–1292. https://doi.org/10.1016/j.jhazmat.2008.09.096

Ford, R. G., Wilkin, R. T., & Puls, R. W. (2007). *Monitored natural attenuation of inorganic contaminants in ground water* (Vol. 2). Naiontal Risk Management Research Laboratory, US Environmental Protection Agency.

Fouad, D., Bachra, Y., Ayoub, G., Ouaket, A., Bennamara, A., Knouzi, N., & Berrada, M. (2020). A Novel Drug Delivery System Based on Nanoparticles of Magnetite Fe 3 O 4 Embedded in an Auto Cross-Linked Chitosan. In *Chitin and Chitosan - Physicochemical Properties and Industrial Applications [Working Title]*. IntechOpen. https://doi.org/10.5772/intechopen.94873

Freundlich, H. K. (1909). Akademische Verlagsgesellschaft. *Leipzig, Germany*, *385*, 386.

Gai, X., Wang, H., Liu, J., Zhai, L., Liu, S., Ren, T., & Liu, H. (2014). Effects of feedstock and pyrolysis temperature on biochar adsorption of ammonium and nitrate. *PLoS ONE*, *9*(12), 1–19. https://doi.org/10.1371/journal.pone.0113888

Garg, U. K., Kaur, M. P., Garg, V. K., & Sud, D. (2008). Removal of Nickel(II) from aqueous solution by adsorption on agricultural waste biomass using a response surface methodological approach. *Bioresource Technology*, *99*(5), 1325–1331. https://doi.org/10.1016/j.biortech.2007.02.011

Gherbi, N. (2008). Etude expérimentale et identification du processus de rétention des cations métalliques par des matériaux naturels. *These de Doctorat*, 163. http://archives.umc.edu.dz/bitstream/handle/123456789/5391/GHE5243.pdf?sequence=1

Giles, C. H., Smith, D., & Huitson, A. (1974). A general treatment and classification of the solute adsorption isotherm. I. Theoretical. *Journal of Colloid and Interface Science*, *47*(3), 755–765. https://doi.org/10.1016/0021-9797(74)90252-5

González-García, P. (2018). Activated carbon from lignocellulosics precursors: A review of the synthesis methods, characterization techniques and applications. *Renewable and Sustainable Energy Reviews*, *82*(August 2017), 1393–1414. https://doi.org/10.1016/j.rser.2017.04.117

Hadj-Otmane, C., Ouakouak, A., Touahra, F., Grabi, H., Martín, J., & Bilal, M. (2022). Date palm petiole–derived biochar: effect of pyrolysis temperature and adsorption properties of hazardous cationic dye from water. *Biomass Conversion and Biorefinery*, *0123456789*.

https://doi.org/10.1007/s13399-022-03127-3

Hameed, B. H., & Ahmad, A. A. (2009). Batch adsorption of methylene blue from aqueous solution by garlic peel, an agricultural waste biomass. *Journal of Hazardous Materials*, *164*(2–3), 870–875. https://doi.org/10.1016/j.jhazmat.2008.08.084

HAMIMED, F. (2016). *Élaboration DE BILLES à BASE D'ALGINATE. Étude Rhéologique ET de COMPORTEMENT*. These de doctorat (Chimie et Physique des Polymères), UNIVERSITE M'HAMED BOUGARRA - BOUMERDES.

Hammoudi, N., Ziani Cherif, H., Borsali, F., Benmansour, K., & Meghezzi, A. (2020). Preparation of active antimicrobial and antifungal alginate-montmorillonite/lemon essential oil nanocomposite films. *Materials Technology*, *35*(7), 383–394. https://doi.org/10.1080/10667857.2019.1685292

Hariani, P. L., Faizal, M., Ridwan, R., Marsi, M., & Setiabudidaya, D. (2013). Synthesis and Properties of Fe3O4 Nanoparticles by Co-precipitation Method to Removal Procion Dye. *International Journal of Environmental Science and Development*, *4*(3), 336–340. https://doi.org/10.7763/ijesd.2013.v4.366

Harper, T. R., & Kingham, N. W. (1992). Removal of arsenic from wastewater using chemical precipitation methods. *Water Environment Research*, *64*(3), 200–203. https://doi.org/10.2175/wer.64.3.2

Hassan, M., Deb, A. K., Qi, F., Liu, Y., Du, J., Fahy, A., Ahsan, M. A., Parikh, S. J., & Naidu, R. (2021). Magnetically separable mesoporous alginate polymer beads assist adequate removal of aqueous methylene blue over broad solution pH. *Journal of Cleaner Production*, *319*(May), 128694. https://doi.org/10.1016/j.jclepro.2021.128694

Hassan, M., Naidu, R., Du, J., Qi, F., Ahsan, M. A., & Liu, Y. (2022). Magnetic responsive mesoporous alginate/β-cyclodextrin polymer beads enhance selectivity and adsorption of heavy metal ions. *International Journal of Biological Macromolecules*, *207*(March), 826–840. https://doi.org/10.1016/j.ijbiomac.2022.03.159

Heidarinejad, Z., Dehghani, M. H., Heidari, M., Javedan, G., Ali, I., & Sillanpää, M. (2020). Methods for preparation and activation of activated carbon: a review. *Environmental Chemistry Letters*, *18*(2), 393–415. https://doi.org/10.1007/s10311-019-00955-0

Heydaripour, J., Gazi, M., Oladipo, A. A., & Gulcan, H. O. (2019). Porous magnetic resin-g-chitosan beads for adsorptive removal of phenolic compounds. *International Journal of*

Biological Macromolecules, *123*, 1125–1131. https://doi.org/10.1016/j.ijbiomac.2018.11.168

Ho, Y.-S., & McKay, G. (1998). Sorption of dye from aqueous solution by peat. *Chemical Engineering Journal*, *70*(2), 115–124.

Hong, H. J., Jeong, H. S., Kim, B. G., Hong, J., Park, I. S., Ryu, T., Chung, K. S., Kim, H., & Ryu, J. (2016). Highly stable and magnetically separable alginate/Fe3O4 composite for the removal of strontium (Sr) from seawater. *Chemosphere*, *165*, 231–238. https://doi.org/10.1016/j.chemosphere.2016.09.034

Horsfall, M., & Abia, A. A. (2003). Sorption of cadmium(II) and zinc(II) ions from aqueous solutions by cassava waste biomass (Manihot sculenta Cranz). *Water Research*, *37*(20), 4913–4923. https://doi.org/10.1016/j.watres.2003.08.020

Huff, M. D., & Lee, J. W. (2016). Biochar-surface oxygenation with hydrogen peroxide. *Journal of Environmental Management*, *165*, 17–21. https://doi.org/10.1016/j.jenvman.2015.08.046

Hussain, F., Shah, S. Z., Ahmad, H., Abubshait, S. A., Abubshait, H. A., Laref, A., Manikandan, A., Kusuma, H. S., & Iqbal, M. (2021). Microalgae an ecofriendly and sustainable wastewater treatment option: Biomass application in biofuel and bio-fertilizer production. A review. *Renewable and Sustainable Energy Reviews*, *137*(December 2020), 110603. https://doi.org/10.1016/j.rser.2020.110603

Isarain-Chávez, E., De La Rosa, C., Godínez, L. A., Brillas, E., & Peralta-Hernández, J. M. (2014). Comparative study of electrochemical water treatment processes for a tannery wastewater effluent. *Journal of Electroanalytical Chemistry*, *713*, 62–69. https://doi.org/10.1016/j.jelechem.2013.11.016

Jain, M., Garg, V. K., & Kadirvelu, K. (2013). Cadmium(II) sorption and desorption in a fixed bed column using sunflower waste carbon calcium-alginate beads. *Bioresource Technology*, *129*, 242–248. https://doi.org/10.1016/j.biortech.2012.11.036

Jeon, C. (2018). Adsorption behavior of cadmium ions from aqueous solution using pen shells. *Journal of Industrial and Engineering Chemistry*, *58*, 57–63. https://doi.org/10.1016/j.jiec.2017.09.007

Jin, X., Liu, R., Wang, H., Han, L., Qiu, M., & Hu, B. (2022). Functionalized porous nanoscale Fe3O4 particles supported biochar from peanut shell for Pb(II) ions removal from landscape wastewater. *Environmental Science and Pollution Research*, *29*(25), 37159–37169.

https://doi.org/10.1007/s11356-021-18432-z

JORA. (2011). No Title p . *JOURNAL OFFICIEL DE LA REPUBLIQUE ALGERIENNE*, *34*, 6. https://www.joradp.dz/FTP/jo-francais/2011/F2011034.pdf

Kadirvelu, K., Faur-Brasquet, C., & Le Cloirec, P. (2000). Removal of Cu(II), Pb(II), and Ni(II) by adsorption onto activated carbon cloths. *Langmuir*, *16*(22), 8404–8409. https://doi.org/10.1021/la0004810

Kalaitzidou, K., Zouboulis, A., & Mitrakas, M. (2020). Cost evaluation for Se(IV) removal, by applying common drinking water treatment processes: Coagulation/precipitation or adsorption. *Journal of Environmental Chemical Engineering*, *8*(5). https://doi.org/10.1016/j.jece.2020.104209

Karge, H. G., & Weitkamp, J. (Eds.). (2008). *Adsorption and Diffusion* (Vol. 7). Springer Berlin Heidelberg. https://doi.org/10.1007/978-3-540-73966-1

Kataria, N., & Garg, V. K. (2018). Green synthesis of Fe3O4 nanoparticles loaded sawdust carbon for cadmium (II) removal from water: Regeneration and mechanism. *Chemosphere*, *208*, 818–828. https://doi.org/10.1016/j.chemosphere.2018.06.022

Kavand, M., Eslami, P., & Razeh, L. (2020). The adsorption of cadmium and lead ions from the synthesis wastewater with the activated carbon: Optimization of the single and binary systems. *Journal of Water Process Engineering*, *34*(August 2019), 101151. https://doi.org/10.1016/j.jwpe.2020.101151

Khaled-Khodja, S., Cherif, S., & Durand, G. (2018). Seasonal assessment of metal trace element contamination by PCA in Seybouse Wadi (Algeria). *Water Science and Technology: Water Supply*, *18*(6), 1897–1905. https://doi.org/10.2166/ws.2018.010

Khalid, M., Joly, G., Renaud, A., & Magnoux, P. (2004). Removal of phenol from water by adsorption using zeolites. *Industrial and Engineering Chemistry Research*, *43*(17), 5275–5280. https://doi.org/10.1021/ie0400447

Khelfaoui, M., Benaissa, A., Kherraf, S., Medjram, M. S., Bouras, I., & Mehri, K. (2022). Assessment of Groundwater and Surface Water Pollution by Hazardous Metals using Multivariate Analysis and Metal pollution Index around the old Sidi Kamber Mine, NE Algeria. *Pollution*, *8*(3), 889–903. https://doi.org/10.22059/POLL.2022.335695.1294

Krou, N. J. (2010). *Etude expérimentale et modélisation d'un procédé séquentiel AD-OX d'élimination de polluants organiques*.

Kulkarni, S., & Kaware, J. (2014). Regeneration and Recovery in Adsorption- a Review. *International Journal of Innovative Science, Engineering & Technology(IJISET)*, *1*(8), 61–64.

Kumar, R., & Wyman, C. E. (2008). An improved method to directly estimate cellulase adsorption on biomass solids. *Enzyme and Microbial Technology*, *42*(5), 426–433. https://doi.org/10.1016/j.enzmictec.2007.12.005

Kyzas, G. Z., & Kostoglou, M. (2014). Green adsorbents for wastewaters: A critical review. *Materials*, *7*(1), 333–364. https://doi.org/10.3390/ma7010333

Lagergren, S. (1898). Zur theorie der sogenannten adsorption geloster stoffe. *Kungliga Svenska Vetenskapsakademiens. Handlingar*, *24*, 1–39.

Langmuir, I. (1918). THE ADSORPTION OF GASES ON PLANE SURFACES OF GLASS, MICA AND PLATINUM. *Journal of the American Chemical Society*, *40*(9), 1361–1403. https://doi.org/10.1021/ja02242a004

Lata, S., Singh, P. K., & Samadder, S. R. (2015). Regeneration of adsorbents and recovery of heavy metals: a review. *International Journal of Environmental Science and Technology*, *12*(4), 1461–1478. https://doi.org/10.1007/s13762-014-0714-9

Leyva-Ramos, R., Rivera-Utrilla, J., Medellin-Castillo, N. A., & Sanchez-Polo, M. (2010). Kinetic modeling of fluoride adsorption from aqueous solution onto bone char. *Chemical Engineering Journal*, *158*(3), 458–467. https://doi.org/10.1016/j.cej.2010.01.019

Li, B., Yang, L., Wang, C. quan, Zhang, Q. pei, Liu, Q. cheng, Li, Y. ding, & Xiao, R. (2017). Adsorption of Cd(II) from aqueous solutions by rape straw biochar derived from different modification processes. *Chemosphere*, *175*, 332–340. https://doi.org/10.1016/j.chemosphere.2017.02.061

Li, H., Li, S., Jin, L., Lu, Z., Xiang, M., Wang, C., Wang, W., Zhang, J., Li, C., & Xie, H. (2022). Activation of peroxymonosulfate by magnetic Fe3S4/biochar composites for the efficient degradation of 2,4,6-trichlorophenol: Synergistic effect and mechanism. *Journal of Environmental Chemical Engineering*, *10*(1), 107085. https://doi.org/10.1016/j.jece.2021.107085

Li, H., Li, Z., Liu, T., Xiao, X., Peng, Z., & Deng, L. (2008). A novel technology for biosorption and recovery hexavalent chromium in wastewater by bio-functional magnetic beads. *Bioresource Technology*, *99*(14), 6271–6279. https://doi.org/10.1016/j.biortech.2007.12.002

Li, N., & Bai, R. (2005). Copper adsorption on chitosan–cellulose hydrogel beads: behaviors and mechanisms. *Separation and Purification Technology*, *42*(3), 237–247.

Li, Y., Liu, F., Xia, B., Du, Q., Zhang, P., Wang, D., Wang, Z., & Xia, Y. (2010). Removal of copper from aqueous solution by carbon nanotube/calcium alginate composites. *Journal of Hazardous Materials*, *177*(1–3), 876–880. https://doi.org/10.1016/j.jhazmat.2009.12.114

Li, Y., Wang, S., Shen, Z., Li, X., Zhou, Q., Sun, Y., Wang, T., Liu, Y., & Gao, Q. (2020). Gradient Adsorption of Methylene Blue and Crystal Violet onto Compound Microporous Silica from Aqueous Medium. *ACS Omega*, *5*(43), 28382–28392. https://doi.org/10.1021/acsomega.0c04437

Li, Y., Zimmerman, A. R., He, F., Chen, J., Han, L., Chen, H., Hu, X., & Gao, B. (2020). Solvent-free synthesis of magnetic biochar and activated carbon through ball-mill extrusion with Fe3O4 nanoparticles for enhancing adsorption of methylene blue. *Science of the Total Environment*, *722*, 137972. https://doi.org/10.1016/j.scitotenv.2020.137972

Liang, L., Xi, F., Tan, W., Meng, X., Hu, B., & Wang, X. (2021). Review of organic and inorganic pollutants removal by biochar and biochar-based composites. *Biochar*, *3*(3), 255–281. https://doi.org/10.1007/s42773-021-00101-6

Liu, C., Ye, J., Lin, Y., Wu, J., Price, G. W., Burton, D., & Wang, Y. (2020). Removal of Cadmium (II) using water hyacinth (Eichhornia crassipes) biochar alginate beads in aqueous solutions. *Environmental Pollution*, *264*, 114785. https://doi.org/10.1016/j.envpol.2020.114785

Liu, J., Hu, C., & Huang, Q. (2019). Adsorption of Cu2+, Pb2+, and Cd2+ onto oiltea shell from water. *Bioresource Technology*, *271*(July 2018), 487–491. https://doi.org/10.1016/j.biortech.2018.09.040

Liu, Y., & Liu, Y. J. (2008). Biosorption isotherms, kinetics and thermodynamics. *Separation and Purification Technology*, *61*(3), 229–242. https://doi.org/10.1016/j.seppur.2007.10.002

Lussac, G., & Ely, A. (2010). *Synthèse et propriétés de biosorbants à base d ' argiles encapsulées dans des alginates : application au traitement des eaux*. Université de Limoges Faculté des Sciences et Techniques.

Maaloul, N., Oulego, P., Rendueles, M., Ghorbal, A., & Díaz, M. (2021). Enhanced Cu(II) adsorption using sodium trimetaphosphate–modified cellulose beads: equilibrium, kinetics, adsorption mechanisms, and reusability. *Environmental Science and Pollution Research*,

28(34), 46523–46539. https://doi.org/10.1007/s11356-020-10158-8

Mahdi, Z., El Hanandeh, A., & Yu, Q. J. (2019). Preparation, characterization and application of surface modified biochar from date seed for improved lead, copper, and nickel removal from aqueous solutions. *Journal of Environmental Chemical Engineering*, *7*(5), 103379. https://doi.org/10.1016/j.jece.2019.103379

Maliou, E., Malamis, M., & Sakellarides, P. O. (1992). Lead and cadmium removal by ion exchange. *Water Science and Technology*, *25*(1), 133–138. https://doi.org/10.2166/wst.1992.0020

Mandala, R., Hegde, G., Kodali, D., & Kode, V. R. (2023). From Waste to Strength: Unveiling the Mechanical Properties of Peanut-Shell-Based Polymer Composites. *Journal of Composites Science*, *7*(8), 1–22. https://doi.org/10.3390/jcs7080307

Marczewski, A. W. (2010). Application of mixed order rate equations to adsorption of methylene blue on mesoporous carbons. *Applied Surface Science*, *256*(17), 5145–5152. https://doi.org/10.1016/j.apsusc.2009.12.078

Marinho, B. A. (2019). *As (III) and Cr (VI) oxyanion removal from water by advanced oxidation / reduction processes — a review*. 2203–2227.

MARTIN, R. T. (1962). Adsorbed Water on Clay: a Review. In *Clays and Clay Minerals* (pp. 28–70). Elsevier. https://doi.org/10.1016/b978-1-4831-9842-2.50007-9

Meshram, P., Prakash, U., Bhagat, L., Abhilash, Zhao, H., & van Hullebusch, E. D. (2020). Processing of Waste Copper Converter Slag Using Organic Acids for Extraction of Copper, Nickel, and Cobalt. *Minerals*, *10*(3), 290. https://doi.org/10.3390/min10030290

Metin, A. Ü., Doğan, D., & Can, M. (2020). Novel magnetic gel beads based on ionically crosslinked sodium alginate and polyanetholesulfonic acid: Synthesis and application for adsorption of cationic dyes. *Materials Chemistry and Physics*, *256*(July). https://doi.org/10.1016/j.matchemphys.2020.123659

Moosavi, S., Lai, C. W., Gan, S., Zamiri, G., Akbarzadeh Pivehzhani, O., & Johan, M. R. (2020). Application of efficient magnetic particles and activated carbon for dye removal from wastewater. *ACS Omega*, *5*(33), 20684–20697. https://doi.org/10.1021/acsomega.0c01905

Munafò, M., Cecchi, G., Baiocco, F., & Mancini, L. (2005). River pollution from non-point sources: a new simplified method of assessment. *Journal of Environmental Management*, *77*(2), 93–98. https://doi.org/10.1016/j.jenvman.2005.02.016

Nematian, M., Keske, C., & Ng'ombe, J. N. (2021). A techno-economic analysis of biochar production and the bioeconomy for orchard biomass. *Waste Management*, *135*, 467–477.

Nguyen, D. T., Tran, H. N., Juang, R. S., Dat, N. D., Tomul, F., Ivanets, A., Woo, S. H., Hosseini-Bandegharaei, A., Nguyen, V. P., Chao, H. P., Choong, G., Liu, Y., & Templeton, D. M. (2020). Adsorption process and mechanism of acetaminophen onto commercial activated carbon. *Journal of Environmental Chemical Engineering*, *211*(1), 54–65. https://doi.org/10.1016/j.jece.2020.104408

Njoku, V. O., Foo, K. Y., & Hameed, B. H. (2013). Microwave-assisted preparation of pumpkin seed hull activated carbon and its application for the adsorptive removal of 2,4-dichlorophenoxyacetic acid. *Chemical Engineering Journal*, *215–216*, 383–388. https://doi.org/10.1016/j.cej.2012.10.068

Nouioua, A., Ben Salem, D., Ouakouak, A., Rouahna, N., Baigenzhenov, O., & Hosseini-Bandegharaei, A. (2023). Production of biochar from Melia azedarach seeds for the crystal violet dye removal from water: combining of hydrothermal carbonization and pyrolysis. *Bioengineered*, *14*(1), 290–306. https://doi.org/10.1080/21655979.2023.2236843

Oladipo, A. A., Ahaka, E. O., & Gazi, M. (2019). High adsorptive potential of calcined magnetic biochar derived from banana peels for Cu2+, Hg2+, and Zn2+ ions removal in single and ternary systems. *Environmental Science and Pollution Research*, *26*(31), 31887–31899. https://doi.org/10.1007/s11356-019-06321-5

Omer, A. M., El-Sayed, M., Abd El-Monaem, E. M., El-Subruiti, G. M., & Eltaweil, A. S. (2023). Graphene oxide@Fe3O4-decorated iota-carrageenan composite for ultra-fast and highly efficient adsorption of lead (II) from water. *International Journal of Biological Macromolecules*, *253*(P7), 127437. https://doi.org/10.1016/j.ijbiomac.2023.127437

Ouakouak, A. (2017). *Elimination du cuivre, des nitrates et des phosphates des eaux par adsorption sur différents matériaux*. Université Mohamed Khider – Biskra.

Ouakouak, A., Abdelhamid, M., Thouraya, B., Chahinez, H. O., Hocine, G., Hamdi, N., Syafiuddin, A., & Boopathy, R. (2021). Development of a novel adsorbent prepared from dredging sediment for effective removal of dye in aqueous solutions. *Applied Sciences (Switzerland)*, *11*(22). https://doi.org/10.3390/app112210722

Ouakouak, A., Rihani, K., Youcef, L., Hamdi, N., & Guergazi, S. (2020). Adsorption characteristics of Cu (II) onto CaCl2 pretreated algerian bentonite. *Materials Research*

Express, *7*(2). https://doi.org/10.1088/2053-1591/ab5ee4

Oussalah, A., Boukerroui, A., Aichour, A., & Djellouli, B. (2019). Cationic and anionic dyes removal by low-cost hybrid alginate/natural bentonite composite beads: Adsorption and reusability studies. *International Journal of Biological Macromolecules*, *124*(December), 854–862. https://doi.org/10.1016/j.ijbiomac.2018.11.197

Park, S., Lee, J. W., Kim, J. E., Kang, G., Kim, H. J., Choi, Y. K., & Lee, S. H. (2022). Adsorptive Behavior of Cu2+ and Benzene in Single and Binary Solutions onto Alginate Composite Hydrogel Beads Containing Pitch Pine-Based Biochar. *Polymers*, *14*(17). https://doi.org/10.3390/polym14173468

Patel, M., Chaubey, A. K., Pittman, C., & Mohan, D. (2022). Aqueous ibuprofen sorption by using activated walnut shell biochar: process optimization and cost estimation†. *Environmental Science: Advances*, *1*(4), 530–545. https://doi.org/10.1039/d2va00015f

Pawar, S. N., & Edgar, K. J. (2012). Alginate derivatization: A review of chemistry, properties and applications. *Biomaterials*, *33*(11), 3279–3305. https://doi.org/10.1016/j.biomaterials.2012.01.007

Petrov, K. D., & Chubarov, A. S. (2022). Magnetite Nanoparticles for Biomedical Applications. *Encyclopedia*, *2*(4), 1811–1828. https://doi.org/10.3390/encyclopedia2040125

Pradhan, S., Abdelaal, A. H., Mroue, K., Al-Ansari, T., Mackey, H. R., & McKay, G. (2020). Biochar from vegetable wastes: agro-environmental characterization. *Biochar*, *2*(4), 439–453. https://doi.org/10.1007/s42773-020-00069-9

Prasannamedha, G., Kumar, P. S., Shivaani, S., & Kokila, M. (2022). Sodium alginate/magnetic hydrogel microspheres from sugarcane bagasse for removal of sulfamethoxazole from sewage water: Batch and column modeling. *Environmental Pollution*, *307*(March), 119523. https://doi.org/10.1016/j.envpol.2022.119523

Qiao, K., Tian, W., Bai, J., Wang, L., Zhao, J., Song, T., & Chu, M. (2020). Removal of high-molecular-weight polycyclic aromatic hydrocarbons by a microbial consortium immobilized in magnetic floating biochar gel beads. *Marine Pollution Bulletin*, *159*(July), 111489. https://doi.org/10.1016/j.marpolbul.2020.111489

Qiao, K., Tian, W., Bai, J., Zhao, J., Du, Z., Song, T., Chu, M., Wang, L., & Xie, W. (2020). Synthesis of floatable magnetic iron/biochar beads for the removal of chromium from aqueous solutions. *Environmental Technology and Innovation*, *19*, 100907.

https://doi.org/10.1016/j.eti.2020.100907

Qiu, C., Jiang, L., Gao, Y., & Sheng, L. (2023). Effects of oxygen-containing functional groups on carbon materials in supercapacitors: A review. *Materials and Design*, *230*, 111952. https://doi.org/10.1016/j.matdes.2023.111952

Rajapaksha, A. U., Chen, S. S., Tsang, D. C. W., Zhang, M., Vithanage, M., Mandal, S., Gao, B., Bolan, N. S., & Ok, Y. S. (2016). Engineered/designer biochar for contaminant removal/immobilization from soil and water: Potential and implication of biochar modification. *Chemosphere*, *148*, 276–291. https://doi.org/10.1016/j.chemosphere.2016.01.043

Raymond Desjardins, B. S. A. et M. I. (1997). *Le traitement des eaux* (Presses internationales Polytechnique (Ed.); 2eme éditi). Presses internationales Polytechnique.

Redlich, O., & Peterson, D. L. (1959). A Useful Adsorption Isotherm. *Journal of Physical Chemistry*, *63*(6), 1024–1024. https://doi.org/10.1021/j150576a611

Reffas A. (2010). Étude De L'Adsorption De Colorants Organiques (Rouge Nylosan Et Bleu De Méthylene) Sur Des Charbons Actifs Préparés À Partir Du Marc De Café. *Journal of Chemical Information and Modeling*, *53*(9), 1689–1699.

Rivas, S. C. M., Corral, R. I. A., Félix, M. del C. F., Rubio, A. R. I., Moreno, L. V., & Montfort, G. R. C. (2019). Removal of cadmium from aqueous solutions by saccharomyces cerevisiae-alginate system. *Materials*, *12*(24), 4128. https://doi.org/10.3390/ma1224128

Rocher, V. (2008). Synthèse et caractérisation de billes d'alginate magnétiques pour l'élimination de polluants organiques dans les effluents par séparation magnétique. In *Thése de doctorat*. Université Pierre et Marie Curie.

Rocher, V., Siaugue, J. M., Cabuil, V., & Bee, A. (2008). Removal of organic dyes by magnetic alginate beads. *Water Research*, *42*(4–5), 1290–1298. https://doi.org/10.1016/j.watres.2007.09.024

Rouahna, N., Ben Salem, D., Bouchareb, I., Nouioua, A., Ouakouak, A., Fadel, A., Hamdi, N., & Boopathy, R. (2023). Reduction of Crystal Violet Dye from Water by Pomegranate Peel–Derived Efficient Biochar: Influencing Factors and Adsorption Behaviour. *Water, Air, and Soil Pollution*, *234*(5), 324. https://doi.org/10.1007/s11270-023-06338-0

Rouquerol, J., Rouquerol, F., Llewellyn, P., Maurin, G., & Sing, K. (2013). *Adsorption by powders and porous solids: principles, methodology and applications*. Academic press.

Ryłko-Polak, I., Komala, W., & Białowiec, A. (2022). The Reuse of Biomass and Industrial Waste in Biocomposite Construction Materials for Decreasing Natural Resource Use and Mitigating the Environmental Impact of the Construction Industry: A Review. In *Materials* (Vol. 15, Issue 12). https://doi.org/10.3390/ma15124078

Sahli, L., Afri-Mehennaoui, F. Z., El Okki, M. E. H., Blaise, C., & Mehennaoui, S. (2011). Spatial and seasonal variations and ecotoxicological significance of sediment trace metal concentrations in Kebir-Rhumel basin (Northeast of Algeria). *Water Science and Technology*, *64*(8), 1759–1766. https://doi.org/10.2166/wst.2011.693

Sakhiya, A. K., Vijay, V. K., & Kaushal, P. (2022). Efficacy of rice straw derived biochar for removal of Pb+2 and Zn+2 from aqueous: Adsorption, thermodynamic and cost analysis. *Bioresource Technology Reports*, *17*(January), 100920. https://doi.org/10.1016/j.biteb.2021.100920

Salah, N. H. S. H. (2012). *Etude de la dégradation photocatalytique de polluants organiques en présence de dioxyde de titane, en suspension aqueuse et en lit fixe.* Université de Grenoble; Université Mentouri (Constantine, Algérie).

San-Pedro, L., Méndez-Novelo, R., Hernández-Núñez, E., Flota-Bañuelos, M., Medina, J., & Giacomán-Vallejos, G. (2020). Selection of the Activated Carbon Type for the Treatment of Landfill Leachate by Fenton-Adsorption Process. *Molecules*, *25*(13), 3023. https://doi.org/10.3390/molecules25133023

Sardella, F., Gimenez, M., Navas, C., Morandi, C., Deiana, C., & Sapag, K. (2015). Conversion of viticultural industry wastes into activated carbons for removal of lead and cadmium. *Journal of Environmental Chemical Engineering*, *3*(1), 253–260. https://doi.org/10.1016/j.jece.2014.06.026

Schaffner, M., Bader, H.-P., & Scheidegger, R. (2009). Modeling the contribution of point sources and non-point sources to Thachin River water pollution. *Science of The Total Environment*, *407*(17), 4902–4915. https://doi.org/10.1016/j.scitotenv.2009.05.007

Serp, D., Cantana, E., Heinzen, C., Von Stockar, U., & Marison, I. W. (2000). Characterization of an encapsulation device for the production of monodisperse alginate beads for cell immobilization. *Biotechnology and Bioengineering*, *70*(1), 41–53. https://doi.org/10.1002/1097-0290(20001005)70:1<41::aid-bit6>3.0.co;2-u

Shafiee, M., Foroutan, R., Fouladi, K., Ahmadlouydarab, M., Ramavandi, B., & Sahebi, S.

(2019). Application of oak powder/Fe 3 O 4 magnetic composite in toxic metals removal from aqueous solutions. *Advanced Powder Technology*, *30*(3), 544–554. https://doi.org/10.1016/j.apt.2018.12.006

Shaheen, S. M., Niazi, N. K., Hassan, N. E. E. E., Bibi, I., Wang, H., Tsang, D. C. W. C. W. W., Ok, Y. S., Bolan, N., & Rinklebe, J. (2019). Wood-based biochar for the removal of potentially toxic elements in water and wastewater: a critical review. *International Materials Reviews*, *64*(4), 216–247. https://doi.org/10.1080/09506608.2018.1473096

Slasli, M. A. (2002). *Modélisation de l'adsorption par les charbons microporeux: Approches théorique et expérimentale*. Université de Neuchâtel.

Sočo, E., & Kalembkiewicz, J. (2016). Comparison of adsorption of Cd(II) and Pb(II) ions on pure and chemically modified fly ashes. *Chemical and Process Engineering*, *37*(2), 215–234. https://doi.org/10.1515/cpe-2016-0018

Sud, D., Mahajan, G., & Kaur, M. P. (2008). Agricultural waste material as potential adsorbent for sequestering heavy metal ions from aqueous solutions - A review. *Bioresource Technology*, *99*(14), 6017–6027. https://doi.org/10.1016/j.biortech.2007.11.064

Sun, L.-M., & Meunier, F. (2003). Adsorption: aspects théoriques. *Techniques de l'ingénieur. Technologies de l'eau*, *2*(J2730).

Teng, D., Zhang, B., Xu, G., Wang, B., Mao, K., Wang, J., Sun, J., Feng, X., Yang, Z., & Zhang, H. (2020). Efficient removal of Cd(II) from aqueous solution by pinecone biochar: Sorption performance and governing mechanisms. *Environmental Pollution*, *265*(Ii), 115001. https://doi.org/10.1016/j.envpol.2020.115001

Thines, K. R., Abdullah, E. C., Mubarak, N. M., & Ruthiraan, M. (2017). Synthesis of magnetic biochar from agricultural waste biomass to enhancing route for waste water and polymer application: A review. *Renewable and Sustainable Energy Reviews*, *67*, 257–276. https://doi.org/10.1016/j.rser.2016.09.057

Thommes, M., Kaneko, K., Neimark, A. V., Olivier, J. P., Rodriguez-Reinoso, F., Rouquerol, J., & Sing, K. S. W. W. (2015). Physisorption of gases, with special reference to the evaluation of surface area and pore size distribution (IUPAC Technical Report). *Pure and Applied Chemistry*, *87*(9–10), 1051–1069. https://doi.org/10.1515/pac-2014-1117

Tomul, F., Arslan, Y., Kabak, B., Trak, D., Kendüzler, E., Lima, E. C., & Tran, H. N. (2020). Peanut shells-derived biochars prepared from different carbonization processes:

Comparison of characterization and mechanism of naproxen adsorption in water. *Science of the Total Environment*, *726*, 137828. https://doi.org/10.1016/j.scitotenv.2020.137828

Tran, H. N. (2022). Improper Estimation of Thermodynamic Parameters in Adsorption Studies with Distribution Coefficient K D(q e/ C e) or Freundlich Constant (K F): Considerations from the Derivation of Dimensionless Thermodynamic Equilibrium Constant and Suggestions. *Adsorption Science and Technology*, *2022*. https://doi.org/10.1155/2022/5553212

Tran, H. N., Lee, C. K., Vu, M. T., & Chao, H. P. (2017). Removal of Copper, Lead, Methylene Green 5, and Acid Red 1 by Saccharide-Derived Spherical Biochar Prepared at Low Calcination Temperatures: Adsorption Kinetics, Isotherms, and Thermodynamics. *Water, Air, and Soil Pollution*, *228*(10). https://doi.org/10.1007/s11270-017-3582-3

Tran, H. N., You, S. J., & Chao, H. P. (2016a). Effect of pyrolysis temperatures and times on the adsorption of cadmium onto orange peel derived biochar. *Waste Management and Research*, *34*(2), 129–138. https://doi.org/10.1177/0734242X15615698

Tran, H. N., You, S. J., & Chao, H. P. (2016b). Thermodynamic parameters of cadmium adsorption onto orange peel calculated from various methods: A comparison study. *Journal of Environmental Chemical Engineering*, *4*(3), 2671–2682. https://doi.org/10.1016/j.jece.2016.05.009

Tran, H. N., You, S. J., Hosseini-Bandegharaei, A., & Chao, H. P. (2017). Mistakes and inconsistencies regarding adsorption of contaminants from aqueous solutions: A critical review. *Water Research*, *120*, 88–116. https://doi.org/10.1016/j.watres.2017.04.014

Tseng, R. L., Wu, P. H., Wu, F. C., & Juang, R. S. (2014). A convenient method to determine kinetic parameters of adsorption processes by nonlinear regression of pseudo-nth-order equation. *Chemical Engineering Journal*, *237*, 153–161. https://doi.org/10.1016/j.cej.2013.10.013

Um-e-Laila, Hussain, A., Nazir, A., Shafiq, M., & Firdaus-e-Bareen. (2021). Potential Application of Biochar Composite Derived from Rice Straw and Animal Bones to Improve Plant Growth. *Sustainability*, *13*(19), 11104. https://doi.org/10.3390/su131911104

Verduzco-Navarro, I. P., Rios-Donato, N., Jasso-Gastinel, C. F., Martínez-Gómez, Á. de J., & Mendizábal, E. (2020). Removal of cu(II) by fixed-bed columns using alg-ch and alg-chs hydrogel beads: Effect of operating conditions on the mass transfer zone. *Polymers*, *12*(10),

1–18. https://doi.org/10.3390/polym12102345

Vijayalakshmi, K., Gomathi, T., Latha, S., Hajeeth, T., & Sudha, P. N. (2016). Removal of copper(II) from aqueous solution using nanochitosan/sodium alginate/microcrystalline cellulose beads. *International Journal of Biological Macromolecules*, *82*(Ii), 440–452. https://doi.org/10.1016/j.ijbiomac.2015.09.070

Visa, M., Bogatu, C., & Duta, A. (2010). Simultaneous adsorption of dyes and heavy metals from multicomponent solutions using fly ash. *Applied Surface Science*, *256*(17), 5486–5491. https://doi.org/10.1016/j.apsusc.2009.12.145

Vo, A. T., Nguyen, V. P., Ouakouak, A., Nieva, A., Doma, B. T., Tran, H. N., & Chao, H. P. (2019). Efficient removal of Cr(VI) from water by biochar and activated carbon prepared through hydrothermal carbonization and pyrolysis: Adsorption-coupled reduction mechanism. *Water (Switzerland)*, *11*(6). https://doi.org/10.3390/w11061164

Walsh, A. (1955). The application of atomic absorption spectra to chemical analysis. *Spectrochimica Acta*, *7*, 108–117.

Wan, S., Zhao, W., Xiong, D., Li, S., Ye, Y., & Du, L. (2022). Novel alginate immobilized TiO2 reusable functional hydrogel beads with high photocatalytic removal of dye pollutions. *Journal of Polymer Engineering*, *42*(10), 978–985.

Wang, B., Wan, Y., Zheng, Y., Lee, X., Liu, T., Yu, Z., Huang, J., Ok, Y. S., Chen, J., & Gao, B. (2019). Alginate-based composites for environmental applications: a critical review. *Critical Reviews in Environmental Science and Technology*, *49*(4), 318–356. https://doi.org/10.1080/10643389.2018.1547621

Wang, F., Zeng, Q., Su, W., Zhang, M., Hou, L., & Wang, Z. L. (2019). Adsorption of Bisphenol A on Peanut Shell Biochars: The Effects of Surfactants. *Journal of Chemistry*, *2019*. https://doi.org/10.1155/2019/2428505

Wang, H., Gao, B., Wang, S., Fang, J., Xue, Y., & Yang, K. (2015). Removal of Pb(II), Cu(II), and Cd(II) from aqueous solutions by biochar derived from KMnO4 treated hickory wood. *Bioresource Technology*, *197*(3), 356–362. https://doi.org/10.1016/j.biortech.2015.08.132

Wang, J., & Wang, S. (2019a). Preparation, modification and environmental application of biochar: A review. *Journal of Cleaner Production*, *227*, 1002–1022. https://doi.org/10.1016/j.jclepro.2019.04.282

Wang, J., & Wang, S. (2019b). Preparation , modi fi cation and environmental application of

biochar : A review. *Journal of Cleaner Production*, *227*, 1002–1022. https://doi.org/10.1016/j.jclepro.2019.04.282

Wang, S., Kwak, J. H., Islam, M. S., Naeth, M. A., Gamal El-Din, M., & Chang, S. X. (2020). Biochar surface complexation and Ni(II), Cu(II), and Cd(II) adsorption in aqueous solutions depend on feedstock type. *Science of the Total Environment*, *712*, 136538. https://doi.org/10.1016/j.scitotenv.2020.136538

Wang, W., Zhang, H., Zhang, L., Wan, H., Zheng, S., & Xu, Z. (2015). Adsorptive removal of phosphate by magnetic Fe3O4@C@ZrO2. *Colloids and Surfaces A: Physicochemical and Engineering Aspects*, *469*, 100–106. https://doi.org/10.1016/j.colsurfa.2015.01.002

Wasewar, K. L., Singh, S., & Kansal, S. K. (2020). Process intensification of treatment of inorganic water pollutants. In *Inorganic Pollutants in Water* (pp. 245–271). Elsevier. https://doi.org/10.1016/B978-0-12-818965-8.00013-5

Wathukarage, A., Herath, I., Iqbal, M. C. M. M., & Vithanage, M. (2019). Mechanistic understanding of crystal violet dye sorption by woody biochar: implications for wastewater treatment. *Environmental Geochemistry and Health*, *41*(4), 1647–1661. https://doi.org/10.1007/s10653-017-0013-8

Weber Jr, W. J., Morris, J. C., & Stumm, W. (1962). Determination of Alkylbenzenesulfonates by Ultraviolet Spectrophotometry. *Analytical Chemistry*, *34*(13), 1844–1845.

Weber, K., & Quicker, P. (2018). Properties of biochar. *Fuel*, *217*(December 2017), 240–261. https://doi.org/10.1016/j.fuel.2017.12.054

Wei, Y., Han, B., Hu, X., Lin, Y., Wang, X., & Deng, X. (2012). Synthesis of Fe3O4 nanoparticles and their magnetic properties. *Procedia Engineering*, *27*(2011), 632–637. https://doi.org/10.1016/j.proeng.2011.12.498

Weng, C. H., Tsai, C. Z., Chu, S. H., & Sharma, Y. C. (2007). Adsorption characteristics of copper(II) onto spent activated clay. *Separation and Purification Technology*, *54*(2), 187–197. https://doi.org/10.1016/j.seppur.2006.09.009

WHO. (2011). Guidelines for drinking-water quality. *WHO Chronicle*, *38*(4), 104–108.

Wu, S., Sun, A., Zhai, F., Wang, J., Xu, W., Zhang, Q., & Volinsky, A. A. (2011). Fe3O4 magnetic nanoparticles synthesis from tailings by ultrasonic chemical co-precipitation. *Materials Letters*, *65*(12), 1882–1884. https://doi.org/10.1016/j.matlet.2011.03.065

Xiao, Z., Zhang, L., Wu, L., & Chen, D. (2019). Adsorptive removal of Cu(II) from aqueous

solutions using a novel macroporous bead adsorbent based on poly(vinyl alcohol)/sodium alginate/KMnO4 modified biochar. *Journal of the Taiwan Institute of Chemical Engineers*, *102*, 110–117. https://doi.org/10.1016/j.jtice.2019.05.010

Yadav, S., Asthana, A., Singh, A. K., Chakraborty, R., Vidya, S. S., Susan, M. A. B. H., & Carabineiro, S. A. C. C. (2021). Adsorption of cationic dyes, drugs and metal from aqueous solutions using a polymer composite of magnetic/β-cyclodextrin/activated charcoal/Na alginate: Isotherm, kinetics and regeneration studies. *Journal of Hazardous Materials*, *409*(August 2020), 124840. https://doi.org/10.1016/j.jhazmat.2020.124840

Yakout, S. M., El, A., Daifullah, H. M., & El-Reefy, S. A. (2015). Pore Structure Characterization of Chemically Modified Biochar Derived From Rice Straw. *Environmental Engineering and Management Journal*, *14*(2), 473–480. http://omicron.ch.tuiasi.ro/EEMJ/

Yang, B., Tong, X., Deng, Z., & Lv, X. (2016). The adsorption of Cu species onto pyrite surface and its effect on pyrite flotation. *Journal of Chemistry*, *2016*.

Yang, H., Yan, R., Chen, H., Lee, D. H., & Zheng, C. (2007). Characteristics of hemicellulose, cellulose and lignin pyrolysis. *Fuel*, *86*(12–13), 1781–1788. https://doi.org/10.1016/j.fuel.2006.12.013

Yang, N., Wang, R., Rao, P., Yan, L., Zhang, W., Wang, J., & Chai, F. (2019). The fabrication of calcium alginate beads as a green sorbent for selective recovery of Cu(II) from metal mixtures. *Crystals*, *9*(5). https://doi.org/10.3390/cryst9050255

Yang, T., & Lua, A. C. (2003). Characteristics of activated carbons prepared from pistachio-nut shells by physical activation. *Journal of Colloid and Interface Science*, *267*(2), 408–417. https://doi.org/10.1016/S0021-9797(03)00689-1

Yang, Z. F., Li, L. Y., Hsieh, C. Te, & Juang, R. S. (2018). Co-precipitation of magnetic Fe3O4 nanoparticles onto carbon nanotubes for removal of copper ions from aqueous solution. *Journal of the Taiwan Institute of Chemical Engineers*, *82*, 56–63. https://doi.org/10.1016/j.jtice.2017.11.009

Yu, C., Wang, M., Dong, X., Shi, Z., Zhang, X., & Lin, Q. (2017a). Removal of Cu(II) from aqueous solution using Fe3O4-alginate modified biochar microspheres. *RSC Advances*, *7*(84), 53135–53144. https://doi.org/10.1039/c7ra10185f

Yu, C., Wang, M., Dong, X., Shi, Z., Zhang, X., & Lin, Q. (2017b). Removal of Cu (ii) from aqueous solution using Fe 3 O 4–alginate modified biochar microspheres. *RSC Advances*,

7(84), 53135–53144.

Zare, K., Sadegh, H., Shahryari-Ghoshekandi, R., Asif, M., Tyagi, I., Agarwal, S., & Gupta, V. K. (2016). Equilibrium and kinetic study of ammonium ion adsorption by Fe3O4 nanoparticles from aqueous solutions. *Journal of Molecular Liquids*, *213*, 345–350. https://doi.org/10.1016/j.molliq.2015.08.045

Zeng, H., Qi, W., Zhai, L., Wang, F., Zhang, J., & Li, D. (2021). Magnetic biochar synthesized with waterworks sludge and sewage sludge and its potential for methylene blue removal. *Journal of Environmental Chemical Engineering*, *9*(5), 105951. https://doi.org/10.1016/j.jece.2021.105951

Zhang, F., Wang, X., Yin, D., Peng, B., Tan, C., Liu, Y., Tan, X., & Wu, S. (2015). Efficiency and mechanisms of Cd removal from aqueous solution by biochar derived from water hyacinth (Eichornia crassipes). *Journal of Environmental Management*, *153*, 68–73. https://doi.org/10.1016/j.jenvman.2015.01.043

Zhang, H., Omer, A. M., Hu, Z., Yang, L. Y., Ji, C., & Ouyang, X. kun. (2019). Fabrication of magnetic bentonite/carboxymethyl chitosan/sodium alginate hydrogel beads for Cu (II)adsorption. *International Journal of Biological Macromolecules*, *135*, 490–500. https://doi.org/10.1016/j.ijbiomac.2019.05.185

Zhang, W., Ou, J., Wang, B., Wang, H., He, Q., Song, J., Zhang, H., Tang, M., Zhou, L., Gao, Y., & Sun, S. (2021). Efficient heavy metal removal from water by alginate-based porous nanocomposite hydrogels: The enhanced removal mechanism and influencing factor insight. *Journal of Hazardous Materials*, *418*(March). https://doi.org/10.1016/j.jhazmat.2021.126358

Zhang, X., Lv, L., Qin, Y., Xu, M., Jia, X., & Chen, Z. (2018). Removal of aqueous Cr(VI) by a magnetic biochar derived from Melia azedarach wood. *Bioresource Technology*, *256*(January), 1–10. https://doi.org/10.1016/j.biortech.2018.01.145

Zhao, N., Zhao, C., Lv, Y., Zhang, W., Du, Y., Hao, Z., & Zhang, J. (2017). Adsorption and coadsorption mechanisms of Cr(VI) and organic contaminants on H3PO4 treated biochar. *Chemosphere*, *186*(Vi), 422–429. https://doi.org/10.1016/j.chemosphere.2017.08.016

Zhao, Y., Carvajal, M. T., Won, Y. Y., & Harris, M. T. (2007). Preparation of calcium alginate microgel beads in an electrodispersion reactor using an internal source of calcium carbonate nanoparticles. *Langmuir*, *23*(25), 12489–12496. https://doi.org/10.1021/la701795y

Zhao, Y. G., Shen, H. Y., Pan, S. D., Hu, M. Q., & Xia, Q. H. (2010). Preparation and characterization of amino-functionalized nano-Fe 3O4 magnetic polymer adsorbents for removal of chromium(VI) ions. *Journal of Materials Science*, *45*(19), 5291–5301. https://doi.org/10.1007/s10853-010-4574-5

Zhou, Q., Liao, B., Lin, L., Qiu, W., & Song, Z. (2018). Adsorption of Cu(II) and Cd(II) from aqueous solutions by ferromanganese binary oxide–biochar composites. *Science of the Total Environment*, *615*, 115–122. https://doi.org/10.1016/j.scitotenv.2017.09.220

Zhu, Y., Fan, W. H., Zhang, K., Xiang, H. D., & Wang, X. R. (2020). Nano-manganese oxides-modified biochar for efficient chelated copper citrate removal from water by oxidation-assisted adsorption process. *Science of the Total Environment*, *709*, 136154. https://doi.org/10.1016/j.scitotenv.2019.136154

Scientific production during the doctoral journey

Scientific production during the doctoral journey

1- International publications

- Published Paper (***Class A⁺/Q1, May 2023***): **Dhirar Ben Salem**, Abdelkader Ouakouak, Touahra Fouzia, Noureddine Hamdi, Abdelazeem S. Eltaweil, Asad Syed, Raj Boopathy, and Hai Nguyen Tran: Easy separable, floatable and recyclable magnetic biochar/alginate beads as super-adsorbent for adsorbing copper ions in water media. Bioresource Technology. (2023). 129225, ISSN 0960-8524. https://doi.org/10.1016/j.biortech.2023.129225

- Published Paper (***Class A, May 2023***): Noureddine Rouahna, **Dhirar Ben Salem**, Imane Bouchareb, Asma Nouioua, Abdelkader Ouakouak, Ammar Fadel, and Raj Boopathy: Reduction of Crystal Violet Dye from Water by Pomegranate Peel–Derived Efficient Biochar: Influencing Factors and Adsorption Behaviour. Water Air Soil Pollut 234, 324 (2023). https://doi.org/10.1007/s11270-023-06338-0

- Published Paper (***Class A, July 2023***): Nouioua, Asma., **Ben Salem, Dhirar**., Ouakouak, Abdelkader., Rouahna, Noureddine., Baigenzhenov, Omirserik., & Hosseini-Bandegharaei, Ahmad. (2023). Production of biochar from Melia azedarach seeds for the crystal violet dye removal from water: combining of hydrothermal carbonization and pyrolysis. Bioengineered, 14(1), 290-306. https://doi.org/10.1080/21655979.2023.2236843

2- International communications

- **Dhirar Ben Salem**, Abdelkader Ouakouak, Fouzia Touahra, Julia Martin and Noureddine Hamdi. "Preparation of floatable and separable biochar/alginate beads for the effective adsorption of heavy metals cations in water", 2nd International Conference on Engineering and Applied Natural Sciences on 15-18 October in 2022 at Konya, Turkey.

- **Dhirar Ben Salem**, Abdelkader Ouakouak, Fouzia Touahra, Maria Bernardo and Noureddine Hamdi. "High-strength Magnetic Beads as Efficient and Reusable Adsorbent of Heavy Metals Recovery", 4th International Conference on Applied Engineering and Natural Sciences 2022, November 10-13/2022, Konya, Turkey.

- **Dhirar Ben Salem**, Abdelkader Ouakouak, Fouzia Touahra and Noureddine Hamdi. "Preparation of a Magnetic Hybrid Adsorbent from Low-cost Biochar for the Effective Removal of Cu (II) from Water", 1st International Seminar on Process Engineering & Environment ISCPE 2023, Mars 14-15/2023, Biskra, Algeria.

3- National Communications

- **Dhirar Ben Salem**, Chahinez Hadj-Otmane, Abdelkader Ouakouak, Fouzia Touahra and Julia Martin. "Effective Removal of Toxic Chromium from Water by Peanut Shells-Derived Biochar Prepared in Single-Step Pyrolysis", The first national Seminar on Green Chemistry and Natural Products (GCNP'22), Mars 14-15/ 2022, El Oued, Algeria.

- **Dhirar Ben Salem**, Abdelkader Ouakouak, Chahinez Hadj-Otmane, Mohamed Khechai and Julia Martin. "Biochar Based Separable Beads adsorbent for Cd (II) Removal from water : Kinetic and Reusability studies", Le 1er Séminaire National sur la Gestion Durable des des Ressources en Eaux et Valorisation des Sous Produits GDRE-VSP 2022, November 14-15/ 2022, Algiers, Algeria.

- **Dhirar Ben Salem**, Abdelkader Ouakouak, Asma Nouioua, Fouzia Touahra and Julia Martin. "Adsorption Mechanism of Chromium (VI) on Various Adsorbents: Comparative study", 1st National Conference on Materials, Energy & Environment 2022, November 23-24/ 2022, Biskra, Algeria.